Improvement of Renal Function by Acteoside and Its Reactive Metabolites from Total Glycoside of the Leaves of *Rehmannia glutinosa* Libosch.

NAN SI

CONTENTS

ABBREVIATIONS

6-keto-PGF1α	6-keto-prostaglandin F1α
ACT	acteoside
AngII	angiotensin II
AUC	area under the curve
BCAA	branched-chain amino acids
CA	caffeic acid
CE	collision energy
CGN	chronic glomerulonephritis
CGRP	calcitonin gene-related peptide
ConA	concanavalin A
CTGF	connective tissue growth factor
Dihuang	Rehmanniae Radex
Dihuangye	the leaves of *Rehmannia glutinosa* Libosch.
DM	diabetes mellitus
DN	diabetic nephropathy
DOPAC	3,4-Dihydroxyphenylacetic acid
DOPE	3,4-dihydroxyphenylethanol
DP	declustering potential
DTG	Total glycosides of Dihuangye
ECM	extracellular matrices
ET	endothelin
FC	fold change
FN	fibronectin
GAPDH	human glyceraldehyde-3-phosphate dehydrogenase
GBM	glomerular basement membrane
Glu	glucose
Glu A	glucuronic acid
GO	gene ontology
HE	hematoxylin–eosin
HG	high glucose
HVA	homovanillic acid
IL-1	interleukin 1

IL-6	interleukin 6
Irb	irbesartan
KEGG	kyoto encyclopedia of genes and genomes
LC-MS	liquid chromatography-mass spectrometry
LPS	lipopolysaccharide
MMPs	matrix metalloproteinases
MOPE	homovanillyl alcohol
MT1-MMP	membrane type 1-MMP
MTT	3-(4,5)-dimethylthiazolyl (-Z-Y1)-3, 5-diphenyltetrazolium bromide
NHDF	normal human dermal fibroblasts
OPLS-DA	orthogonal partial least squares discriminant analysis
PAN	puromycin
PAS	periodic acid-Schiff
PCA	principal component analysis
PHN	passive Heymann nephritis
PI3K	potent inhibitor of phosphatidylinositol3-kinase
PLSD	protected least significant difference
PPI	protein-protein interaction
QC	quality control
Rha	rhamnose
ROC	receiver operating characteristic
RT	reverse transcription
SDS-PAGE	sodium dodecyl sulfatepolyacrylamide gel electrophoresis
SEM	standard error of the mean
STZ	streptozotocin
TCM	traditional Chinese medicine
T2D	type 2 diabetes
T2DM	type 2 diabetes mellitus
TICs	total ion chromatograms
TGF-β	transforming growth factor-β
TIMPs	tissue inhibitors of metalloproteinases
TNF-α	tumour necrosis factor α
TXB2	thromboxane B2
UmACR	urinary microalbumin/creatinine ratio

UHPLC-Q/TOF MS	ultra-high-performance liquid chromatography coupled with quadrupole time-of-flight tandem mass spectrometry
VIP	variable importance in projection
WB	western blot
WT	wild-type
X	pyrocatechol

INTRODUCTION

Rehmannia glutinosa Libosch. is an excellent product of medicinal and food origin in traditional Chinese medicine (TCM), first recorded in the (Sheng Nong's herbal classic). Rehmanniae Radix (Dihuang) as a commonly used TCM is officially listed in the Pharmacopoeia of the People's Republic of China[1]. The leaves of *Rehmannia glutinosa* Libosch. (Dihuangye) are the aboveground part of Dihuang although not as widely used and often discarded as waste, but also had a long history of TCM, as early as in the Tang Dynasty[2] (Dietetic Materia Medica) was recorded. It has similar effects as Dihuang. The Valuable Prescriptions for Emergency has also recorded that "The Dihuangye was mashed and applied every day, and salt soup was washed first to treat skin ulceration on cheeks[3]. For turned waste into treasure, Dihuangye was officially included in the Beijing Traditional Chinese Medicine Standards in 1998[2].

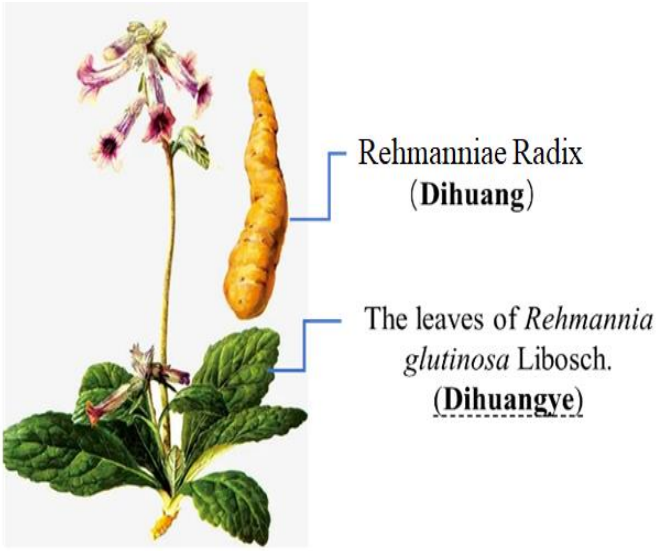

Rehmannia glutinosa Libosch.

Both Dihuangye and Dihuang have various pharmacological effects, such as improving immunity, enhancing hematopoietic function, and anti-tumorigenesis[4]. In Chinese medicine, they are prescribed as a health tonic, urological, skin disease, and women's medicine[3] (The Pharmaceutical Society of Japan). There are many similar chemical components such as iridoid glycosides, phenylethanol glycosides, and amino acids in Dihuang and Dihuangye. Recent studies have shown that the content of some iridoid glycosides and phenylethanol glycosides in Dihuangye is higher than in Dihuang[5].

Dihuangye's Total Glycoside (DTG) capsule, which is made by phenylethanol glycoside group in the Dihuangye, has been developed by our team as a new Class II Chinese drug for the treatment of renal disease. Since DTG capsule has been officially launched into the market from 2011, it has the effect of nourishing yin and tonifying kidney, promoting blood circulation, and

blood cooling[3]. In addition, the drug has been shown to exhibit good therapeutic effects in reducing urinary protein[6], chronic nephritis[7], and diabetic nephropathy (DN)[8]. Thereby, DTG capsule has a favorable reputation to improve kidney function and protecting kidney with a high degree of safety. However, the main active ingredients of DTG capsule as TCM preparations are unclear, which seriously affects the clinical usage and global promotion.

Acteoside (ACT, $C_{29}H_{36}O_{15}$) is known as verbascoside and widely exists in various TCM of the Verbenaceae, Labiatae, Xanthaceae and Miscanthaceae families, especially in the Dihuangye[9]. It is worth mentioning that ACT is the main component in DTG accounting for about 35%, and that in DTG capsule about 12% (Capsule preparation made from DTG as raw material with an appropriate amount of starch added). Moreover, it has been reported that metabolites of ACT are detectable in diabetic nephropathy (DN) animals treated with DTG[10]. Therefore, ACT is suggested to be an active candidate of DTG and/or DTG capsule for treating kidney diseases. However, it is not known whether acteoside and/or its metabolites improve renal dysfunction and exert renoprotective activity.

In this study, to identify the major active components of DTG capsules for the treatment of renal failure and to analyze the medicinal effects of these components, I have characterized *in-vivo* metabolites of ACT in animal models of renal failure, and investigated the effects of these components on renal function *in vivo* and *in vitro*. In CHAPTER 1, I have identified ACT metabolites in a rat model of chronic glomerulonephritis treated with ACT. In addition, I have demonstrated the therapeutic effects of ACT and its metabolites on renal damage in the rat model. In CHAPTER 2, I have demonstrated the improvement effects of ACT and its metabolites on renal damage in a mouse model of diabetic nephropathy. Furthermore, in CHAPTER 3, to elucidate the molecular mechanism of the improvement effects of ACT and their metabolites on renal injury, I have demonstrated the pharmacological actions of acteoside and their metabolites on cellular functions in three types of renal glomerulus-derived cells under inflammatory and high-glucose conditions *in vitro*.

CHAPTER 1 Identification of ACT and its metabolites and their renal protective effects in a rat model of chronic glomerulonephritis (CGN)

1.1 Introduction

ACT is a compound composed of two glycosides; 3,4-dihydroxyphenylethanol (DOPE) and caffeic acid (CA), in which glucose (Glu) and rhamnose (Rha) have a wide range of biological activities such as anti-inflammatory[11-12], antitumor[13], hepatoprotective[14], osteoblast proliferation and differentiation[15], neuroprotective[16], and immunomodulatory activities[17]. In addition to such diverse biological activities, ACT is characterized by its lack of teratogenic activity and high safety properties[18]. For the last few years, ACT has been increasingly studied in the field of nephrology, and its biological activity in the treatment of kidney disease has been gradually discovered and recognized[19-20].

The identification of metabolites of ACT *in vivo* is indispensable for illustrating its metabolic patterns and proposed mechanisms. Previous studies have reported that ACT is a prodrug and converted to active metabolites or intermediates to perform pharmacological actions in gastrointestinal tract and liver[21-23]. The metabolic behaviors of ACT *in vivo* have shown that the metabolites were concentrated on less polar compounds[24]. However, such metabolic behavior of ACT remains unclear in a disease animal model, which might differ from normal animal model. Furthermore, such data obtained in a pathological model might be more meaningful than that in a normal one for clinical applications. Moreover, an in-depth study of metabolic profile of ACT by oral administration is considered to be essential for understanding both physiological and pathological conditions.

In this Chapter, I have examined metabolite identification in normal and passive Heymann nephritis (PHN) rats as a model for CGN by an ultra-high-performance liquid chromatography coupled with quadrupole time-of-flight tandem mass spectrometry (UHPLC-Q/TOF MS)[25-26]. Comprehensive metabolites of ACT in rat plasma, feces, and urine after its oral administration were studied. In addition, metabolites in urine samples were validated after ACT administration into the pathological rat model to evaluate the clinical efficacy of ACT in CGN. Furthermore, I have investigated the renoprotective effect and possible mechanisms of ACT on adhesion

molecule and inflammatory cytokine production, vasoactive substance balance, platelet aggregation, the level of transforming growth factors and matrix proteins *in vivo* and *in vitro*.

1.2 Materials and Methods

1.2.1 Extraction, purification, and structural identification of ACT

1.2.1.1 Extraction and purification

ACT was isolated from Dihuangye. Dry leaves of *Rehmannia glutinosa* Libosch. were extracted twice, each for 60 min with ethanol. The extracts were combined and concentrated, and then placed overnight. Supernatant was added to the processed macroporous resin SP825 chromatography column, eluted according to priority: water, 15% ethanol, and 95% ethanol. The 95% ethanol elute was collected and concentrated to small volume, and then dried by low-temperature and vacuum. The dry matters were pulverized into a fine powder (60 mesh). The powder was extracted with acetone, and then dried and pulverized into a fine powder (80 mesh). Recrystallization with methanol-chloroform to be white crystal, and the purity of ACT was ≥98%.

1.2.1.2 Physical and chemical properties of the crystal

FUP 151□153°C; UV λ_{max}^{MeOH} (nm): 208 (4.30), 217 (4.45), 292 (4.10), 329 (4.25); IR υ_{max}^{KBr} (cm^{-1}): 3424 (OH), 2931 (C-H), 1701 (conjester), 1629 (C=C), 1604, 1523; FAB-MS (m/z): 623 $[M]^-$; ^{1}H-NMR (500M DMSO-d6, TMS):δPPM:0.966 (d, J=6 Hz, 3H, Rha.CH_3), 2.699 (t, J=8.5Hz, 2H, Phenylethanol H_β), 4.356 (d, J=8Hz, 1H, Glc. H_1), 4.722 (t, J=9.5Hz, 1H, Glc. H_4), 5.024 (s, 1H, Rha, H_1), 6.201 (d, J=16 Hz, 1H, caffeic acid H_α), 6.484~7.028 (6H, aromatic proton signal), 7.460 (d, J=15.5Hz, 1H, caffeic acid H_β), 8.688, 8.751, 9.187, 9.623 (4×OH). Data of ^{13}C-NMR were shown in **Table 1-1**. Compared with the literatures[27], it was proved to be the ACT (CAS 61276-17-3) (**Figure 1-1**).

Table 1-1 ^{13}C-NMR chemical shifts of the parts of ACT

CA	1	125.515	**DOPE**	1	129.082
	2	114.725		2	116.310
	3	145.571		3	145.007
	4	148.475		4	143.567
	5	113.567		5	115.777
	6	121.446		6	119.556
	β’	145.571		β	35.019
	α’	115.464		α	70.293
	co	165.719			
Glc	1	102.273	**Rha**	1	101.253
	2	74.514		2	70.537
	3	79.041		3	70.537
	4	69.112		4	71.634
	5	74.514		5	68.761
	6	60.790		6	18.194

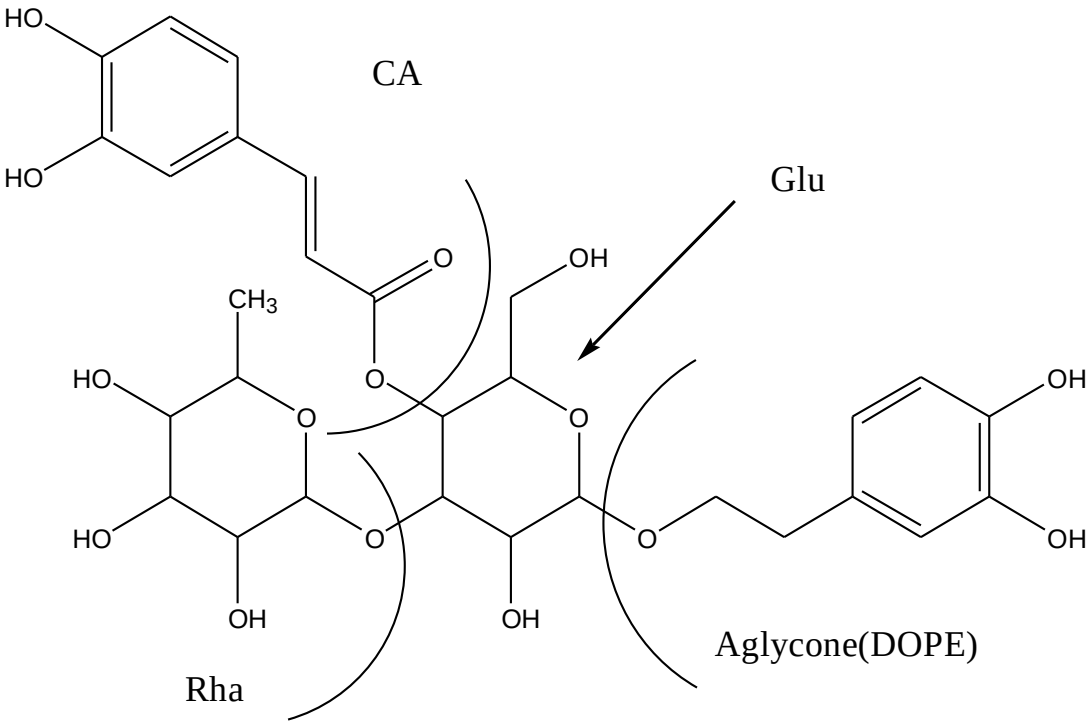

Figure 1-1 The structure of ACT

1.2.2 Chemicals and reagents

Prednisone acetate tablets (Pred) (lot: 0606027) were purchased from Tianjin Lisheng Pharmaceutical Co., Ltd. (Tianjin, China). DOPE was purchased from Tokyo Chemical Industry Co., Ltd. (Tokyo, Japan); DOPAC and homovanillic acid (HVA) were purchased from Acros Organics (New Jersey, USA); and pyrocatechol (X) was purchased from Sinopharm Chemical Reagent Co., Ltd. (Beijing, China). Homovanillyl alcohol (MOPE) was purchased from Sigma Aldrich (Steinheim, Germany). The purity of the reference substances was ≥ 98%. Methanol for extraction was obtained from Honeywell Burdick and Jackson (Swedesboro, NJ, USA). HPLC-grade acetonitrile was purchased from Merck Company (Rahway, NJ, USA). MS grade formic acid was purchased from Thermo Fisher Scientific (San Jose, CA, USA). All the other chemicals and reagents were of analytical grade.

1.2.3 Materials

Freund's adjuvant, complete and incomplete (Cat# F5881 and F5506), concanavalin A (ConA) (Cat# C-2631), lipopolysaccharide (LPS) (Cat# L-4391), and IgG from rabbit serum (Cat# I5006) were purchased from Sigma-Aldrich (St. Louis, USA). Urinary protein reagent (Cat# UP1570) was purchased from Randox Laboratories (UK). ELISA kits for albumin (Cat# Y002) and creatinine (Cat# 1032) were purchased from Beijing Beihua Kangtai Clinical Reagents Co., Ltd (Beijing, China). Immunohistochemical staining kit (Cat# SP9001) was purchased from Beijing Zhongshan Jinqiao Biotechnology Co., Ltd (Beijing, China). ELISA kits for endothelin (ET), calcitonin gene-related peptide (CGRP), 6-keto-prostaglandin F1α (6-keto-PGF1α), thromboxane B2 (TXB2) were purchased from Liberation Army General Hospital Science and Technology Development Center (Beijing, China). Anti-CD3 (Cat# MR5301), anti-CD4 (Cat# MR5104), and anti-CD8 (Cat# MR5206) were purchased from Caltag Laboratories (USA). ELISA kits for interleukin 6 (IL-6) (Cat# 2705KI), tumor necrosis factor α (TNF-α) (Cat# 551225) were purchased from BD Biosciences (USA). Transforming growth factor-β (TGF-β) rabbit polyclonal antibody (Cat# SC-146) was purchased from Santa Cruz Biotechnology (USA). Fibronectin (FN) rabbit polyclonal antibody (Cat# orb10665) was obtained from Dako Cytomation (Denmark). Proteinase K (Cat# 39450-01-6) was purchased from Merck (Germany). Anti-rabbit IgG (20060123) was purchased from Academy of Military Medical Sciences (Beijing, China). MTT was from Sigma-Aldrich, subassembly by Kehai Company. Fetal bovine serum (FBS), trypsin-EDTA solution (0.25%: 0.02%), Dulbecco's

modified Eagle's medium (DMEM), DMEM/F12, penicillin-streptomycin liquid were purchased from GIBCO (Gaithersburg, USA).

1.2.4 Animals

CGN rat model: Male Sprague-Dawley (SD) rats were used for the PHN model. One hundred and forty male rats were purchased from Beijing Vital River Laboratory Animal Technology Co. Ltd, SCXK (jing) 2002-0003 (Beijing, China), animal feeding place during the experiment: Animal Room, Medical Laboratory Animal Center, China Academy of Chinese Medical Sciences, Experimental facility License SYXK (Beijing) 2005-0028. Eight male Japanese white rabbits with initial body weights of 2 to 2.5 kg were used. The rabbits were purchased from National Institute for the Control of Pharmaceutical and Biological Products, SCXK (jing) 2005-0004 (Beijing, China), animal feeding place during the experiment: Institute of Basic Theory, China Academy of Chinese Medical Sciences, Experimental Facility License SYXK (Beijing) 2005-0024.

Normal rats for metabolic validation research: Eight SD rats, male, 240-260 g, provided by Vital River Laboratory Animal Technology Co., Ltd, approved No. SCXK (jing) 2012-0001. The animal experiment was reviewed and approved by the Animal Ethics Committee of Institute of Chinese Materia Medica, China Academy of Chinese Medical Sciences, resolution number: 20152023. Six SD rats in the ACT group and two rats in the blank group for metabolic research. ACT was dissolved in saline solution with the concentration of 5.0 mg/mL. After fasted for 12 h, the rats were given an oral dosage of 50 mg/kg ACT. At the same time, the blank group was orally administered with the same dose of saline solution. Plasma samples were collected at 0, 0.5, 1, 2, 4, 8, 24, and 48 h. Urine samples were collected from each rat using metabolic cages during intervals of 0-2, 2-4, 4-8, and 8-24 h. Feces were collected daily for 2 days. All samples were stored at -20 ℃ until analysis.

Puromycin (PAN) nephropathy model rats[28] for metabolic validation research: twenty-one male SD rats (6 weeks) were purchased from Beijing Vital River Laboratory Animal Technology Co. Ltd and raised in the Animal Center of Peking University First Hospital (clean grade). The animal experiment was reviewed and approved by the Animal Ethics Committee of Peking University First Hospital, resolution number: J201644. After 3 days of environment adaptation, they were randomly divided into 3 groups, the PAN + ACT group for this study. On day 0 of the experiment, groups 2 and 3 were given a single intraperitoneal injection of PAN

(American Sigma P7130) 15 mg/100 g, and the PAN + ACT group was given 10 mg/kg ACT daily by gavage. Urine samples were collected at 0, 5, 10, 15, and 20 days and stored at -20°C until analysis.

All animal experiments were conducted according to the standards recommended by the drug non-clinical pharmacokinetics of guiding principles (China Food and Drug Administration) and the experimental animal drug delivery technology. All animals were housed under controlled conditions of light and darkness (12:12 h). The temperature was 18-23 ℃ and the relative humidity was 40-70%. Standard rat pellet diet and standard rabbit pellet feed were purchased from Beijing Keaojieli Feed Co., Ltd (Beijing, China). Tap water were available ad libitum. Animal studies were conducted according to Guide for the Care and Use of Laboratory Animals (National Institutes of Health).

1.2.5 Sample preparation for metabolic research

The plasma and urine samples were mixed with 6-fold volumes of 0.1% Vitamin C/water-MeOH (1:9) by vortex mixing. The feces samples were homogenized with 60 volumes of 0.1% Vitamin C/water-MeOH (1:9), vortex-mixed for 1 min. After ultrasonic extraction for 30 min, the extract centrifuged at 15000 rpm at 4 ℃ for 15 min. The supernatant was evaporated under nitrogen. The residues were reconstituted with 100 μL MeOH and centrifuged at 15000 rpm at 4 ℃ for 10 min. The supernatant was injected into the chromatographic system for analysis.

1.2.6 Chromatographic and mass spectrometry conditions

An Agilent 1290 Infinity II UHPLC system and 6530 Q-TOF with a dual AJS/ESI ion source were used. Samples were separated on a YMC-Pack ODS-AQ C18 column (4.6 mm × 150 mm, 5 μm). The column temperature was maintained at 30 °C. The flow rate was 0.5 mL/min. The mobile phase consisted of water containing 0.01% formic acid (A) and acetonitrile (B). For the metabolite identification of the glomerulonephritis model urine sample conditions, the online LTQ Orbitrap Velos Pro (Thermo Fisher Scientific Inc.) combined with UHPLC via an ESI interface was used. LC separation was carried out on an Agilent Eclipse XDB-C18 (4.6 mm × 150 mm, 3.5 μm) column. The mass spectra were recorded in simultaneous negative NEF-ionization full-scan mode in the range of *m/z* 100~1000. The ESI source parameters were set as follows: collision energy, 20 eV; sheath gas temperature, 350 ℃; gas temperature, 325 ℃; sheath gas flow rate, 11 arb; nebulizer rate, 40 psi; gas flow rate, 8 L/min; and injection volume,

1 μL. The data were analyzed by Agilent Center Metabolite ID Software B.04.00 (G2211AA), and then the metabolites were verified with the endogenous metabolite database “Scripps Center for Metabolomics” and unique structure analysis software from Agilent “MassHunter MSC (Molecular Structure Corporation)”.

1.2.7 Preparation of chronic glomerulonephritis rats

1.2.7.1 Preparation of anti-glomerular basement membrane serum

Healthy SD rats anesthetized with urethane were perfused in the abdominal aorta under sterile conditions until the kidney was bloodless. Under sterile ice bath conditions, the kidney cortex was cut up, ground and passed through a 200-mesh wire mesh and centrifuged at 1500 rpm for 10 min. The sediment was taken, and Fever's complete adjuvant (Fever's incomplete adjuvant from the second immunization) was added. The sample was then ground and mixed thoroughly to form an emulsion containing 10% kidney tissue. The rabbits were immunized with the emulsion at 1 mL/each by subcutaneous multipoint injection once a week 12 times. For the first immunization, BCG vaccine plasma was added at a concentration of 4 mg/mL. Five days after the last injection, rabbit serum was obtained from the carotid artery. After inactivation of the complement in a 56 °C water bath and absorption with rats for 1 h, the serum was centrifuged to obtain nephrotoxic serum. The anti-glomerular basement membrane serum was aseptically divided and stored in a low temperature freezer at -20 °C.

1.2.7.2 Construction of rat models

A total of 120 rats were reselected, thus leaving 10 rats as the control group. The other rats were pre-immunized by subcutaneous multipoint injection of rabbit IgG 5 mg (IgG 5 mg mixed well with 1 mL of Freund's complete adjuvant). Six days later, the rat was injected with 0.06 mL/kg anti-glomerular basement membrane serum via the tail vein. After 14 days, the urine of the rats was collected in a metabolic cage, and the 24-h urine protein was measured. Serum was collected from the orbital vein, and the creatinine level in the serum was determined. The animals were randomly grouped. ACT was prepared with distilled water at concentrations of 1 mg/mL, 2 mg/mL and 4 mg/mL. Pred were prepared in distilled water to prepare a suspension at a concentration of 0.7 mg/mL.

1.2.8 Detection index

On the 7th and 14th days of administration, the rats were anesthetized with pentobarbital sodium 30 mg/kg, and blood was taken from the abdominal aorta. Serum creatinine concentrations were determined using commercially available kits with a semiautomatic biochemical analyzer. The serum levels of TNF-α and IL-6 were determined by ELISA kits in accordance with the manufacturer's instructions. The leukocyte expression of CD3, CD4, CD8, and CD18 was measured by flow cytometry. Twenty-four-hour urine protein was measured using urine protein assay kits. Blood was anticoagulated with 3.8% sodium citrate (anticoagulant:blood = 1:9). Platelet-rich plasma was centrifuged, and the maximum percentage of platelet aggregation was determined. Plasma levels of ET, CGRP, TXB2, and 6-keto-PGF1α were determined by radioimmunoassay, and the anticoagulant used was peptidase-inhibiting EDTA 2Na. After the animals were sacrificed, the kidneys were removed and fixed in neutral formalin. The kidneys were dehydrated, paraffin-embedded and sectioned according to routine procedures, and the expression of TGF-β and fibronectin (FN) was detected by immunohistochemistry.

Ninety milligrams of spleen were ground with RPMI-1640 medium containing 10% FBS to an approximately 10 mL volume. Cell counts were performed on each tube and the cell count was adjusted to 5×10^6 cells/mL. Splenocyte suspension from each rat was added separately to a 24-well culture plate at 800 μL cell suspension per well. The cells were treated with 200 μL LPS or ConA. The final concentration of LPS or ConA was 5 μg/mL. The cells were incubated in a 5% CO_2 incubator at 37 ℃ for 96 h. The plate was centrifuged at 2000 rpm for 10 min. Then, 600 μL of supernatant per well was collected to test the levels of IL-6 and TNF-α. The rest of the supernatant was discarded, and 200 μL of MTT was added at 0.5 mg/mL and incubated for 2 h. The supernatant was centrifuged and aspirated. DMSO was added to lyse the precipitated cells, and the optical density (OD) was measured at a wavelength of 570 nm. The OD value was used to represent the lymphocyte proliferative activity.

1.2.9 Cell culture

RAW 264.7 cells were purchased from Cell Center, Institute of Basic Medical Sciences Chinese Academy of Medical Sciences (Beijing, China). RAW 264.7 cells were cultured in RPMI-1640 medium containing 10% FBS and sub-cultured twice weekly. Cells were digested with 0.25% trypsin, dispersed with high glucose DMEM culture medium containing 10% FBS

to single cells, adjusted to 1×10^5 cells/mL and inoculated into 96-well plates at 100 μL/well. After 24 h of cell culture, the culture fluid was aspirated and discarded. The culture wells were divided into the normal control group, LPS group and LPS + ACT different concentration groups. After incubation for 24 h in a 5% CO_2 incubator at 37 °C, the plates were removed, and the supernatant was collected for the determination of IL-6 and TNF-α by ELISA.

1.2.10 Statistical analysis

SPSS 25.0 software (IBM Corp, Armonk, New York, USA) was used for the statistical analysis. The results are presented as the mean ± standard error of the mean (SEM). One-way ANOVA was used to determine differences among groups. If the distribution of the variables was not parametric, the data were analyzed using the nonparametric Mann–Whitney test. Comparisons between groups were made using Kruskal–Wallis one-way ANOVA on ranks with pairwise multiple comparisons made by Dunnett's method. The statistical significance level was defined as $P < 0.05$. The figure asterisk indicates statistical significance. A graph of the resulting data was created using GraphPad Prism 7.0 software (GraphPad Software Inc., San Diego, CA, USA).

1.3 Results

1.3.1 Metabolite profiles in plasma, feces, and urine samples

A total of 5 metabolites (**M25, M30, M40, M44, M46**) were identified within 0-48 h (0, 0.5, 1, 2, 4, 8, 24, and 48 h) pooled plasma samples from rats (**Figure 1-2**). After oral administration of ACT, **M44** and **M46** were detected at 0.5 h and almost disappeared at 8 h. **M25, M30** and **M40** could be detected at 0.5 h and reached their highest levels at 2 h, then gradually decreased, and disappeared 48 h later. The metabolites of ACT in fecal samples (**M1~4, M44, M46**) were summarized (**Figure 1-3**). After oral administration of ACT, **M44** and **M46** were detected at 24 h and almost disappeared 48 h later. **M1~4** could be detected at 24 h and 48 h in fecal samples. In particular, **M2** was detected at 24 h and gradually decreased 48 h later. The metabolites of ACT in urine samples were displayed (**Figure 1-4**). The prototype and isomer of ACT were not detected in urine samples. However, the prototype and isomers for DOPE (**M13**), DOPAC (**M16**), HVA (**M28**), C-4 (**M29** and **M49**) and C-6 (**M26** and **M36**) could be detected. Most of the metabolites were found after 4 h of dosing, up to 8 h, and then

decreased gradually at 48 h later (**Table 1-2**).

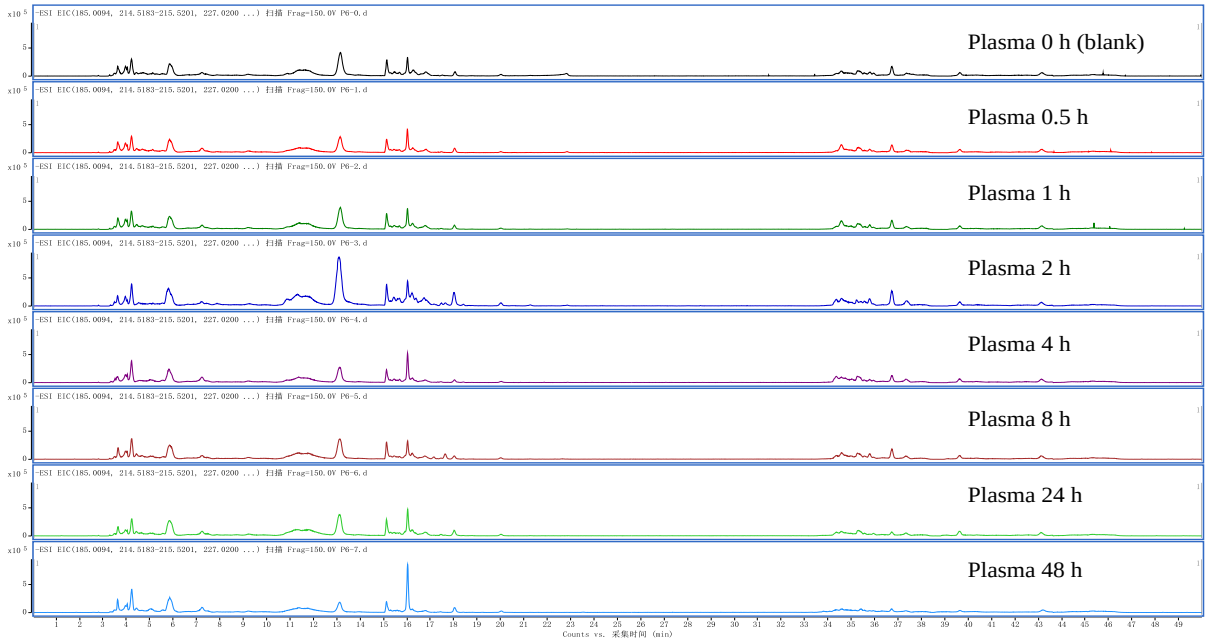

Figure 1-2 The total ion chromatograms of rat plasma samples at 0 h (blank), 0.5, 1, 2, 4, 8, 24, and 48 h after oral administration of ACT by UHPLC-Q/TOF MS in negative ion mode

The unit of vertical axis is ion strength (unified scale), and the horizontal axis represents the retention time (min). These results can preliminarily determine the temporal trend of changes in blood components.

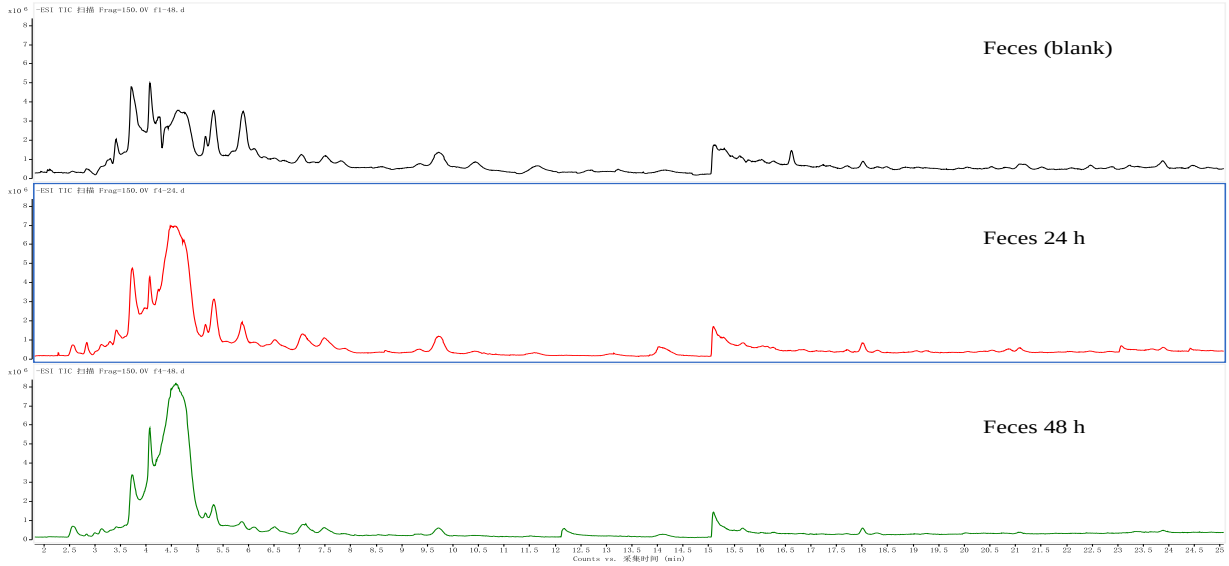

Figure 1-3 The total ion chromatograms of rat feces samples at 0 (blank), 24, and 48 h after oral administration of ACT by UHPLC-Q/TOF MS in negative ion mode.

The unit of vertical axis is ion strength (unified scale), and the horizontal axis represents the retention time (min). These results can preliminarily determine the temporal trend of changes in feces components.

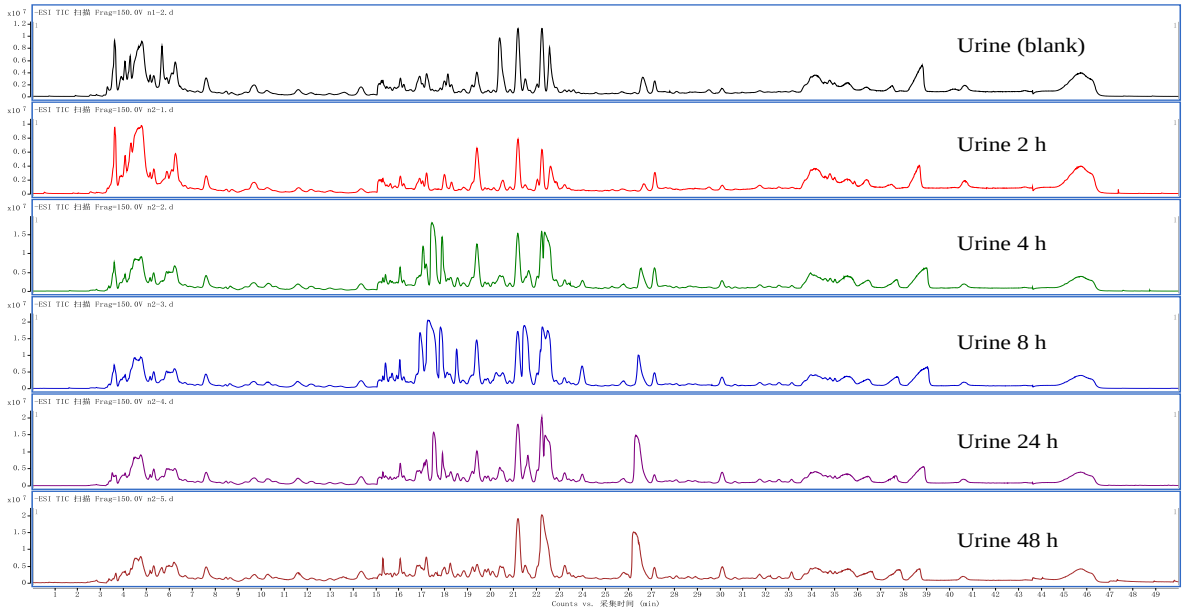

Figure 1-4 The total ion chromatograms of rat urine samples at 0 (blank), and 2, 4, 8, 24, and 48 h after oral administration of ACT by UHPLC-Q/TOF MS in negative ion mode.

The unit of vertical axis is ion strength (unified scale),and the horizontal axis represents the retention time (min). These results can preliminarily determine the temporal trend of changes in urine components.

Table 1-2 Metabolites of ACT in rats

NO.	t_R (min)	Molecular formula	Exact mass (Da)	Measured mass (Da)	Diagnostic product ions	Error (ppm)	Biotransformation Pathways	Source
M1	4.08	$C_{15}H_{16}O_{12}$	387.0558	387.0598	222.8205, 197.0089, 181.0098, 179.0003	10.33	HVA Carboxylation + Glucuronidation	F
M2	4.31	$C_{14}H_{14}O_{12}$	373.0402	373.043	197.0067, 178.9932	7.63	DOPAC Carboxylation + Glucuronidation	F
M3	4.39	$C_{14}H_{14}O_{11}$	357.0452	357.0484	181.0141	8.86	CA Demethylation + Oxidation + Glucuronidation	F
M4	4.43	$C_{15}H_{16}O_{12}$	387.0558	387.0593	211.0224, 193.0156, 181.0168, 179.0019	9.04	HVA Hydroxylation + Glucuronidation isomers	F
M5*	6.98	$C_8H_{10}O_7S$	249.0063	249.008	167.0360, 149.0249, 123.0455, 108.0212, 80.9654	6.63	DOPE Hydroxylation and Sulfation	U

M6	15.19	$C_{15}H_{20}O_{10}$	359.0973	359.0994	231.0488, 197.0465, 175.0236	5.92	HVA Glucuronidation + Hydroxylation	U
M7	15.41	$C_{29}H_{38}O_{18}$	673.1974	673.1955	329.0877, 297.0629, 294.0716, 249.0095	-2.88	ACT Hydrogenation + Oxidation	U
M8	15.42	$C_{14}H_{18}O_9$	329.0867	329.0901	175.0247, 153.0538, 123.0472, 113.0255	10.31	DOPE Glucuronide Conjugation	U
M9*	15.62	$C_8H_{10}O_7S$	249.0063	249.0085	169.0495, 155.9877, 123.0459, 94.9815, 80.9641	8.64	DOPE Hydroxylation and Sulfation isomers	U
M10	15.71	$C_{14}H_{18}O_9$	329.0867	329.0885	175.0229, 153.0569, 123.0307 113.0248	5.44	DOPE Glucuronide Conjugation	U
M11	15.9	$C_8H_8O_8S$	262.9856	262.9878	183.0305, 140.0354, 124.0114, 123.0107, 95.0088	8.31	DOPAC Hydroxylation and Sulfation	U
M12	15.91	$C_{15}H_{20}O_9$	343.1024	343.105	267.0425, 223.0810, 193.0298, 167.0717, 152.0473, 113.0224, 96.9686	7.7	MOPE Glucuronide Conjugation	U
M13*	16	$C_8H_{10}O_3$	153.0546	153.0558	123.0438	7.71	DOPE Parent	U
M14*	16.18	$C_8H_{10}O_9S_2$	312.9682	312.97	233.0125, 153.0563, 123.0461, 69.9602	5.59	DOPE Di-Sulfate Conjugation	U
M15	16.2	$C_{15}H_{18}O_{10}$	357.0816	357.0836	237.0408, 181.0556, 177.0193, 151.0403, 137.0607, 123.0465	5.54	HVA Glucuronide Conjugation	U
M16*	16.21	$C_8H_8O_4$	167.0339	167.0341	149.0198, 137.0280, 123.0465, 109.0280	1.29	DOPAC Parent	U
M17*	16.53	$C_8H_8O_7S$	246.9907	246.993	123.0463, 80.9620	9.31	DOPAC Sulfate Conjugation	U
M18*	16.74	$C_{11}H_{13}NO_5$	238.071	238.0725	160.0409	6.31	HVA Glycine Conjugation	U
M19*	16.95	$C_8H_{10}O_6S$	233.0114	233.0135	153.0559, 123.0455, 96.9598	8.86	DOPE Sulfate Conjugation	U

M20*	17.15	$C_9H_{12}O_7S$	263.022	263.024	183.0680, 137.0606, 96.9551	7.61	MOPE Hydroxylation and Sulfation	U
M21	17.18	$C_{13}H_{17}NO_6S$	314.0693	314.071	234.0155, 158.0834, 114.0942	5.46	DOPE N-Acetylcysteine Conjugation and Desaturation	U
M22	17.33	$C_8H_{10}O_9S_2$	312.9682	312.9717	233.0126, 153.0553, 123.0443, 96.9604	11.02	DOPE Di-Sulfate Conjugation isomers	U
M23*	17.39	$C_8H_{10}O_6S$	233.0114	233.0132	153.0557, 123.0452, 96.9593	7.57	DOPE Sulfate Conjugation isomers	U
M24	18.39	$C_{15}H_{16}O_9$	339.0711	339.0733	341.0915, 207.0283, 163.0393	6.61	CA deoxidization and Glucuronidation	U
M25	18.41	$C_{17}H_{23}N_3O_9S$	444.1071	444.1124	391.1607, 170.0846, 145.0154, 112.9863	11.88	DOPE Gluthation conjugation + Demethylation	P
M26*	18.49	$C_{15}H_{18}O_9$	341.0867	341.0889	261.2780, 165.0573, 121.0666, 113.0257	6.43	C-6 (CA deoxidization and hydrogenation and Glucuronidation)	U
M27*	18.52	$C_9H_{10}O_7S$	261.0063	261.0085	243.1253, 225.1141, 181.0510, 168.0442, 138.0300, 122.0367,98.0255	8.24	HVA Sulfate Conjugation	U
M28*	18.77	$C_9H_{10}O_4$	181.0495	181.0509	137.0530, 122.0304, 109.0225	7.54	HVA Parent	U
M29	18.82	$C_{14}H_{20}O_7$	299.1125	299.1141	220.0600, 176.0670, 119.0497	5.25	C-4 Parent	U
M30	18.88	$C_{15}H_{16}O_{11}$	371.0609	371.0634	253.0336, 225.0415, 195.0303, 177.0796, 165.0187, 137.0233, 109.0279	6.77	CA Hydroxylation + Glucuronidation	P
M31*	19.09	$C_9H_{12}O_6S$	247.0271	247.0289	167.0696, 152.0458, 137.0640, 123.0469, 96.9614	7.35	MOPE Sulfate Conjugation	U
M32*	19.39	$C_9H_{12}O_6S$	247.0271	247.0295	167.0739, 152.0451,	9.78	MOPE Sulfate Conjugation isomers	U

					123.0457, 96.9614			
M33	19.46	$C_{14}H_{22}O_{10}$	349.1129	349.115	173.0835, 155.0735, 129.0928, 113.0253,	5.95	C-4 Hydrolysis + Di-Oxidation	U
M34*	19.86	$C_9H_{10}O_7S$	261.0063	261.0084	181.0507, 137.0607, 121.0286, 109.0305, 96.9598	7.86	HVA Sulfate Conjugation isomers	U
M35	19.89	$C_{25}H_{37}NO_{14}S$	606.1851	606.1864	359.0030, 275.0257, 195.0693, 149.0515, 132.0318	2.14	C-1 N-Acetylcysteine Conjugation and Desaturation	U
M36	19.97	$C_{15}H_{18}O_9$	341.0867	341.0881	261.0126, 165.0596, 121.0646, 113.0209	4.08	CA deoxidization and Glucuronidation	U
M37	20.07	$C_{14}H_{19}NO_6S$	328.0849	328.0865	250.0686, 199.0425, 184.0189	4.77	MOPE N-Acetylcysteine Conjugation and Desaturation	U
M38*	20.22	$C_8H_{10}O_2$	137.0597	137.0608	166.7807, 122.0374	7.98	MOPE Hydroxymethylene Loss	U
M39	20.52	$C_9H_{10}O_7S$	261.0063	261.0082	181.0510, 135.0466, 122.0267, 96.9602	7.09	HVA Sulfate Conjugation isomers	U
M40	21.28	$C_{15}H_{14}O_{10}$	353.0503	353.0518	204.9983, 177.0175, 149.0304, 123.0456, 105.0339	4.18	CA unsaturation+ Glucuronidation	P
M41*	21.38	$C_9H_8O_7S$	258.9907	258.9928	179.0348, 135.0450, 96.9728	8.11	CA Sulfate Conjugation	U
M42*	22.37	$C_9H_{10}O_7S$	261.0063	261.0087	261.0848, 217.0573, 181.0876, 166.0258, 138.0628, 96.7918	9	HVA Sulfate Conjugation isomers	U
M43	22.51	$C_9H_{10}O_{10}S_2$	340.9632	340.9656	263.0582, 170.0828, 136.3526, 122.0515, 96.9603	7.14	HVA Di-Sulfate Conjugation	U
M44	22.86	$C_{29}H_{36}O_{15}$	623.197	623.1979	461.1722, 315.1133, 179.0372, 161.0258, 135.0460, 113.0251	1.37	Acteoside parent	PF

M45*	23.99	$C_9H_{10}O_3$	165.0546	165.0559	121.0566, 119.0498	7.75	MOPE Hydroxylation and Dehydration	U
M46	24.31	$C_{29}H_{36}O_{15}$	623.197	623.2008	461.1751, 315.0246, 161.0246	6.02	Acteoside isomers	PF
M47	24.42	$C_{14}H_{20}O_9$	331.1024	331.1048	253.0693, 177.1114, 153.0563, 117.0203	7.37	DOPE Glucuronidation + Hydrogenation	U
M48*	25.75	$C_9H_8O_3$	163.039	163.0401	119.0505, 106.0410	6.93	HVA Alcohols Dehydration	U
M49	25.8	$C_{14}H_{20}O_7$	299.1125	299.1145	221.0457, 177.0519, 133.0362, 120.0403	6.59	C-4 Parent isomers	U

Note: source: P, plasma; U, urine; F, feces. Compounds labeled ***** were those detected in urine samples of glomerulonephritis model rats.

1.3.2 Identification of metabolites by Q-TOF MS

1.3.2.1 Metabolites of ACT

Compared with the reference standard, **M44** was identified as ACT. ACT is composed of 4 chemical moieties, including CA, DOPE (phenylethanoid aglycone), glucose (central saccharide) and rhamnose (Rha). Furthermore, they might be transformed to C1-6, HVA, MOPE, DOPAC and X. **M44** (t_R = 22.86 min) produced an $[M-H]^-$ ion at *m/z* 623.1979 ($C_{29}H_{35}O_{15}$, err. 1.37 ppm). In the MS/MS analysis, the $[M-H]^-$ ion produced an ion at *m/z* 461.1722 ($C_{20}H_{29}O_{12}$) by loss of the CA moiety, which produced an ion at *m/z* 315.1133 ($C_{14}H_{19}O_8$) by continuous loss of the Rha moiety. The CA moiety was also found at *m/z* 179.0372 ($C_9H_7O_4$), and it produced ions at *m/z* 161.0258 ($C_9H_5O_3$) and *m/z* 135.0460 ($C_8H_7O_2$) through the loss of H_2O and CO_2, respectively (**Figure 1-5A**). **M7** ($C_{29}H_{37}O_{18}$, *m/z* 673.1955) and **M46** ($C_{29}H_{35}O_{15}$, *m/z* 623.2053) in negative mode were detected. **M44** and **M46** were detected in plasma and feces. **M7** and **M46** were detected in urine samples. The molecular weight of **M7** showed an increase of 50 Da (H_2O_3) over ACT. The fragment ion at *m/z* 329.0877 ($C_{14}H_{18}O_9$) of M7 had more O than the fragment ion at *m/z* 315 $[M-H-CA-Rha]^-$ of ACT, suggesting that M7 was a hydrogenation and oxidation product of ACT and that one of the oxidation sites was at DOPE part. **M49** (t_R = 25.8 min) showed an $[M-H]^-$ ion at *m/z* 299.1145 ($C_{14}H_{19}O_7$, err. 6.59 ppm). In the MS/MS analysis, the fragment ion at 221.0457 ($C_{11}H_9O_5$) was generated by splitting from the glucose substituent. The ion at *m/z* 177.0519 ($C_{10}H_9O_3$) was triggered by the loss of CO_2 (NL 44 Da) from *m/z* 221. The ion at *m/z* 120.0403 ($C_4H_8O_4$) was

produced from the glucose substituent. **M29** (t_R = 18.82 min) showed $[M-H]^-$ ions at *m/z* 299.1141 ($C_{14}H_{19}O_7$, err. 5.25 ppm), displayed MS data similar to those of **M49** in negative ion mode. **M29** and **M49** were speculated to be two metabolites that were ACT removed from the CA and Rha moieties.

1.3.2.2 Metabolites of CA

Seven types of metabolites of CA, namely, **M3, M24, M26, M30, M36, M40** and **M41,** were detected in the plasma, feces and urine, and they were in consistent with the fragmentation pattern. **M30** (t_R = 18.88 min) showed an $[M-H]^-$ ion at *m/z* 371.0634 ($C_{15}H_{15}O_{11}$, err. 6.77 ppm) in plasma and feces. It showed an increase of $C_6H_8O_7$ over CA. The fragment ion at *m/z* 195.0303 ($C_9H_7O_5$) was due to the loss of 176 Da (Glu A), and *m/z* 195 had more O than the fragment ion at *m/z* 179 of CA, which suggested that hydroxylation and glucuronide occur in the structure of M30. The fragment ions at *m/z* 177.0196 ($C_9H_5O_4$), *m/z* 165.0187 ($C_8H_5O_4$), and *m/z* 137.0233 ($C_7H_5O_3$) were generated from *m/z* 195 by losses of H_2O, CHO and CO. **M3** (t_R = 4.39 min) showed an $[M-H]^-$ ion at *m/z* 357.0484 ($C_{14}H_{13}O_{11}$, err. 8.86 ppm) in feces. The main product ion was at *m/z* 181.0141 ($C_8H_6O_5$) by losing Glu A, which might be the product after oxidation and hydroxylation of the CA acrylic groups. **M41** (*m/z* 258.9928, $C_9H_7O_7S$, 8.11 ppm) was more SO_3 than CA, detected in urine. The fragment ions at *m/z* 179.0348 ($C_9H_7O_4$, $[M-H-SO_3]^-$) and 135.0450 ($C_8H_7O_2$, $[M-H-SO_3-H_2O]^-$) were similar to CA. The ion at *m/z* 96.9728 indicated sulfate conjugation. M41 was deduced as a CA sulfate conjugation metabolite.

M40 (t_R = 21.28 min) showed an $[M-H]^-$ ion at *m/z* 353.0518 ($C_{15}H_{13}O_{10}$, err. 4.18 ppm). The ion at *m/z* 177.0175 ($C_9H_5O_4$) was due to the neutral loss of $C_6H_8O_6$ (NL 176 Da) in the MS/MS analysis. The fragment ions at *m/z* 149.0304 ($C_8H_5O_3$), *m/z* 123.0456 ($C_7H_7O_2$) and *m/z* 105.0339 (C_7H_6O) were from the CA group, suggesting that the CA group had a higher desaturation signal. M40 was probably a glucosidaldehyde derivative of one more molecule of unsaturation CA. **M26** (t_R = 18.49 min) and **M36** (t_R = 19.97 min) gave $[M-H]^-$ ions at *m/z* 341.0889 ($C_{15}H_{17}O_9$, err. 6.43 ppm) and *m/z* 341.0881 ($C_{15}H_{17}O_9$, err. 4.08 ppm). M26 and M36 had the same fragment ions. The ion at *m/z* 165.0573 ($C_9H_9O_3$) was due to the neutral loss of $C_6H_8O_6$ (NL 176 Da) in the MS/MS analysis. The fragment ion at *m/z* 121.0666 (C_8H_9O) was generated by the loss of CO_2 from *m/z* 165. They all came from the CA group. **M26** and **M36** were isomers of each other. They were probably a glucosidaldehyde derivative of deoxidization

and hydrogenation CA. **M24** (t_R = 18.39 min, *m/z* 339.0733, $C_{15}H_{15}O_9$) was less 2H than M26 and M36. The ion at *m/z* 163.0393 ($C_9H_7O_3$) was due to the neutral loss of $C_6H_8O_6$ (NL 176 Da). **M24** was probably a glucosidaldehyde derivative of deoxidization CA.

1.3.2.3 Metabolites of DOPE

A total of 12 metabolites of the DOPE type were detected in the biological samples. Compared with the reference standard, **M13** was identified as DOPE. **M13** (t_R = 16 min) produced an $_{[M-H]^-}$ ion at *m/z* 153.0558 ($C_8H_9O_3$, err. 7.71 ppm). In the MS/MS analysis, the base peak at *m/z* 123.0450 ($C_7H_7O_2$) was attributed to the loss of the CH_2O moiety (**Figure 1-5B**). The other metabolites were **M25**, **M5**, **M8**, **M9**, **M10**, **M13**, **M14**, **M19**, **M21**, **M22**, **M23** and **M47**, which were mainly detected in plasma and urine. **M25** was detected in plasma, while the other 13 metabolites were all detected in urine. **M5** and **M9** were isomers of each other, as **M8** and **M10**; **M14** and **M22**; **M19** and **M23**.

The metabolic pathways of DOPE mainly included sulfation, glucuronidation, demethylation and glutathione-binding **M25** (*m/z* 331.1048, $C_{17}H_{23}N_3O_9S$) and N-acetylcysteine binding **M21** (*m/z* 314.0710, $C_{13}H_{17}NO_6S$). Two isomers, **M19** (t_R = 16.95 min) and **M23** (t_R = 17.39 min), displayed similar MS data in negative ion mode and gave the same $[M-H]^-$ ions at *m/z* 233.0135 and *m/z* 233.0135 ($C_8H_9O_6S$, err. 8.86 ppm and 7.57 ppm). The fragment ion at *m/z* 153.0557 ($C_8H_9O_3$, $[M-H-SO_3]^-$) was DOPE. The ion at *m/z* 96.9593 indicated sulfate conjugation. They were mono-sulfated metabolites of DOPE. At the same time, two di-sulfated metabolites **M14** (*m/z* 312.9700, $C_8H_9O_9S_2$, 5.59 ppm) and **M22** (*m/z* 312.9717, $C_8H_9O_9S_2$, 11.02 ppm) as well as two hydroxylated-mono-sulfated metabolites **M5** (*m/z* 249.0080, $C_8H_9O_7S$, 6.63 ppm) and **M9** (*m/z* 249.0085, $C_8H_9O_7S$, 8.64 ppm) were tentatively detected. There were 6 sulfated products of DOPE type. Two isomers, **M8** (t_R = 15.42 min, *m/z* 329.0901, $C_{14}H_{17}O_9$) and **M10** (t_R = 15.71 min, *m/z* 329.0885, $C_{14}H_{17}O_9$, 5.44 ppm) had the same base peak at *m/z* 153.0557 ($C_8H_9O_3$) due to the neutral loss of $C_6H_8O_6$ (NL 176 Da). The fragment ion at *m/z* 123.0472 ($C_7H_7O_2$) was attributed to the loss of the CH_2O moiety from the ion at *m/z* 153. They were glucuronide products of DOPE type. **M47** was a hydroxylated mono-glucuronide metabolite product.

1.3.2.4 Metabolites of MOPE

In the three kinds of biological samples, we detected 7 MOPE metabolites. These metabolites were **M12**, **M20**, **M31**, **M32**, **M37**, **M38** and **M45**, which were all detected in urine.

M31 and **M32** were isomers of each other. MOPE ($C_9H_{11}O_3$, *m/z* 167.0711) generated an $[M-H-CH_3]^-$ ion at *m/z* 152.0476 ($C_8H_9O_3$) (**Figure 1-6A**). **M12** (t_R = 15.91 min) showed an $[M-H]^-$ ion at *m/z* 343.1050, ($C_{15}H_{19}O_9$, err. 7.7 ppm), and it was identified as MOPE+$C_6H_8O_6$. The product ions were at *m/z* 167.0717 ($C_9H_{11}O_3$) and 152.0473 ($C_8H_8O_3$), which was consistent with MOPE. The ion at *m/z* 193.0298 was indicative of glucuronic acid. Therefore, **M12** was the glucuronide conjugation metabolite of MOPE. The MS/MS fragments of **M31** (*m/z* 247.0289, $C_9H_{11}O_6S$, 7.35 ppm) and **M32** (*m/z* 247.0295, $C_9H_{11}O_6S$, 9.78 ppm) all contained MOPE fragments and sulfating special fragments. The metabolic pathway of **M31** and **M32** was speculated to be MOPE sulfate conjugation. **M45** (*m/z* 165.0559, $C_9H_9O_3$, 7.75 ppm) was less H_2 than MOPE. Its fragment ions were at *m/z* 121.0566 (C_8H_9O) and *m/z* 119.0498 (C_8H_7O) with the metabolic pathway of MOPE hydroxylation and dehydration.

1.3.2.5 Metabolites of HVA

Compared with the reference standard, **M28** was identified as HVA. **M28** (t_R = 18.77 min) produced an $[M-H]^-$ ion at *m/z* 181.0505 ($C_9H_9O_4$, err. 7.54 ppm). The $[M-H]^-$ ion produced a fragment ion at *m/z* 137.0607 ($C_8H_9O_2$) by the loss of CO_2, which produced a ion at *m/z* 122.0373 ($C_7H_6O_2$) via loss of CH_3 (**Figure 1-6B**). A total of 12 HVA metabolites had been detected in biological samples. These metabolites were **M1**, **M4**, **M6**, **M15**, **M18**, **M27**, **M28**, **M34**, **M39**, **M42**, **M43** and **M48**, mainly detected in feces and urine. **M27**, **M34** and **M39** were isomers. **M1** and **M4** were detected in feces, the other metabolites were all detected in urine. **M4** (t_R = 4.43 min) exhibited a quasi-molecular ion at *m/z* 387.0593 ($C_{15}H_{15}O_{12}$, err. 9.04 ppm) in the full mass spectrum. The $[M-H]^-$ ion dissociated into *m/z* 211.0224 ($C_9H_7O_6$) ascribed to the loss of glucuronic acid residue (176 Da). The fragment ions at *m/z* 193.0156 ($C_9H_5O_5$) and *m/z* 181.0168 ($C_8H_5O_5$) were generated from *m/z* 211 by the loss of H_2O and CH_2O. **M1** (t_R = 4.08 min) displayed the same $[M-H]^-$ ions at *m/z* 387.0598. **M1** and **M4** were hydroxylation + glucuronidation metabolites product. **M15** (t_R = 16.2 min) displayed an $[M-H]^-$ ion at *m/z* 357.0836 ($C_{15}H_{17}O_{10}$, err. 5.54 ppm) in the full mass spectrum. The fragment ion at *m/z* 181.0556 ($C_9H_9O_4$) was due to the neutral loss of 176 Da (Glu A). The ion at *m/z* 181 produced a fragment ion at *m/z* 137.0607 ($C_8H_9O_2$) by the loss of CO_2, which was the signal of HVA. **M15** was a HVA metabolite of glucuronide conjugation. **M27** (t_R = 18.52 min) displayed an $[M-H]^-$ ion at *m/z* 261.0085 ($C_9H_9O_7S$, err. 8.24 ppm) in the full mass spectrum. The fragment ion at *m/z* 181.0502 ($C_9H_9O_4$) was due to loss of SO_3 (80 Da). **M27** was a sulfated metabolite

of HVA. **M43** had more SO_3 than **M27**, which was judged as the metabolites of HVA di-sulfate conjugation.

1.3.2.6 Metabolites of DOPAC

Compared with the reference standard, **M16** was identified as DOPAC. **M16** (t_R = 16.21 min) produced an $_{[M-H]^-}$ ion at *m/z* 167.0347 ($C_8H_7O_4$, err. 1.29 ppm). In the MS/MS analysis, the fragment ions at *m/z* 152.0133 ($C_7H_4O_4$) and *m/z* 123.0451 ($C_7H_7O_2$) through the loss of CH_3 and CO_2 (**Figure 1-5C**). There were 4 DOPAC metabolites, including **M2**, **M11**, **M16** and **M17**. They were detected in plasma, feces, and urine. **M2** (t_R = 4.31 min) showed an $[M-H]^-$ ion at *m/z* 373.043 ($C_{14}H_{13}O_{12}$, err. 7.63 ppm) and had more $C_6H_6O_8$ than DOPAC. The ion at *m/z* 197.0067 ($C_8H_5O_6$) was due to the neutral loss of $C_6H_8O_6$ (NL 176 Da) in the MS/MS analysis. There had a glucuronic acid group. **M2** was deduced as a carboxylation and glucuronidation product of DOPAC. **M11** (t_R = 15.9 min) and **M17** (t_R = 16.53 min) gave $[M-H]^-$ ions at *m/z* 262.9878 ($C_8H_7O_8S$, err. 8.31 ppm) and *m/z* 246.993 ($C_8H_7O_7S$, err. 9.31 ppm). M17 had more O than M11. The fragment ion at 183.0305 ($C_8H_8O_5$) of M11 was generated by the loss of SO_3. M17 had obvious DOPAC fragment at *m/z* 123.0463 ($C_7H_7O_2$) by the splitting of SO_3 and CO_2 moieties. They were sulfation metabolites. Thus, **M11** and **M17** were identified as two sulfation metabolites of DOPAC.

1.3.3 Validation of metabolites in urine samples in CGN model rats

Urine samples from PAN nephropathy model rats were obtained. As the results showed above, the metabolites of ACT were mostly eliminated through urine, which was in accordance with ACT treatment for puromycin nephropathy. Urine samples were collected at 0, 5, 10, 15, and 20 days. The results demonstrated that ACT could significantly alleviate the abnormal proteinuria in nephrotic rats from 15 days according to the results of our group research. Taken together, the urine sample at 15 days was analyzed and identified using Thermo LTQ Orbitrap Velos. The metabolites, especially polar metabolites M5, M9, M13, M14, M16, M18, M19, M20, M23, M26, M27, M28, M31, M32, M34, M38, M39, M41, M42, M45 and M48 were validated after ACT was administered to pathological models with the aid of molecular weight and MS/MS information. The results suggested that the sulfated and conjugates of ACT were major metabolites, thus providing a foundation for further experiments to find potential biomarkers in the treatment of puromycin nephropathy by ACT.

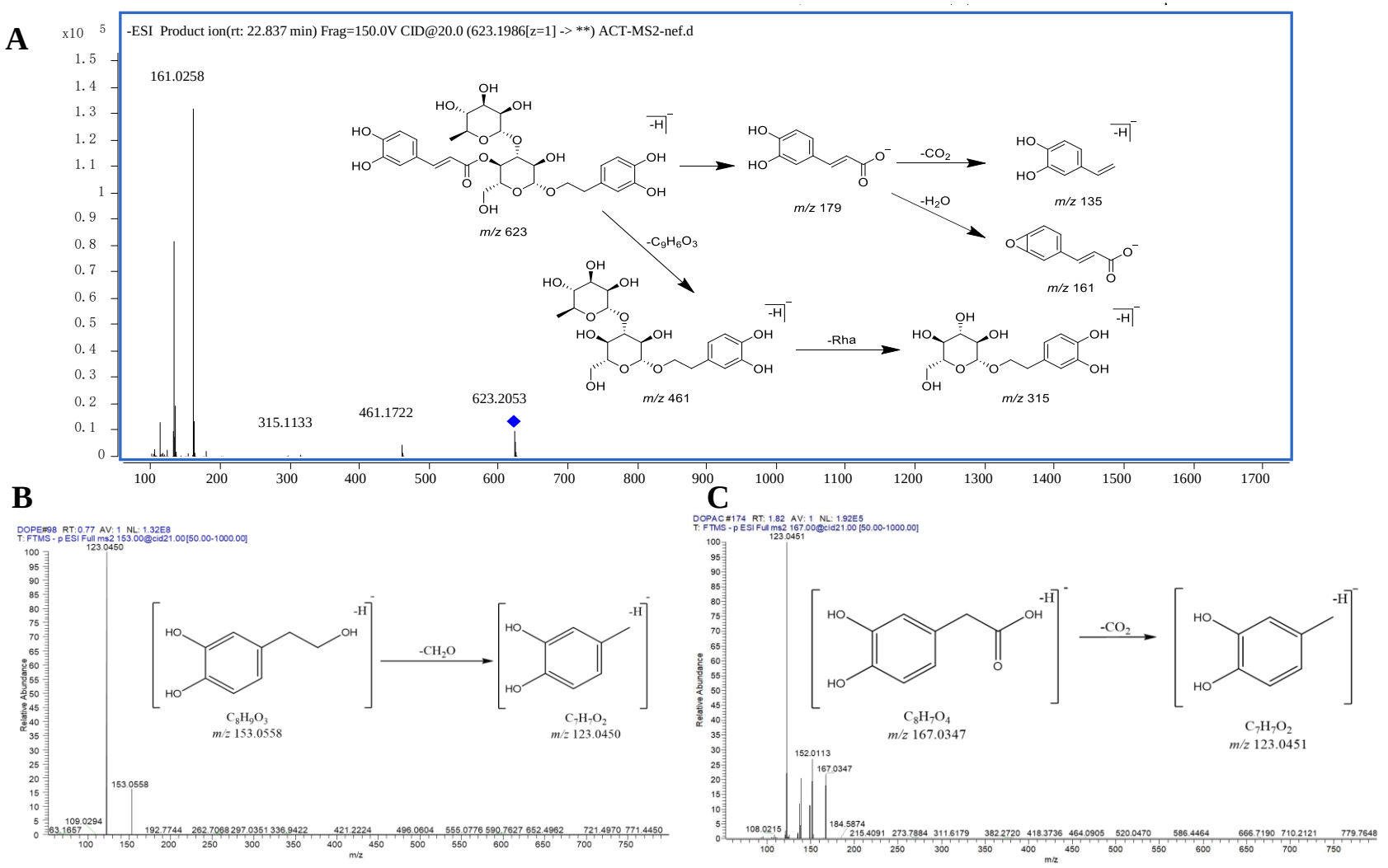

Figure 1-5 The MS/MS spectra of ACT metabolites

The unit of vertical axis is relative abundance, and the horizontal axis represents the mass-to-charge ratio (m/z). The MS/MS spectra of ACT (A), DOPE (B), and DOPAC (C).

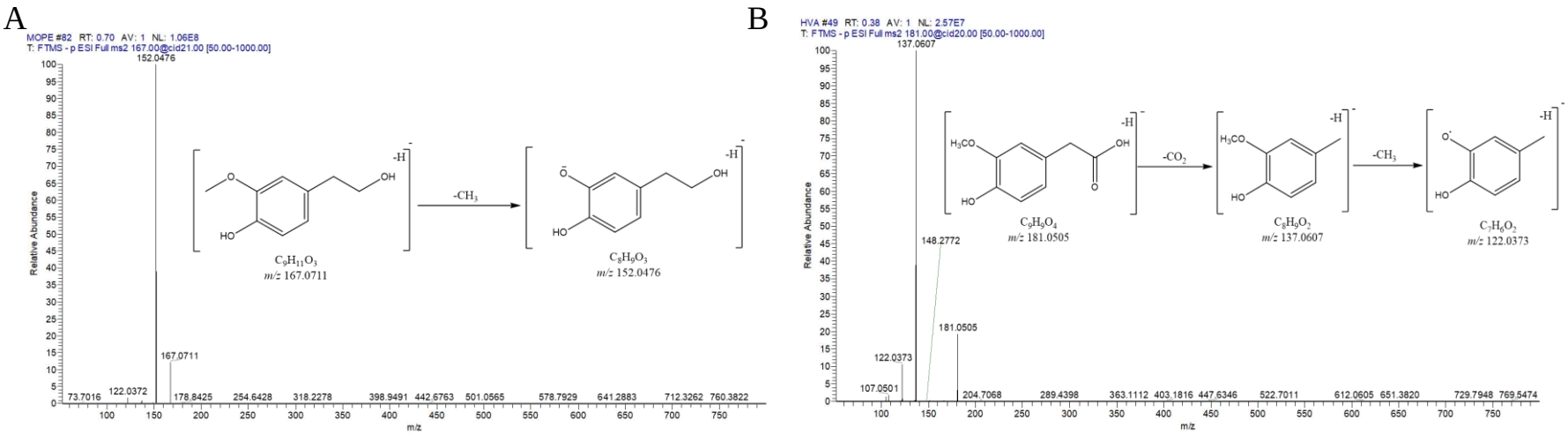

Figure 1-6 The MS/MS spectra of metabolites

The unit of vertical axis is relative abundance, and the horizontal axis represents the mass-to-charge ratio (m/z). A: MOPE; B:HVA.

1.3.4 Therapeutic effect of ACT on CGN rats

1.3.4.1 Effect of ACT on urinary protein and serum creatinine

After modeling with anti-glomerular basement membrane serum, there was a significant effect on the renal function of rats. The concentration of serum creatinine and the 24 h urinary protein were significantly higher in the Mod group than the Con group ($P < 0.001$). After 2 weeks in the ACT-M and ACT-H groups, urinary protein was significantly lower than that in the Mod group ($P < 0.05$ or $P < 0.01$). The concentration of serum creatinine was significantly lower in the ACT-L, ACT-M and ACT-H groups after 2 weeks of administration than in the Mod group ($P < 0.01$ or $P < 0.05$). The results are shown in **Figure 1-7A and B**. The results indicated that ACT significantly improved renal function for immune nephritis, reducing urinary protein and promoting creatinine excretion.

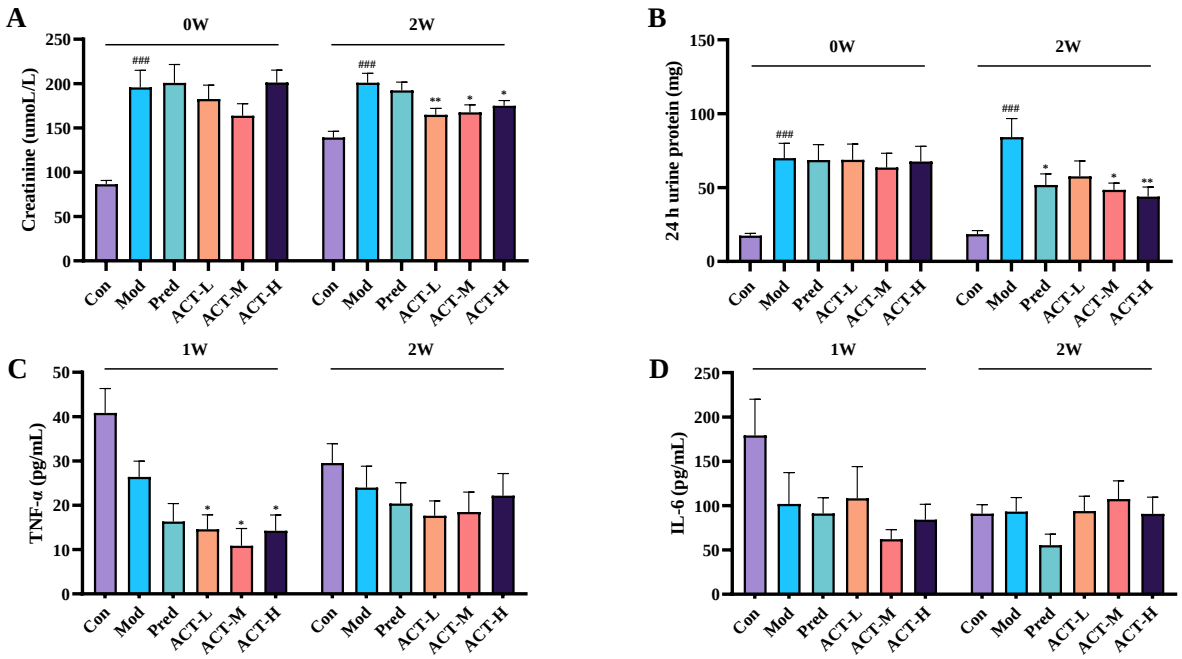

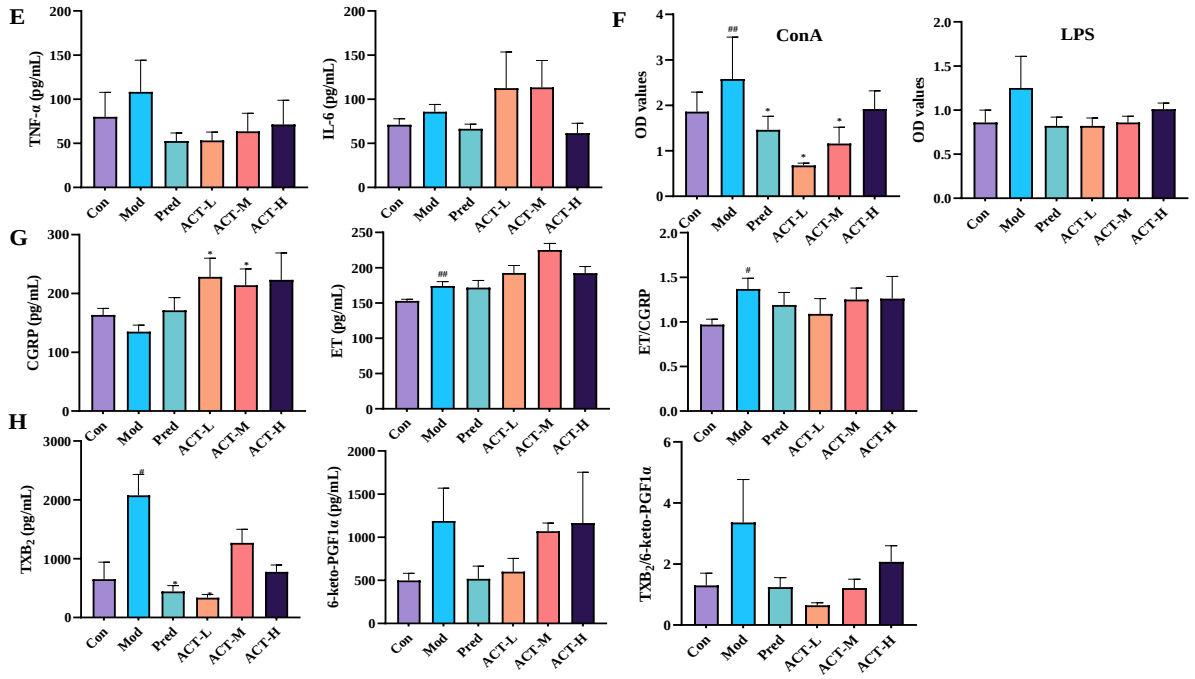

Figure 1-7 The renoprotective effect of ACT

The levels of serum creatinine (A) and 24 h urinary protein (B) in rats. The levels of serum TNF-α (C) and IL-6 (D) in rats. (E) The levels of splenocyte TNF-α and IL-6 in rats. (F) The levels of proliferative activity of spleen lymphocytes in rats stimulated by ConA and LPS. (G) The levels of serum CGRP, ET and ET/CGRP in rats. (H) The levels of serum TXB2, 6-keto-PGF1αand TXB2/6-keto-PGF1α in rats. Positive controls were Pred 7mg/kg, ACT-L 10 mg/kg, ACT-M 20 mg/kg and ACT-H 40 mg/kg and the final concentration of LPS or ConA was 5 μ g/mL. All the results were expressed as the mean ± SEM; $^{\#}P < 0.05$, $^{\#\#}P < 0.01$, $^{\#\#\#}P < 0.001$ (compared to Con group); $^{*}P < 0.05$, $^{**}P < 0.01$, $^{***}P < 0.001$ (compared to Mod group).

1.3.4.2 Effect of ACT on leukocyte adhesion and inflammatory cytokines

The measurement of CD18 expression represented the expression level of β2 integrins. The results showed that the mean fluorescence intensity of CD18 expression was enhanced and the expression positivity rate was increased in the Mod group ($P < 0.05$). ACT significantly inhibited the fluorescence intensity of CD18 expression and decreased the percentage of positive CD18 expression ($P < 0.01$ or $P < 0.05$) (**Table 1-3**). The results suggested that ACT had a significant inhibitory effect on the expression of the leukocyte adhesion molecule β2 integrin in immune nephritis.

Table 1-3 The level of plasma leukocyte CD18 in rats

Group	n	Positive rate (%)	Positive inhibition rate (%)	Average fluorescence intensity	Fluorescence intensity inhibition rate (%)
Con	5	82.52 ± 2.67	8.5	5.46 ± 0.32	4.2
Mod	6	90.2 ± 2.63$^{\#}$	-	5.7 ± 0.22	-
Pred	6	90.27 ± 2.51	-	5.6 ± 0.55	1.8
ACT-L	6	86.93 ± 4.09	3.6	4.51 ± 0.24**	20.9
ACT-M	7	83.57 ± 2.73	7.4	4.64 ± 0.18**	18.6
ACT-H	7	77.14 ± 6.57	14.5	4.72 ± 0.4*	17.2

Inhibition rate (%) = (Mod - experimental group)/ Mod*100; *$P < 0.05$, ** $P < 0.01$, *** $P < 0.001$ (compared to Mod group)

After 1 week of ACT administration, inflammatory cytokine production was significantly inhibited, and the level of serum TNF-α was significantly lower than that in the Mod group ($P < 0.05$). The level of serum IL-6 showed a decreasing trend in the ACT-M and ACT-H groups (**Figure 1-7C and D**). The secretion of TNF-α and IL-6 from splenic lymphocytes in the Mod group tended to increase compared to that in the Con group. After 2 weeks of ACT administration, the secretion level of TNF-α from splenic lymphocytes tended to decrease compared to that in the Mod group; however, the effect on IL-6 was not significant (**Figure 1-7E**).

1.3.4.3 Effect of ACT on the production of IL-6 and TNF-α in LPS-stimulated macrophage RAW 264.7 cells

Macrophage RAW 264.7 cells stimulated by LPS induced a large amount of TNF-α and IL-6 production ($P < 0.01$ or $P < 0.001$, compared with the Con group). ACT inhibited the production of TNF-α and IL-6 in a dose-dependent manner in the dose range of 1.8-1330 μg/mL. The results indicated that ACT had a significant inhibitory effect on macrophage inflammatory cytokine production (**Table 1-4**).

Table 1-4 The levels of TNF-α and IL-6 in macrophage RAW 264.7 cells stimulated by LPS

ACT (μg/mL)	LPS (μg/mL)	IL-6 (pg/mL)	Inhibition rate (%)	TNF-α (ng/mL)	Inhibition rate (%)
blank control		32.91 ± 11.44	-	1.34 ± 0.05	-
0	1	240.75 ± 39.05$^{###}$	-	2.57 ± 0.35$^{##}$	-
1.8	1	225.77 ± 32.42	6.2	1.58 ± 0.17*	38.4
5.6	1	199.68 ± 16.19	17.1	1.68 ± 0.19*	34.5
16.7	1	173.73 ± 16.59	27.8	1.78 ± 0.05*	30.7
50	1	128.96 ± 3.73*	46.4	1.65 ± 0.05*	35.7
150	1	97.11 ± 3.83**	59.7	1.2 ± 0.45**	53.2
443	1	52.26 ± 16.93**	78.3	0.86 ± 0.12**	66.7
1330	1	0	100	0.08 ± 0.01***	96.9

$^{\#}P < 0.05$, $^{\#\#}P < 0.01$, $^{\#\#\#}P < 0.001$ (compared to blank control group); $^{*}P < 0.05$, $^{**}P < 0.01$, $^{***}P < 0.001$ (compared to ACT-0 μg/mL group)

1.3.4.4 Immunomodulatory effects of ACT

LPS mainly induced the proliferation of B lymphocytes, while ConA mainly induced T lymphocytes. The proliferative activity of spleen lymphocytes in the Mod group was significantly increased after stimulation with mitogen ConA ($P < 0.05$, compared with the Con group). There was a tendency for their proliferative activity to increase after LPS stimulation, suggesting that T lymphocytes in the nephritis model showed higher responsiveness to ConA stimulation. ACT-L and ACT-M had significant effects on the proliferation of ConA-stimulated lymphocytes ($P < 0.05$, compared with the Mod group). ACT at doses of 10, 20 and 40 mg/kg also inhibited the proliferation of LPS-stimulated lymphocytes. The results indicated that ACT had an inhibitory effect on the hyperresponsiveness of lymphocytes stimulated by mitogen, with a more pronounced inhibitory effect on T lymphocytes (**Figure 1-7F**). CD3 was significantly lower in the ACT-L and ACT-M groups than in the Mod group ($P < 0.01$ or $P < 0.05$). There was no significant effect on CD4, CD8 or the CD4/CD8 ratio in the ACT dose groups. The results indicated that ACT had an overall suppressive effect on T lymphocytes but no significant effects on the distribution of CD4 and CD8 cell subpopulations (**Figure 1-8A**). IgG was

significantly higher in the Mod group ($P < 0.01$, compared with the Con group), and IgM tended to increase, while IgA had no significant effect, indicating the presence of humoral immune enhancement in the Mod group. No significant effects were observed in the ACT dose groups on IgG, IgM and IgA compared with the Mod group. Serum immunoglobulin might not be the main target of ACT (**Figure 1-8B**).

1.3.4.5 Effect of ACT on vasomotor function and platelet aggregation

ET is a highly active vasoconstrictor. CGRP is an ET antagonist and one of the most potent vasodilators. ET was significantly higher in the Mod group ($P < 0.01$), while CGRP was lower and the ratio of ET/CGRP was significantly higher compared to the Con group ($P < 0.05$). The results indicated that the nephritis model had strong vasoconstrictor activity and weak vasodilator activity, which could affect the blood perfusion of organs. There was no significant decrease in ET in any ACT dose group. However, ACT at doses of 10, 20 and 40 mg/kg significantly increased CGRP, with a significant difference between the 10 and 20 mg/kg groups compared with the Mod group ($P < 0.05$). This results in a tendency for ET/CGRP to decrease. Thus, the comprehensive result was an enhanced vasodilatory effect (**Figure 1-7G**).

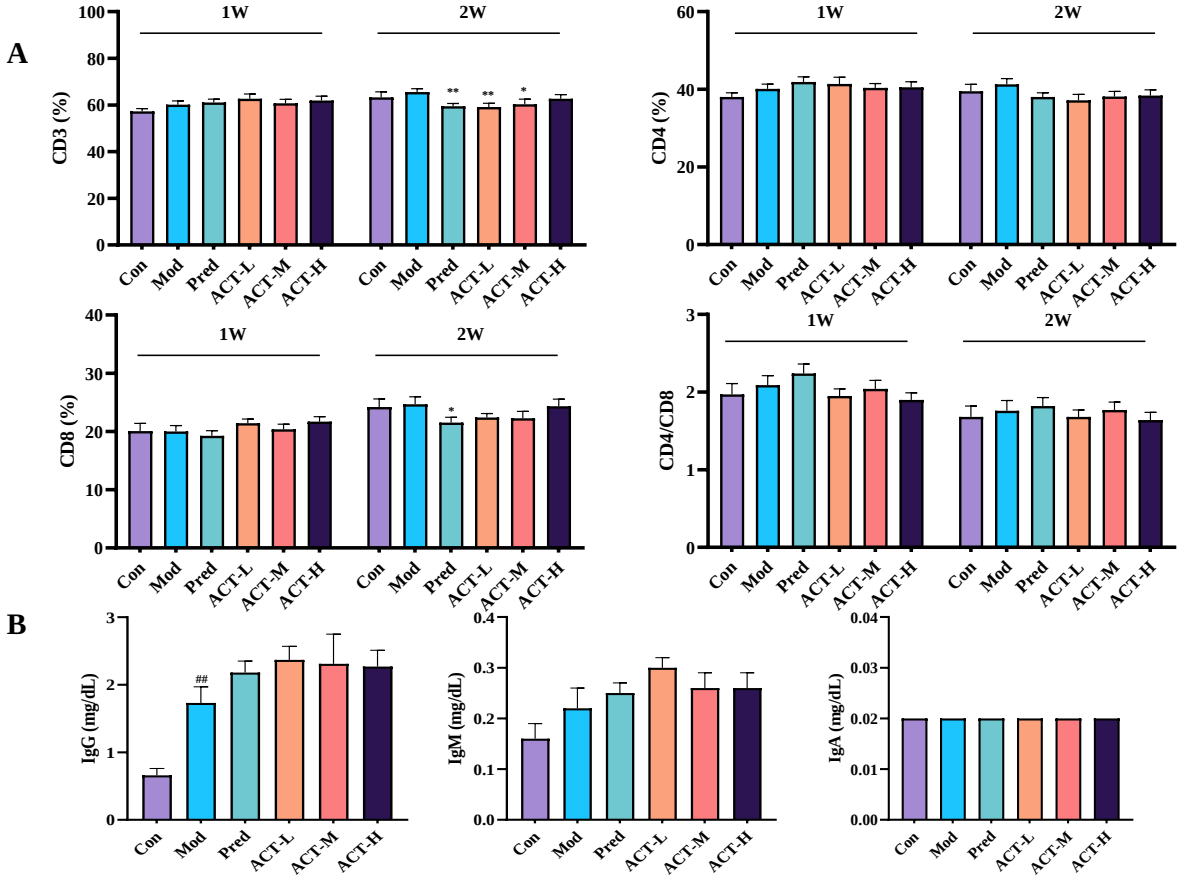

Figure 1-8 Immunomodulatory effects of ACT

The leukocyte expression of CD3, CD4, CD8, and CD18 was measured by flow cytometry. A: The percentage of plasma CD3, CD4, CD8 and CD4/CD8 in rat, the number of the animals in each group was 10, 16, 15, 15, 15, 16; B: the levels of serum IgG, IgM and IgA in rats. Positive controls were Pred 7mg/kg, ACT-L 10 mg/kg, ACT-M 20 mg/kg and ACT-H 40 mg/kg..All the results were expressed as the mean ± SEM; $^{\#}P < 0.05$, $^{\#\#}P < 0.01$, $^{\#\#\#}P < 0.001$ (compared to Con group); $^{*}P < 0.05$, $^{**}P < 0.01$, $^{***}P < 0.001$ (compared to Mod group).

TXB_2 was significantly higher in the Mod group than in the Con group ($P < 0.01$), and 6-keto-PGF1α and the TXB_2/6-Keto-PGF1α ratio were also significantly higher. The Mod rats had enhanced vasoconstrictor activity and platelet aggregation, thus possibly affecting organ blood perfusion. TXB_2, 6-keto-PGF1α and the TXB_2/6-keto-PGF1α ratio in the ACT-M and ACT-H groups tended to decrease compared to that in the Mod group. The reduction was significantly different in the ACT-L group ($P < 0.05$). ACT regulated the balance of TXB_2/6-keto-PGF1α, improving vasodilatory function (**Figure 1-7H**).

The platelet aggregation rate was significantly higher in the Mod group ($P < 0.01$, relative to the Con group). The platelet aggregation rate was significantly lower in the ACT-L, ACT-M and ACT-H groups than in the Mod group ($P < 0.01$ or $P < 0.001$). The results indicated that ACT had an inhibitory effect on platelet aggregation (**Table 1-5**).

Table 1-5 The effect on platelet aggregation

Group	n	Platelet aggregation rate (%)	Inhibition rate (%)
Con	5	43.5 ± 1.13	13.83
Mod	6	50.48 ± 1.29$^{\#\#}$	-
Pred	6	33.55 ± 2.29***	33.54
ACT-L	6	33.78 ± 2.87**	33.08
ACT-M	7	35.93 ± 1.71***	28.82
ACT-H	7	43.53 ± 1.61**	13.77

Inhibition rate (%) = (Mod - experimental group)/ Mod×100

1.3.4.6 Effect of ACT on the expression of TGF-β and FN in kidney

The expression of TGF-β and FN in renal tissues of the Mod group was significantly enhanced, and positive cells were increased and strongly positive compared with that in the Con group. The ACT-L, ACT-M and ACT-H groups significantly inhibited the expression of TGF-β and FN, and the intensity of positive expression became weaker, and the expression of positive cells decreased compared with the Mod group (**Figure 1-9A-D**).

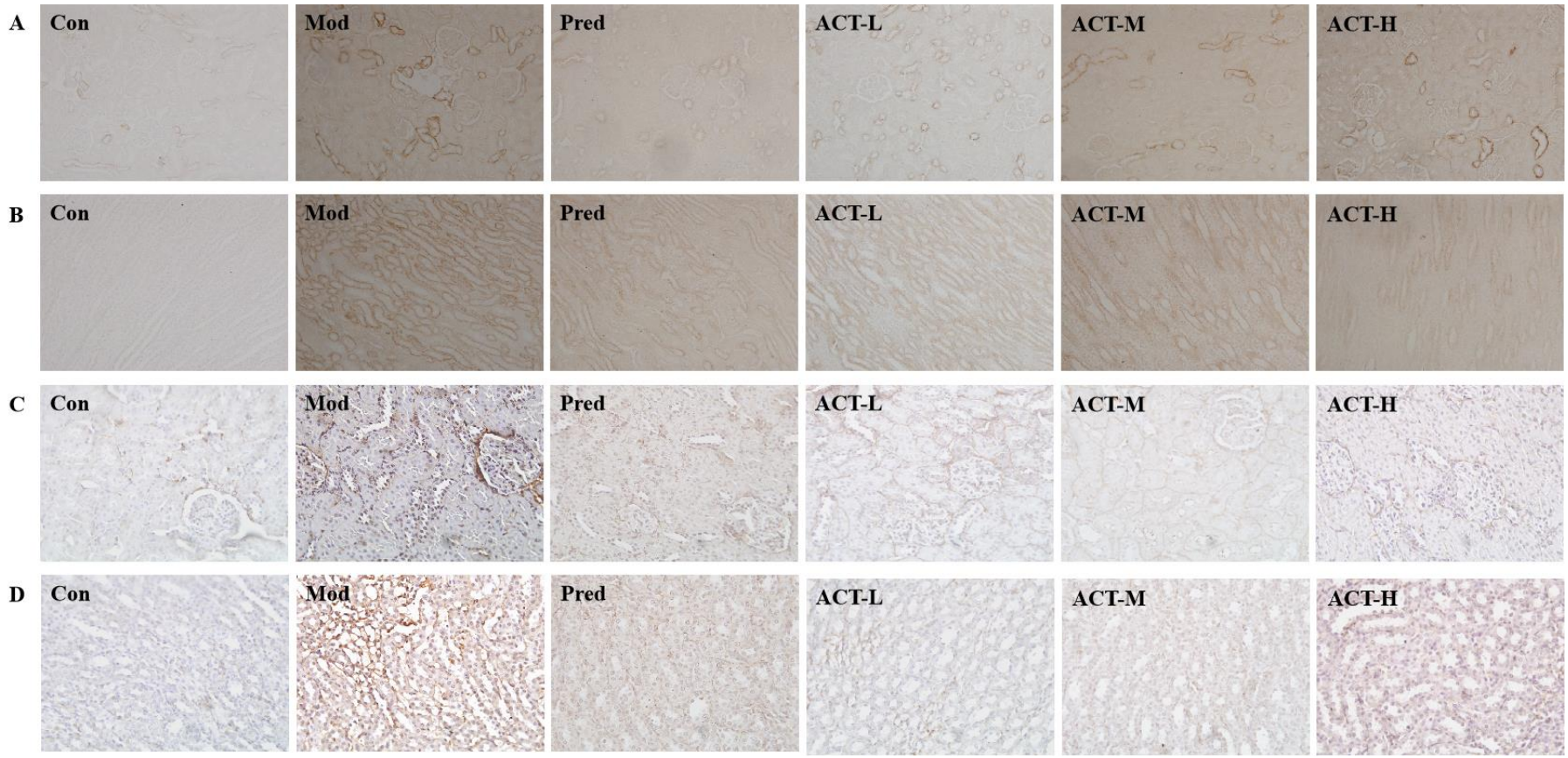

Figure 1-9 Effect of ACT on the expression of TGF-β and FN in kidney

Immunohistochemical detection showed the expression of TGF-β (× 200 magnification) in rat renal cortex (A) and medulla (B), and the expression of FN (× 400 magnification) in rat renal cortex (C) and medulla (D). The photos from left to right are Con, Mod, Pred, ACT-L, ACT-M and ACT-H groups.Positive controls were Pred 7mg/kg, ACT-L 10 mg/kg, ACT-M 20 mg/kg and ACT-H 40 mg/kg.

1.4 Discussion

1.4.1 Study of Metabolites

The metabolism of ACT in rats was studied by using Q-TOF MS. Accurate masses along with fragment ion information were applied to elucidate the structures of metabolites. A total of 49 metabolites were detected, and the metabolic pathways were summarized. Five metabolites were detected in plasma, 6 were found in feces, and the rest were all discovered in urine. In view of the chromatographic peak area, the sulfated derivatives of ACT were identified as major metabolites. ACT and its isomer could be detected in plasma and reached their highest levels at 0.5 h after oral administration, which would provide a clinical reference for clarifying the characteristics of the disposition process *in vivo*.

In the fecal samples, ACT could be discharged in the form of a prototype and isomers, indicating that assimilation and metabolism did not usually occur in the digestive system. Thus, it is suggested that its assimilation mechanism is passive diffusion, which might account for the low bioavailability of phenylethanoid glycosides by oral administration. In urine samples, on the other hand, ACT and its isomers were not discovered, suggesting that the form of ACT existed in the urine mainly as metabolites. These results were in accordance with pharmacokinetic research of ACT and the treatment of glomerulonephritis[29]. Thus, total 41 metabolites were detected in urine. Furthermore, 21 metabolites were validated after the administration of ACT to pathological models. Moreover, this study indicated that ACT was rapidly absorbed into the blood and transferred to the kidney, while the metabolites were discharged via urine. Therefore, the main route of excretion of ACT is likely to be the urinary system. Thus, these results provide a theoretical support for the pharmacological action of ACT in the clinical treatment of CGN and could lay a foundation for finding potential underlying biomarkers.

1.4.2 Possible mechanisms of renal protective actions of ACT in CGN model rats

I demonstrated that ACT significantly reduced the amount of urinary protein and serum creatinine, indicating that it had a significant effect on renal function in immune nephritis.

Based on these results, the following molecular mechanisms are discussed.

(1) Inhibition of leukocyte adhesion and inflammatory cytokine production leading to the reduction of inflammatory responses

The repeated progression and persistence of the inflammatory responses in renal tissues is the main mechanism for the development of chronic nephritis[30]. The inflammatory responses mediated by adhesion molecules and inflammatory cytokines plays an essential role in the pathological mechanisms of CGN[31]. CD18 is a subunit shared by a leukocyte adhesion molecule β2 integrin (CD11a/CD18, CD11b/CD18, CD11c/CD18)[32]. Clinical studies have shown that the production of β2 integrin is increased in proliferative CGN kidney tissues, either within glomerulus or interstitial tubule[33-36], indicating the local inflammatory activity and distribution. Renal cells are targets for the biological effects of cytokines. The excessive production of cytokines could exacerbate glomerular pathological changes and cause abnormal glomerular tissue structure and function[37]. When an inflammatory response occurs, macrophages are stimulated to produce large amounts of inflammatory cytokines. TNF-α could cause proliferation of renal lamina propria cells, stimulating the expression of adhesion molecules and excessive production of extracellular matrix, which directly leads to the damage of mesangial cells[38]. In addition, TNF-α stimulates the adhesion of polymorphonuclear leukocytes and stimulates endothelial cells to express tissue factors[39]. TNF-α initiates coagulation and promotes thrombosis in the renal vessels[40], which in turn contributes to the progression of nephritis. Together with TNF-α, IL-6 is the main cytokine mediating the inflammatory responses in the body and plays an important role in the pathology of some diseases, leading to so-called IL-6-related diseases[41]. Clinical observations have shown that plasma TNF-α and IL-6 levels are significantly higher in patients with chronic nephritis than in normal controls, and that changes in their concentrations are significantly and positively correlated with the degree of impairment of renal function[42]. In chronic proliferative glomerulonephritis, mesangial cells continuously secrete IL-6, which binds to the cell surface IL-6 receptor to stimulate the cell proliferation[43-46]. Thus, it is suggested that a vicious cycle of

autocrine regulation exacerbates glomerular pathology along with the abnormal glomerular structure and functions. Furthermore, its possible paracrine role in mediating the immune response in the glomerulus, IL-6 may also be one of the autocrine signals leading to mesangial cell proliferation *in vivo*, suggesting the importance of IL-6 in the development, progression, and regression of CGN[47].

The regulation of the expression of adhesion molecules and the inhibition of inflammatory cytokine production were of great importance for nephritis remission[48]. In this study, ACT significantly reduced the expression level of CD18 accompanied with the suppression of β2 integrin expression in PHN rats. In addition, ACT significantly inhibited TNF-α and IL-6 production. Furthermore, in RAW264.7 macrophages cultured *in vitro*, ACT similarly inhibited TNF-α and IL-6 production. Thus, these results suggest that the pharmacological actions of ACT for nephritis are associated with the inhibition of β2 integrin expression and inflammatory cytokine production in macrophage, which results in the reduction of macrophage adhesion and the inflammatory responses *in vivo*.

(2) Regulation of TXA2 and PGI2 balance to inhibit platelet aggregation and thrombosis, and improve blood flow

TXA2 and PGI2, both metabolites of arachidonic acid, have opposite functions. TXA2 has strong vasoconstrictive and stimulating effects on platelet aggregation[49]. Under normal physiological conditions, TXA2 and PGI2 are in balance to maintain normal vascular tension, blood flow patterns, and proper coagulation factor activity[50]. Once the vascular endothelium is damaged, platelets aggregate in the endothelium, resulting in a dysfunctional balance between vascular endothelium and platelets[51]. The blood becomes hypercoagulable, which leads to thrombosis[52]. Because TXA2 and PGI2 are extremely unstable, their concentrations are generally measured by measuring their metabolites, TXB2 and 6-keto-PGF1α[53]. Clinical studies have shown that TXB2 is significantly higher, while 6-keto-PGF1α is lower in patients with chronic nephritis[54]. Platelets are actively involved in the development of CGN as an inflammatory effector[55]. It has been reported that platelet activation releases a large number of

inflammatory mediators from its internal alpha granules, dense granules and lysosomes, which synergize with renal intrinsic cells or infiltrating inflammatory cells to mediate intraglomerular thrombosis, accelerate the deposition of immune complexes in the glomerulus, stimulate mesangial cell proliferation, and alter glomerular hemodynamics[56]. Recurrent intraglomerular platelet coagulation, thrombosis and ultimately glomerulosclerosis[57]. Due to the important role of platelets in renal immune damage, antiplatelet active drugs are often used clinically to treat CGN. In the present study, ACT reduced TXB2 levels and modulated the TXB2/6-keto-PGF1α ratio. In addition, ACT (10, 20, and 40 mg/kg) suppressed the platelet aggregation rate in the PHN rats. These results suggested that ACT improves the dysfunction of pathological vascular endothelium-platelet balance in nephritis by regulating TXB2/6-keto-PGF1α and inhibiting platelet aggregation and thrombus formation. Thus, ACT is likely to alleviate the development of renal lesions by improving renal hemodynamics and hemorheology and reducing the deposition of circulating immune complexes in the kidney.

(3) Regulating vasomotor function and improving blood perfusion

Glomerular inflammation and platelet aggregation often lead to coagulation disorders. Large amounts of the vasoconstrictor substance ET could be synthesized[58]. CGRP is a physiological antagonist of ET[59]. If the metabolism of ET and CGRP is imbalanced, the inflammatory and hypercoagulable state of nephritis might be exacerbated, resulting in a vicious cycle. In this study, ACT (10 and 20 mg/kg) significantly increased blood CGRP levels and decreased the ET/CGRP ratio in rats with immune nephritis. These results suggested that ACT improves the balance of ET/CGRP metabolism to make dominantly the vasodilating effect in vivo. Thus, the subsequent improvement of renal blood flow is likely to suppress the deposition of circulating immune complexes and inflammatory substances in the kidney, resulting in the reduction of the renal inflammatory response. Furthermore, the increase in renal blood flow may improve blood hypercoagulation by inhibiting blood clotting and thrombosis, which leads to prevent the progression of the disease.

(4) Inhibition of excessive cellular immunity

CGN is an autoimmune disease with an overactive immune responses in the body[60]. In this study, the results in CGN model rats showed the presence of excessive humoral immunity, the high T-cell reactivity to mitogen *in vivo*, the increase of blood IgG levels, and the ConA-induced proliferation activity of splenic lymphocytes in the Mod group. ACT did not decrease the level of blood IgG in rats with nephritis, but did the ConA-induced proliferation activity of splenic lymphocytes. Therefore, these finding suggested that ACT has an inhibitory effect on the hyperreactivity of T lymphocytes to mitogens in the nephritis model.

(5) Inhibition of renal interstitial fibrosis and stromal protein deposition to prevent chronic fibrosis

Excessive extracellular matrix production and accumulation are a pathological mechanism of fibrosis in chronic nephritis[61]. The production of extracellular matrix has been reported to be stimulated by TGF-β, which is associated with overproduction of renal interstitial matrix protein[62]. As FN is a matrix protein that exists in the interstitium during renal fibrosis[63], FN as well as TGF-β are important factors involved in the pathological mechanism of chronic nephritis. In the present study, the production of TGF-β and FN was effectively inhibited by ACT, indicating that ACT might mitigate the fibrosis process of chronic nephritis.

1.5 Conclusion

The study in CHAPTER 1 indicated that a total of 49 metabolites of ACT was identified, of which 21 metabolites were detectable in nephropathy model rats. Furthermore, it is strongly suggested that ACT is a pivotal therapeutic agent in DTG for CGN with the relief of fibrotic lesions by the inhibition of inflammatory responses and macrophage adhesion to interstitial extracellular matrix, regulation of immune function, and the improvement of tissue hemodynamics and hemorheology.

CHAPTER 2 Characterization of renal protective actions of ACT in *db/db* mice with diabetic nephropathy and their network pharmacology analysis

2.1 Introduction

Diabetes mellitus (DM) is a major chronic disease worldwide and characteristic to a metabolic disease characterized by hyperglycemia[64]. Diabetic nephropathy (DN) is the most common complication of DM and known as the major cause of end-stage renal disease[65-67]. On the other hand, a G-T point mutation in leptin receptor encoded by the db gene has been reported to lead to the abnormal translation of leptin receptor protein, resulting in a model of congenital obesity type 2 DM[68]. It has been reported that *db/db* mice develop progressive nephropathy after an episode of overt diabetes, like human diabetic nephropathy[69]. Currently, *db/db* mice are the most widely used animal for establishing type 2 DN models[70].

DTG capsules have definite therapeutic effects by reducing proteinuria levels and hypercoagulable blood in DN patients[8]. In addition, it has been reported that DTG capsules inhibits the growth of high-glucose-induced glomerular mesangial cells by decreasing the TGF-β1 and Wnt/β-catenin signaling pathways[10]. Furthermore, a combined usage of DTG in routine treatment has been reported to actively improve the proteinuria level of DN[71]. In Chapter 1, I have identified ACT as the major active substance of DTG and found that it improves renal abnormality in CGN rats. Thus, this study allows me to speculate that ACT might be an active component of DTG that shows efficacy in DN.

In this Chapter, to clarify the improvement actions of ACT on DN, I have examined the therapeutic effects of ACT and its metabolites in *db/db* mice with symptoms of DN. In addition, for the analysis of metabolites of ACT in the body, I have performed untargeted metabolomics studies by UHPLC-LTQ-Orbitrap MS using urine, serum, and kidney samples. For the pathways enriched by untargeted metabolomics, targeted metabolomics by UHPLC-QQQ-MS/MS was performed in kidney samples for validation. Furthermore, metabolomics and network pharmacology studies were employed to explore the mechanism of ACT against DN.

2.2 Materials and methods

2.2.1 Chemicals and reagents

ACT was isolated from the Dihuangye as CHAPTER 1. The purity of ACT was over 98%. MS grade acetonitrile, methanol, and formic acid were obtained from Thermo Fisher Scientific Inc. (USA), and Wahaha pure water was purchased from Hangzhou Wahaha Group Company (China). Irbesartan (lot number: 1348E20274) was purchased from Zhejiang Huahai Pharmaceutical Co., Ltd. (Linjiang, China). Glucose (lot number: 200904-2) was purchased from Xilong Chemical Co., Ltd. (Foshan, China). ACCU-CHEK blood glucose test strips were purchased from Roche (USA). Blood creatinine and urea nitrogen kits were purchased from Inventec Xiamen Technology Co., Ltd. (Xiamen, China). Urine creatinine and urine microalbumin assay kits were purchased from Shanghai Yaji Biotechnology Co., Ltd. (Shanghai, China). Xylene, anhydrous ethanol, 95% ethanol, n-butanol, phosphomolybdic acid, and aniline blue were purchased from Sinopharm Chemical Reagent Co., Ltd. (Beijing, China). Hematoxylin and eosin (HE) were purchased from Zhuhai Beso Biotechnology Co., Ltd. (Zhuhai, China). Schiff Reagent and Weigert's iron hematoxylin were purchased from Shanghai Solarbio Biotechnology Co., Ltd. (Shanghai, China).

2.2.2 Animals

Seven-week-old SPF grade male B6.BKS(D)-*Lepr* ^{db} /J (*db/db*) mice and seven-week-old male wild-type (WT) C57BL/6 mice, all purchased from Shanghai Model Organisms Co., Ltd., and animal license number was SCXK-(HU)2017-0010. All animals were housed in a Specific Pathogen Free class animal house with 12 h of light per day at 20 ± 1°C and 50 ± 10% relative humidity. The animals were fed a normal water and diet. The study was approved by the Institutional Animal Care and Use Committee of the Beijing animal science Co., Ltd., and the animal ethics approval number was IACUC-2020102007.

All the animals were acclimatized under the above conditions for seven days. The WT mice were as the Control group (Con, n=15). The *db/db* mice were divided into 3 groups by random number grouping and divided into ACT group (ACT, 100 $mg \cdot kg^{-1} \cdot d^{-1}$, n=15) (Ran et al., 2023), Irbesartan group (Irb, 22.75 $mg \cdot kg^{-1} \cdot d^{-1}$, n=15) and administered by gavage. Since Irb has been reported that it is a good treatment drug for diabetes nephropathy[72,73], it was used as positive control in this experiment. The Con and Mod groups were given equal amounts of saline in a gavage volume of 10 $mL \cdot kg^{-1}$. The body weight of each mouse was weighed weekly.

The drug was administered for 8 weeks.

2.2.3 Sample collection and index determination

Fasting blood glucose measurement: Mice were fasted for 12 h, after disinfected, the tail tips were cut off and the blood glucose values were read using a glucometer. Oral glucose tolerance test: Mice were fasted for 12 h, and glucose was garaged at 2 $g \cdot kg^{-1}$ mouse body weight. Blood samples were collected from the tail tip capillaries of the mice and the blood glucose concentration values of the mice after glucose loading were determined by a glucometer.

Mice were relocated to the metabolic chamber and urine samples were collected over a 24 h period while the animals were allowed to drink freely. The 24 h urine specimens were centrifuged at 3,000 rpm for 10 min. Levels of 24 h urine microalbumin and urine creatinine were measured by immunoturbidimetric method using an automatic biochemical analyzer. The ratio of albumin to creatinine in urine was calculated.

After anesthesia with urethane, blood was taken from the heart and the kidney tissue was removed. After 1 h of placing, the supernatant of blood sample was collected by centrifugation at 3000 rpm for 15 min. The left kidney was fixed with 4% paraformaldehyde, dehydrated with ethanol, and then embedded with paraffin. HE, Masson, and periodic acid-Schiff (PAS) staining were performed. Histopathological changes of HE-stained sections were observed under the light microscope. Microscopic examination was focused on glomerular hypertrophy, basement membrane thickening, tubular degeneration, tubular pattern, necrosis, and inflammatory cell infiltration, etc. Semi-quantification of the degree of lesions from mild to severe, and graded score and total score were performed. Five orthotropic glomeruli were randomly selected under 40x objective lens in each PAS-stained section, and glomerular glycogen and glomerular area was measured separately. The glomerular glycogen and glomerular area were stained, and the ratio of glomerular glycogen/glomerular area was calculated and the mean value (Olympus DP71 analysis system) was taken to compare the differences between the groups. Masson-stained sections with blue-colored collagen fibers were scored semi-quantitatively according to the degree of collagen fiber proliferation within the renal tissues, and then the differences in collagen proliferation among the groups were compared. An independent researcher who maintained the confidentiality of the study protocol assessed the histomorphology of each kidney section.

2.2.4 Preparation of metabolomics samples

2.2.4.1 Urine samples preparation

Urine (100 μL) was vortexed with 400 μL of methanol (3 min). The mixture was centrifuged (10000 rpm, 4 ℃) for 20 min. The supernatant was taken for untargeted metabolomics.

2.2.4.2 Serum samples preparation

Serum (50 μL) was mixed with 150 μL methanol: acetonitrile (1:1) by vortex (3 min). After centrifugation (10000 rpm, 20 min), the supernatant was taken for untargeted metabolomics.

2.2.4.3 Kidney tissue samples preparation

Kidney tissues were homogenized 2 times for 2 min with 70% methanol. The homogenate was vortexed for 30 s following to the centrifugation at 12000 rpm for 15 min at 4 ℃. The subsequent supernatant (200 μL) was evaporated and redissolved with 120 μL acetonitrile: water (2:3) for targeted metabolomics.

2.2.4.4 Quality control (QC) sample preparation

To verify the validity of the analytical method, urine, serum, and kidney QC samples were prepared respectively. An aliquot (10 μL) of QC sample extracted from the serum, urine, and kidney samples, separately. QC was inserted after every five samples in the analysis queue.

2.2.5 UHPLC-LTQ-Orbitrap MS-based untargeted metabolomics analysis

The online Dionex Ultimate 3000 UHPLC system (Thermo Fisher Scientific, USA) and LTQ Orbitrap Velos Pro (Thermo Fisher Scientific, USA) were combined via an ESI interface. Samples were separated on a Waters UHPLC HSS T3 column (2.1 mm × 100 mm, 1.8 μm). The mobile phases were water containing 0.1% formic acid (A) and acetonitrile (B). The flow rate was set at 0.3 mL/min with a gradient elution starting with 2% (B) and the following chromatographic conditions were set: 0-3 min maintain 2% (B), 3-8 min maintain to 66% (B), 8-17 min linear gradient to 98% (B), 17-20 min maintain 98% (B), 20-20.1 min linear gradient to 2% (B), 20.1-22 min maintain 2% (B). The column temperature was maintained at 35 ℃.

The injection volume was 8 μL. The analysis was carried out in positive and negative ion modes. The mass resolution of the Fourier transform was 30000 with a full scan in the range of *m/z* 50-1500.

2.2.6 UHPLC-QQQ-MS/MS-based targeted metabolomics analysis

Exion LC-20AC coupled with an AB SCIEX QTRAP® 6500+ (Redwood City, CA, USA) mass spectrometer was used for quantitative analysis. Samples were separated on a Waters ACQUITY UHPLC®HSS PFP column (2.1 mm × 100 mm, 1.8 μm). The mobile phases were water containing 0.1% formic acid (A) and acetonitrile (B). The flow rate was set at 0.3 mL/min with a gradient elution starting with 2% (B) and the following chromatographic conditions were set: 0-4 min maintain 2% (B), 4-6 min linear gradient to 98% (B), 6-10 min maintain 98% (B), 10-10.1 min linear gradient to 2% (B), 10.1-14 min maintain 2% (B). Multiple reaction monitoring (MRM) detection mode was operated. The analysis was carried out in positive and negative ion modes. Parameters for MS and MS/MS analysis, including declustering potential (DP) and collision energy (CE), were optimized (**listed in Table 2-1**).

Table 2-1 The conditions of the MS detection of metabolites based targeted metabolomics analysis

Metabolites	Ion mode	Q1(*m/z*)	Q3(*m/z*)	DP(V)	CE(V)
Cysteine	ESI^+	122	59	40	30.4
Alanine	ESI^+	89.8	44.2	47	17.4
Hypoxanthine	ESI^+	137	119.1	50	28.7
Choline	ESI^+	104	60.1	50	30
Dopamine	ESI^+	154	137	30	15.3
Glycine	ESI^+	76	30.1	40	16.8
Homovanillic acid	ESI^+	183	137.2	40	16
Glutamate	ESI^+	148	84	50	23.7
Citrulline	ESI^+	176	159.2	35	13.6
Glutamine	ESI^+	147	84	40	22.9
Methionine	ESI^+	150	56	40	21.3

Arginine	ESI^+	175.1	70	30	27.1
Lysine	ESI^+	130	84.1	36	22.6
Tyrosine	ESI^+	182	136.1	40	18.7
leucine	ESI^+	132	86.2	25	14.6
Ornithine	ESI^+	133	70.1	30	24
Adrenaline	ESI^+	184.1	166.2	40	14.8
Serine	ESI^+	106	60.1	40	14.7
Threonine	ESI^+	120.1	74	33	20
Aspartic acid	ESI^+	134	74.1	35	19.9
Asparagine	ESI^+	132.9	74	36	21.9
Adenosine	ESI^+	268.1	136.2	30	26.84
γ-Aminobutyric acid	ESI^+	104	87.1	40	14.3
Acetylcholine	ESI^+	146	87.1	40	19.7
Histamine	ESI^+	112	95	30	20
Levodopa	ESI^+	198.2	152.2	45	19.1
Norepinephrine	ESI^+	170	152.1	40	15
Taurine	ESI^+	126	108	50	15
Proline	ESI^+	116	69.9	40	15
Uridine	ESI^+	244.9	113	40	20
Phenylalanine	ESI^+	166.1	120.1	20	19.6
Histidine	ESI^+	156.1	110	30	14.6
urea	ESI^+	61	44	40	24.22
IS-Tryptophan-d5	ESI^+	210	192	13	15.63
Tryptamine	ESI^+	161.1	144	17	16.8
Picolinic acid	ESI^+	124.1	106.1	20	13.42
S-adenosyl homocysteine	ESI^+	385	136	39	23
Kynurenine	ESI^+	209.1	146.2	20	28
5-Hydroxy-tryptophan	ESI^+	221.1	204.2	20	14.8

Serotonin	ESI^+	177.2	160	20	18
L-3-hydroxykynurenine	ESI^+	225	208	10	12.97
Tryptophan	ESI^+	205	188	20	14.12
Indole-3-acetic acid	ESI^+	176	130	20	23.95
Nicotinic acid	ESI^+	124	80	70	27.93
Quinolinic acid	ESI^-	165.9	121.9	-20	-13.88
Kynurenic acid	ESI^-	188	144	-20	-20
Xanthurenic acid	ESI^-	204	160	-20	-20.38
3-OH-anthranilic acid	ESI^-	152	108	-20	-19
ATP	ESI^-	506.1	158.9	-70	-36
ADP	ESI^-	426	159	-45	-34
NAD	ESI^-	662	540	-30	-24
Fumaric acid	ESI^-	115.1	71	-15	-11.14
Aconitic acid	ESI^-	173	85	-14	-17.3
Citric acid	ESI^-	190.9	111.1	-23	-18.21
Malic acid	ESI^-	132.9	115	-30	-15.9
Pyruvic acid	ESI^-	87.2	32	-21	-11.99
Oxoglutaric acid	ESI^-	145.2	101.1	-13	-11.81
Lactic acid	ESI^-	89.1	42.9	-26	-14.21
Succinic acid	ESI^-	117.1	72.8	-27	-16
Glucose	ESI^-	179	135.1	-70	-17.4
AMP	ESI^-	346.2	79	-82	-78.9
NADH	ESI^-	664	346.1	-100	-46.5
IS-puerarin	ESI^-	415	295	-140	-30

2.2.7 Untargeted metabolomics data processing

All the LC-MS data were processed by the Compound Discoverer 3.3 software, providing compound formula, retention time, *m/z*, area, and normalized peak area. QC samples were used

for monitoring the stability and repeatability of the whole liquid quality system. Principal component analysis (PCA) and orthogonal partial least squares discriminant analysis (OPLS-DA) were performed. The *t*-test ($P < 0.05$) and fold change (FC) values (FC > 1.5 or < 0.7) were used as indicators to screen for potential biomarkers with significant differences based on the criteria of variable importance in projection (VIP) values (VIP >1) in predictions obtained from the OPLS-DA model. MetaboAnalyst 5.0 (http://www.metaboanalyst.ca/) was used to analyze the relative metabolic pathways. In all cases, *P* value < 0.05 was statistically significant.

2.2.8 Network pharmacology analysis

The targets of ACT were obtained from Pharmmapper[74] and Swiss Target Prediction databases[75-76]. The related DN targets were searched by using "Diabetic Nephropathy" as a key word from TTD, OMIM, GeneCards, and DrugBank databases[77-79]. The targets were imported to Uniprot database to standardize and remove duplicates. The Venn diagram was obtained from Omicshare website (https://www.omicshare.com/). A protein-protein interaction (PPI) network was constructed by STRING 11.0 database[80]. Enrichment analysis such as Gene ontology (GO) and Kyoto encyclopedia of genes and genomes (KEGG) were established by the Metascape database[81]. According to the "component-target" and the "target-pathway" relationships, the Cytoscape 3.7.2 software was used to generate the "component-target-pathway" network and the network topology parameters.

2.2.9 Statistical analysis

Data were shown as mean ± standard error of the mean (SEM), and SPSS (version 25) was used to analyze the data. When comparing two groups of samples, a *t*-test was used if the distribution was normal and the variances were equal, otherwise a non-parametric rank sum test was used. For comparisons between multiple groups, if the distribution was normal and the chi-square test was satisfied, the SNK test was used after a one-way ANOVA with differences, and the Tamhenian T2 (M) test was used when the variance was not equal. Significant differences were indicated when $P < 0.05$ and trends were indicated when $P < 0.1$. Graphs were made using GraphPad Prism (version 9.5). The graded data were statistically analyzed using a non-parametric rank sum test, with $P < 0.05$ as the test for significance of difference.

2.3 Results

2.3.1 General conditions of mice

The mice in the Con group were in good general condition and agile. In the Mod group, the mice were depressed, the activity was reduced, and the flexibility was weakened. The above conditions of mice in each treatment group were improved. The mice weight gain values in the Mod group were significantly higher than those in the Con group ($P < 0.001$). The body weight gain values of mice in the ACT group were significantly smaller than the Mod group ($P < 0.05$) after 8 weeks of irbesartan and ACT administration (**Figure 2-1A)**. The amount of water consumption in the Mod group was significantly higher than that in the Con group ($P < 0.05$). After irbesartan and ACT administration, there was no significant difference in water consumption between the Mod group and each group (**Figure 2-1B)**. The results of glucose tolerance showed that there was a significant difference between the Mod group and the Con group ($P < 0.05$), but no significant difference between the Mod group and the other groups. In addition, the results of glucose tolerance in each group of mice showed significant differences ($P<0.05$) between the Mod group and the Con group, and there was no significant difference between the ACT treatment group and the Mod group, and there was no statistically significant difference before and after self comparison (Table 2-2).

Table 2-2 The results of the area under the curve (AUC) under the glucose tolerance of mice in each group before and after administration (Mean ± SEM)

Group	n	0W	4W	8W
Con	9	1316.5 ± 43.92	1372.83 ± 45.69	1260.67 ± 38.73
Mod	7	3022.5 ± 184.56$^{###}$	3406.5 ± 132.82$^{###}$	3603.86 ± 123.69$^{###}$
ACT	6	3020.5 ± 304.92	3443.5 ± 272.44	3234.75 ±355.18

2.3.2 Therapeutic effect of ACT on DN mice

The results of urine biochemical indexes showed that the 24 h urinary microalbumin (total mALB) and urinary microalbumin/creatinine ratio (UmACR) were significantly higher in the Mod group than in the Con group ($P < 0.05$). In the Irb and ACT groups, the level of UmACR was lower than that in the Mod group (**Figure 2-1C)**.

As shown in **Figure 2-1D**, HE staining results showed that there was no change in hypertrophy of the glomerulus, thickening of the capillary basement membrane, hyperplasia of the mesangial matrix, degeneration or necrosis of the tubular epithelium, and infiltration of inflammatory cells in the interstitium in the Con group. In the Mod group, the renal glomeruli were moderately hypertrophied, the glomerular cystic cavity was narrowed or even lacunar, the mesangial area was significantly widened, and the mesangial matrix was increased as shown by green arrows. Some of the renal tubules were structurally disorganized, while epithelial cells were hypertrophied and vacuolated as shown by yellow arrows (granular degeneration). Some animals had necrosis of individual cells in the tubules as shown by blue arrows. The inflammatory cell infiltration was visible in the interstitium, as shown by purple arrows, with a significant difference compared with the Con group ($P < 0.01$). In the Irb group, these lesions were slightly reduced compared to the Mod group. In the ACT group, the glomeruli were mildly hypertrophied, and the basement membrane and mesangial matrix were mildly hyperplastic as shown by the black and green arrows, respectively. The tubular epithelial cells were locally vacuolated as shown by the yellow arrow, whereas there was slight reduction of such cells as compared to the model group ($P < 0.1$).

As shown in **Figure 2-1E**, PAS-staining results showed that the glomeruli of the Con group were structurally intact and had no mesangial proliferation. In the Mod group, the glomeruli were widened, the mesangial matrix proliferated, the glomerular capillary lumen was narrowed, and the basement membrane was thickened. The PAS glycogen area ratio of the kidney was significantly increased ($P < 0.01$) in the Mod group rather than the Con group, whereas was significantly lower in the Irb and ACT groups ($P < 0.05$ and $P < 0.01$, respectively).

As shown in **Figure 2-1F**, Masson-staining results showed that the glomeruli and tubules in the Con group were structurally normal. In the Mod group, the collagen in the glomerular thylakoid region and renal tubulointerstitial tissues was more proliferative rather than in the Con group. The capillary basement membrane was thickened to varying degrees as shown by black arrows. The administration of Irb had a moderating effect on the collagen deposition in the interstitium of glomeruli and tubular interstitium of *db/db* mice. The ACT intervention was found to reduce collagen deposition in the glomeruli and tubular interstitium of *db/db* mice ($P < 0.05$).

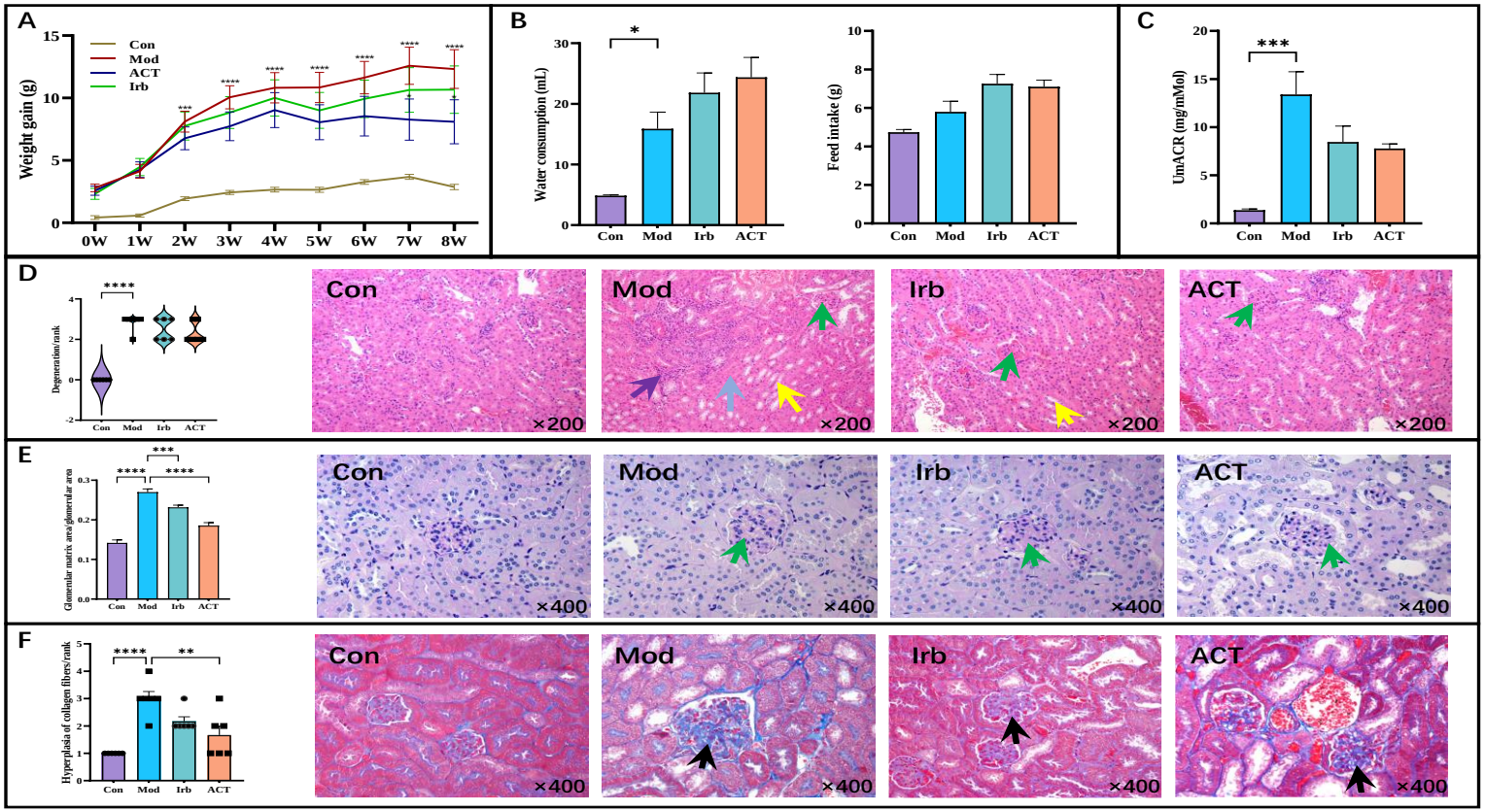

Figure 2-1 Therapeutic effect of ACT on DN mice

The glomerular glycogen and glomerular area was stained and the ratio of glomerular glycogen/glomerular area was calculated and the mean value (Olympus DP71 analysis system) was taken to compare the differences between the groups. Masson-stained sections with blue-colored collagen fibers were scored semi-quantitatively according to the degree of collagen fiber proliferation within the renal tissues, and then the differences in collagen proliferation among the groups were compared. (A) The weight gain of mice in different groups for 8 weeks. (B) Food intake and water consumption of mice in each group. (C) The urinary microalbumin/creatinine ratio (UmACR) of mice in each group. (D) HE staining of kidney tissues (×200). (E) PAS staining of kidney tissues (×400). (F) Masson staining of kidney tissues (×400). *$P < 0.05$, **$P < 0.01$, ***$P < 0.001$, ****$P < 0.0001$ (compared to Mod group).

2.3.3 Multivariate analysis of metabolic profiles

To further explore the potential mechanisms accounting for the protective effects of ACT against DN, the untargeted metabolomics was performed. To maximize the information load, fingerprints of serum, urine, and kidney samples were acquired in both negative and positive modes. 55, 328, and 196 metabolites were identified in serum, urine, and kidney samples, respectively, under the positive mode, while 52, 879, and 51 metabolites were under the negative mode.

PCA analysis exhibited a separation tendency of groups. Unsupervised PCA and the representative total ion chromatograms (TICs) showed that QC samples behaved stably during the process. Furthermore, the PCA score plots (**Figure 2-2A**) showed that the three groups were obviously separated from each other, for both the positive and negative ion modes. This indicated a significant change in metabolites in the different groups, consistent with the appearance of physiological indicators. The first principal component (PC1) explained 96.13%, 91.81%, 91.32%, and 93.41% of the characteristics of the original dataset under positive mode in serum, 4 weeks-urine, 8 weeks-urine, and kidney samples, respectively, while 98.83%, 94.93%, 92.93%, and 93.49% under negative mode.

The OPLS-DA model plots for the Con and Mod groups in positive and negative ion modes were clearly distinguishable (**Figures 2-3, 2-4, 2-5**). It was revealed that the endogenous substance metabolisms of *db/db* mice were obviously disrupted and could use the metabolic profiles to screen for biomarkers. Under positive mode, the parameters of R^2Y and Q^2 in OPLS-DA were 0.987 and 0.909 in serum samples, 0.99 and 0.938 in 4 weeks-urine samples, 0.996 and 0.959 in 8 weeks-urine samples, 0.996 and 0.915 in kidney samples, respectively, between Con and Mod group. Under positive mode, the parameters of R^2Y and Q^2 in OPLS-DA were 0.997 and 0.677 in serum samples, 0.989 and 0.156 in 4 weeks-urine samples, 0.99 and 0.515 in 8 weeks-urine samples, 0.98 and 0.842 in kidney samples, respectively, between Mod and ACT group. Under negative mode, the parameters of R^2Y and Q^2 in OPLS-DA were 0.99 and 0.759 in serum samples, 0.991 and 0.956 in 4 weeks-urine samples, 0.995 and 0.963 in 8 weeks-urine samples, 0.986 and 0.824 in kidney samples, respectively, between Con and Mod group. Under negative mode, the parameters of R^2Y and Q^2 in OPLS-DA were 0.993 and 0.553 in serum samples, 0.969 and 0.752 in 4 weeks-urine samples, 0.992 and 0.879 in 8 weeks-urine samples, 0.891 and 0.78 in kidney samples, respectively, between Mod and ACT group. In the positive mode, there was no significant difference in the urine samples between the ACT and

Mod groups at 4 weeks, while a significant difference at 8 weeks. These results indicated that the difference in the urine samples was more pronounced in the group that was administered for a longer period between the ACT and Mod groups.

2.3.4 Analysis of metabolic pathways

Based on VIP > 1, FC > 1.5 or < 0.7, and $p < 0.05$, the metabolites were filtered as differential metabolites. To explore the metabolic pathways of ACT in *db/db* mice, the differential metabolites were imported to MetaboAnalyst 5.0. As shown in **Figure 2-2B**, the pathways such as pyrimidine metabolism; aminoacyl-tRNA biosynthesis; alanine, aspartate, and glutamate metabolism; and glycine, serine and threonine metabolism were affected significantly in 4 weeks-urine samples between Con and Mod groups. As shown in **Figure 2-2C**, the pathways such as pyrimidine metabolism; alanine, aspartate, and glutamate metabolism; aminoacyl-tRNA biosynthesis; pantothenate and CoA biosynthesis; and β-alanine metabolism were affected significantly in 8 weeks-urine samples between Con and Mod groups. These results showed that pathways associated with amino acid metabolism were markedly changed after the ACT treatment. Ultimately, pathways affected in the urine were suggested to include alanine, aspartate and glutamate metabolism, and amino sugar and nucleotide sugar metabolism. Furthermore, pathways affected in the kidney were suggested to include purine metabolism, arginine biosynthesis, pantothenate and CoA biosynthesis, β-alanine metabolism, and lysine degradation (**Figure 2-2D**).

2.3.5 Network pharmacology analysis

As shown in **Figure 2-6A**, a total of 293 targets of ACT were extracted from Pharmmapper and Swiss Target Prediction databases. After selecting and eliminating the redundancy, **Figure 2 -6B** showed that 1748 targets for DN were obtained, in which there were 122 intersecting targets. In addition, **Figure 2-7** briefly illustrated the process of network pharmacological analysis, indicating that AGE-RAGE signaling pathway in diabetic complications, Fox O signaling pathway, endocrine resistance, MAPK signaling pathway, insulin resistance, PI3K-Akt signaling pathway, and IL-17 signaling pathway were involved in the KEGG pathway (**Figures 2-6C and D)**.

There were 143 nodes (122 targets and 20 pathways and ACT) and 477 edges. The "component-target-pathway" network was shown in **Figure 2-7**. In this network, the targets

such as AKT2, AKT1, MAPK1, HRAS, MAPK10, EGFR, MAPK8, MAPK14, IGF1R, and SRC were located at the central network. This result suggested that ACT may act synergistically on these targets to have pharmacological effects. Furthermore, carbohydrate, lipid, and amino acid metabolism, which mainly affected endocrine and immune system, were found to be highly relevant pathways along with signaling transduction pathways.

2.3.6 Compound-reaction-enzyme-gene network construction

To obtain a comprehensive view of the therapeutic effect of ACT on *db/db* mice, an interaction network was constructed based on metabolomics and network pharmacology in **Figure 2-8**. By matching the potential genes and the differential endogenous metabolites in Medscape, key targets such as AKT2, AKT1, MAPK1, HRAS, MAPK10, EGFR, MAPK8, MAPK14, IGF1R, and SRC were selected. The related key metabolites were adenine, leucine, uracil, adenosine monophosphate, arginine and so on. In addition, urea cycle and metabolisms of arginine, proline, glutamate, aspartate, asparagine, tyrosine, tryptophan, pyrimidine, phosphatidylinositol phosphate, purine, lysine, glycine, serine, alanine, and threonine were affected by such signal pathways.

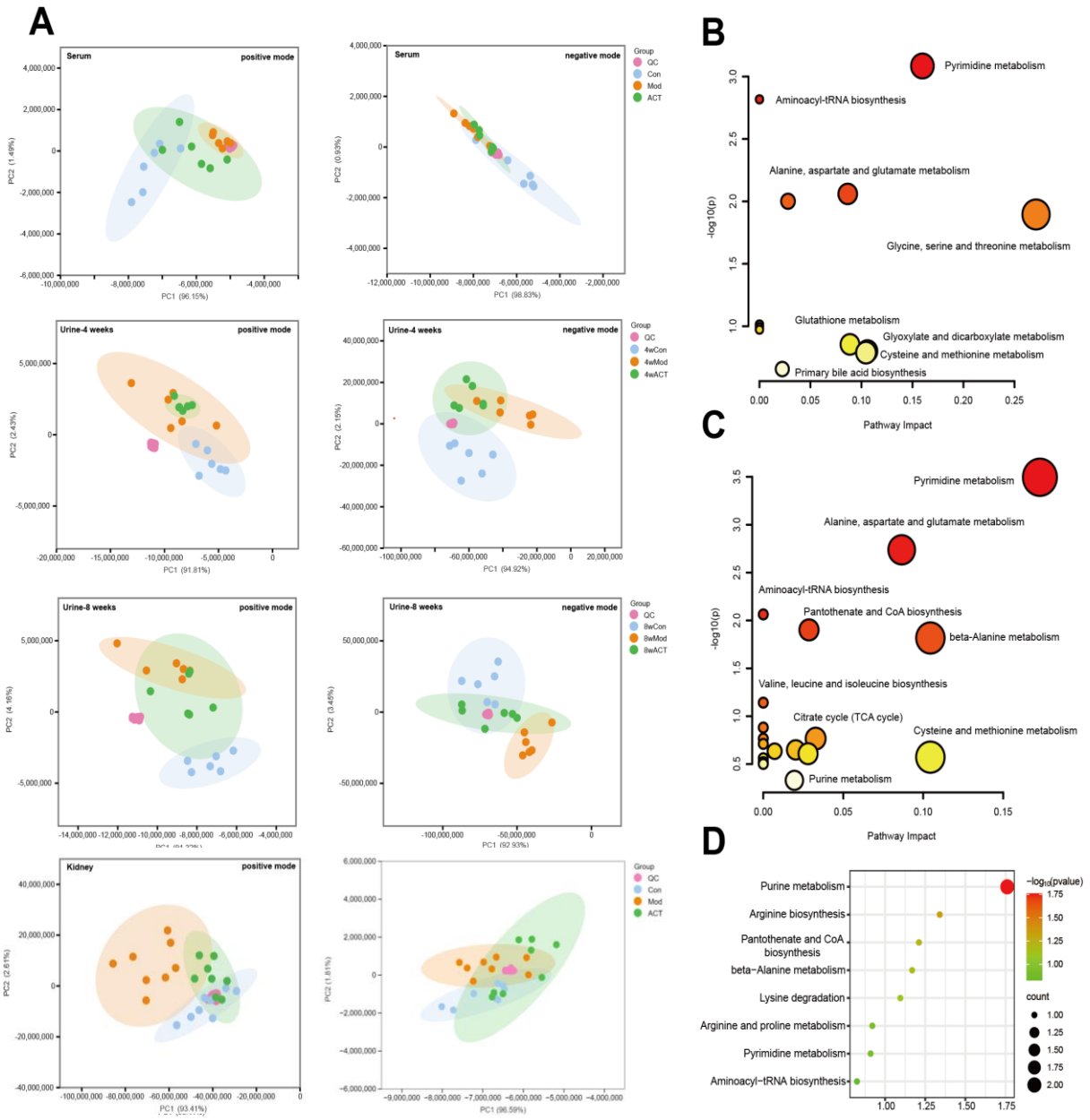

Figure 2-2 Differential metabolite analysis

A total of 293 targets of ACT were extracted from Pharmmapper and Swiss Target Prediction databases. After selecting and eliminating the redundancy. (A) PCA of Con, Mod, ACT group serum, 4 weeks-urine, 8 weeks-urine, and kidney samples in positive and negative mode. (B) Metabolic pathways of significant metabolites in 4 weeks-urine samples between Con and Mod group as visualized using MetaboAnalyst. (C) Metabolic pathways of significant metabolites in 8 weeks-urine samples between Con and Mod group as visualized using MetaboAnalyst. (D) The metabolic pathways of significant metabolites in kidney samples among Con, Mod and ACT group.

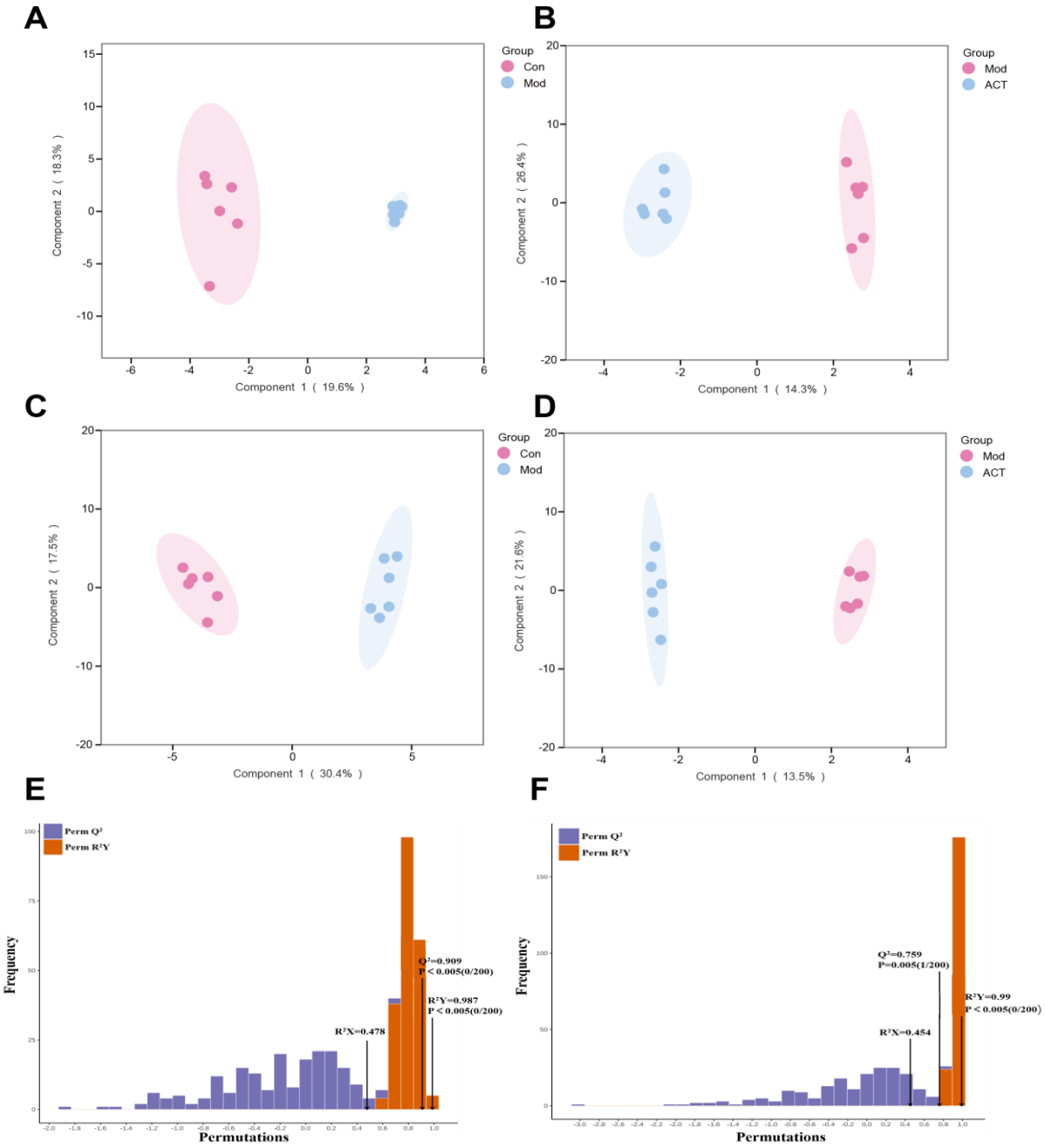

Figure 2-3. Multivariate statistical analysis of Con, Mod, and ACT group in serum samples

(A) Orthogonal projections to latent structures discriminant analysis (OPLS-DA) scores scatter plot between Con and Mod groups in positive mode. (B) OPLS-DA scores scatter plot between Con and Mod groups in negative mode. (C) OPLS-DA scores scatter plot between Mod and ACT groups in positive mode. (D) OPLS-DA scores scatter plot between Mod and ACT groups in negative mode. (E) Results of OPLS-DA permutation test between Con and Mod groups in positive mode. (F) Results of OPLS-DA permutation test between Con and Mod groups in negative mode.

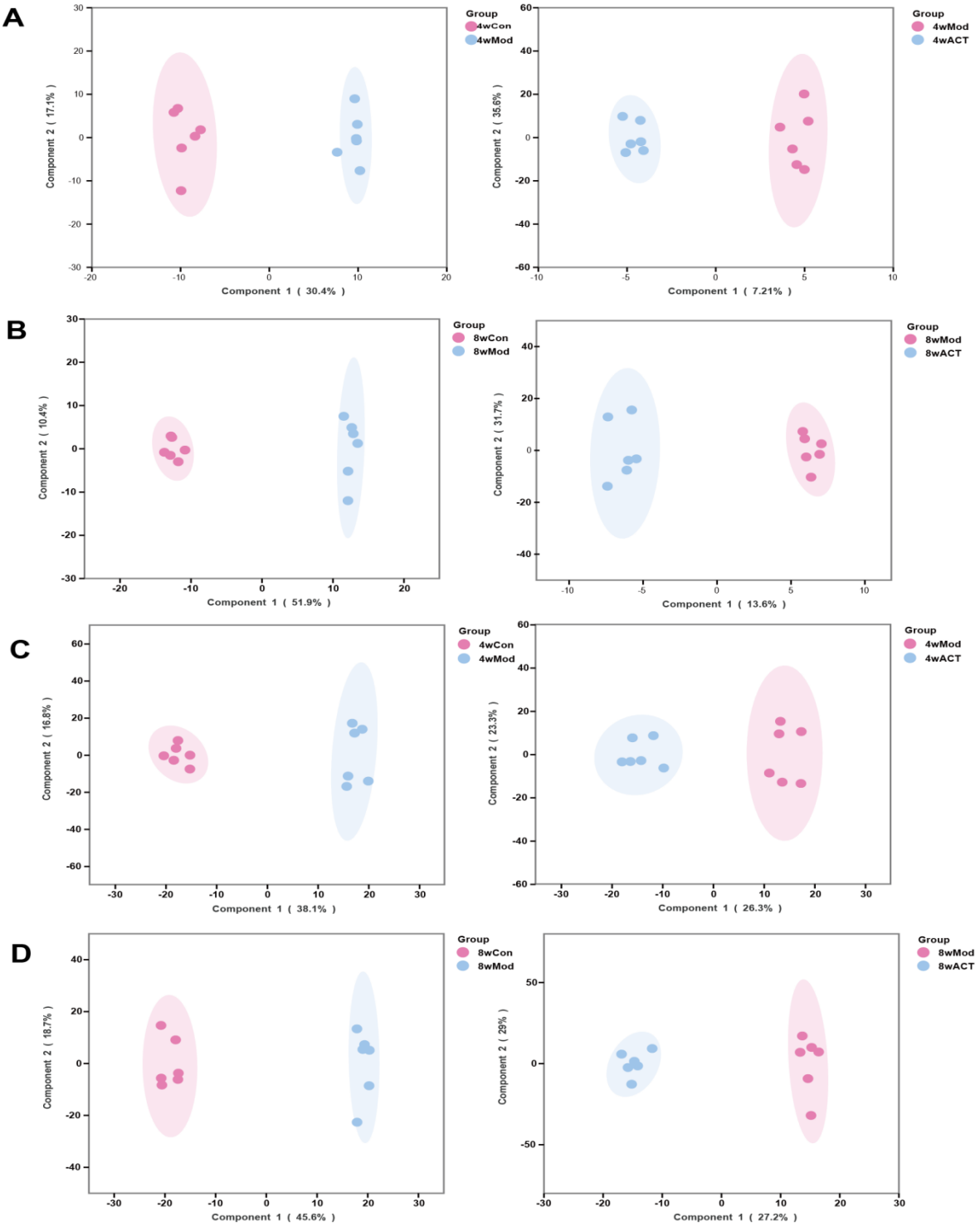

Figure 2-4. Multivariate statistical analysis of Con, Mod, and ACT group in 4 and 8 weeks-urine samples

(A) OPLS-DA scores scatter plot of 4 weeks-urine samples in positive mode. (B) OPLS-DA scores scatter plot of 8 weeks-urine samples in positive mode. (C) OPLS-DA scores scatter plot of 4 weeks-urine samples in negative mode. (D) OPLS-DA scores scatter plot of 8 weeks-urine samples in negative mode.

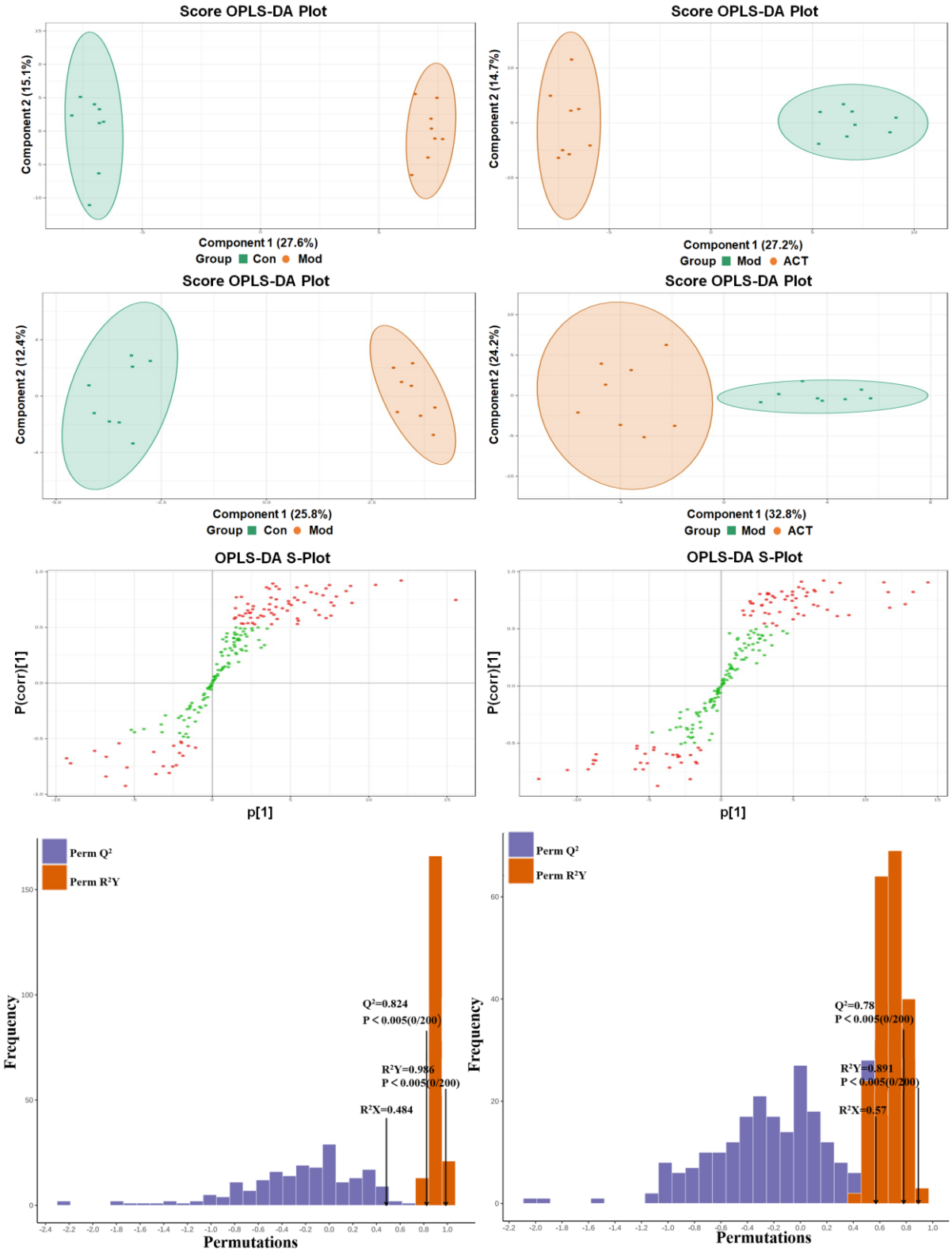

Figure 2-5. Multivariate statistical analysis of Con, Mod, and ACT group in kidney samples

(A) OPLS-DA scores scatter plot between Con and Mod groups in positive mode. (B) OPLS-DA scores scatter plot between Mod and ACT groups in positive mode. (C) OPLS-DA scores scatter plot between Con and Mod groups in negative mode. (D) OPLS-DA scores scatter plot between Mod and ACT groups in negative mode. (E) S-plot analysis of OPLS-DA between Con and Mod groups in positive mode. (F) S-plot analysis of OPLS-DA between Mod and ACT groups in positive mode. (G) Results of OPLS-DA permutation test between Con and Mod groups in negative mode. (H) Results of OPLS-DA permutation test between Mod and ACT in negative mode.

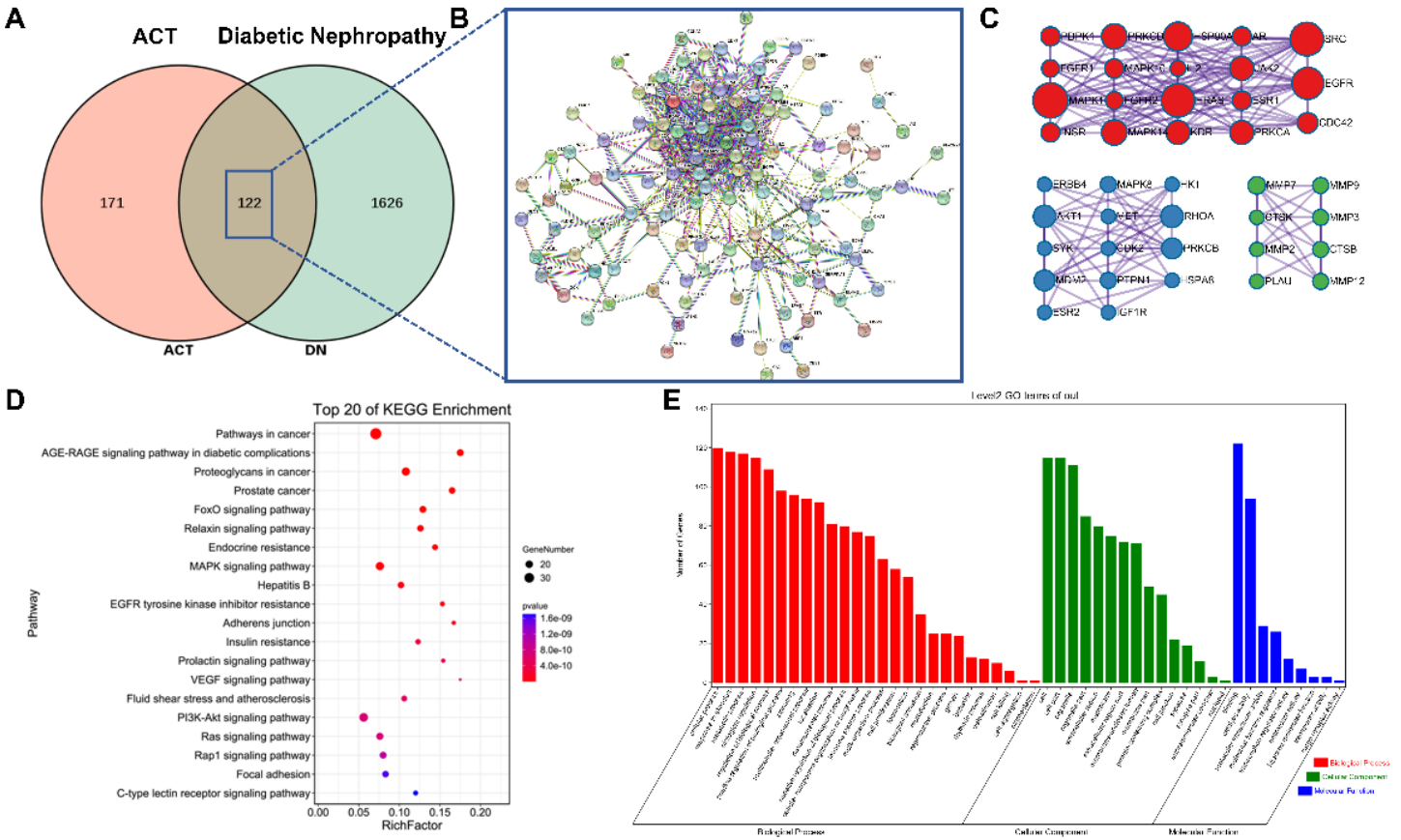

Figure 2-6 Screening and enrichment analysis of ACT-DN targets

That 1748 targets for DN were obtained, in which there were 122 intersecting targets. The targets of ACT were obtained from Pharmmapper[74] and Swiss Target Prediction databases[75-76]. Enrichment analysis such as Gene ontology (GO) and Kyoto encyclopedia of genes and genomes (KEGG) were established by the Metascape database. According to the “component-target” and the “target-pathway” relationships, the Cytoscape 3.7.2 software was used to generate the "component-target-pathway" network and the network topology parameters.(A) 122 overlapping gene symbols between DN and ACT. (B) PPI network analysis. (C) Modules in PPI network. (D) Top 20 pathways of KEGG enrichment analysis. (E) GO enrichment analysis.

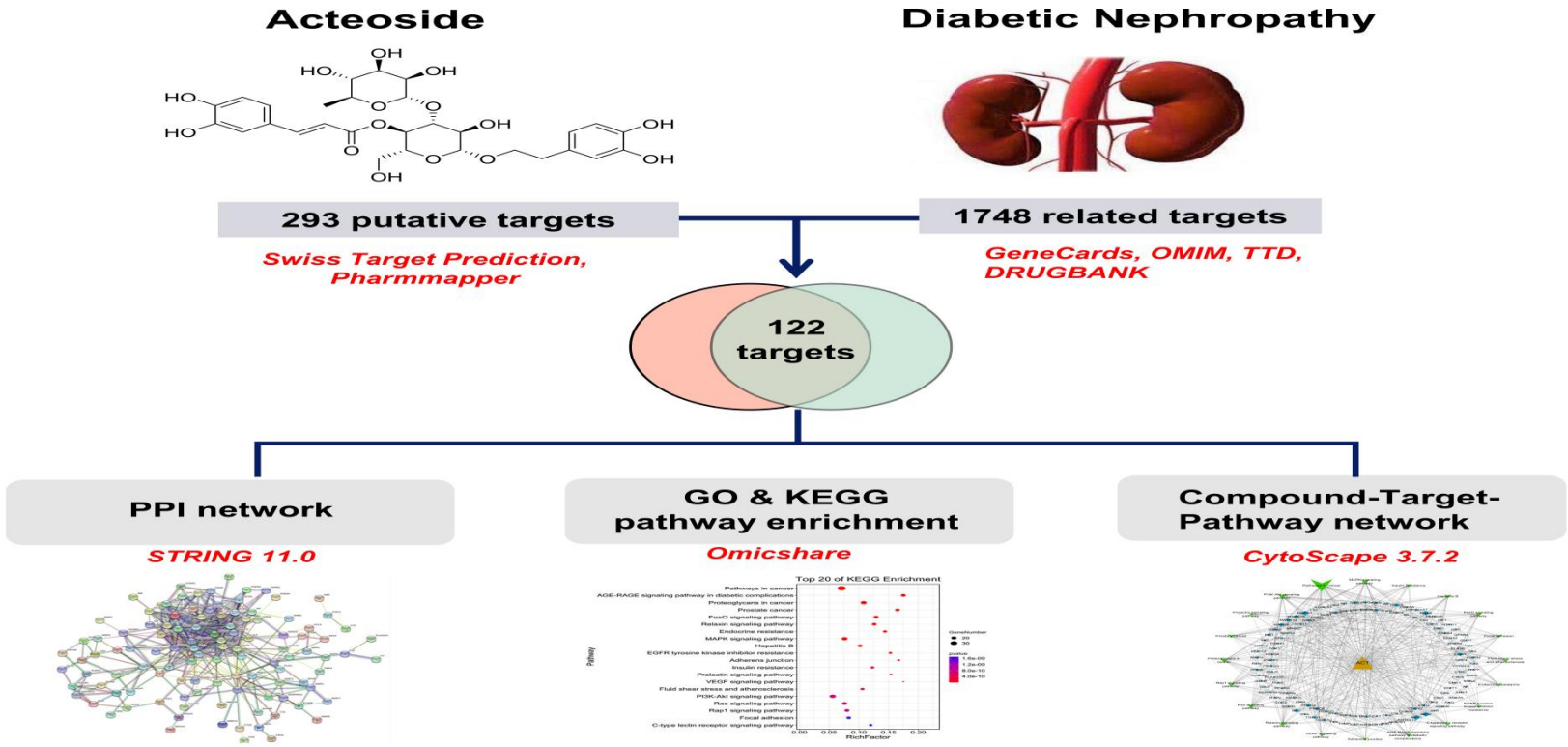

Figure 2-7 The process of network pharmacological analysis

The process of network pharmacological analysis typically involves several key steps. First, the analysis targets are determined, which may include specific compounds or targets. Next, a database search is conducted using the analysis targets as keywords. This involves searching public databases. After collecting the necessary information, a compound-protein interaction network is constructed. This network model integrates the collected data to reflect the interactions between compounds and proteins. Subsequently, network analysis is performed on the established compound-protein network. The aim is to reveal the interaction patterns and pharmacological mechanisms between compounds and targets.

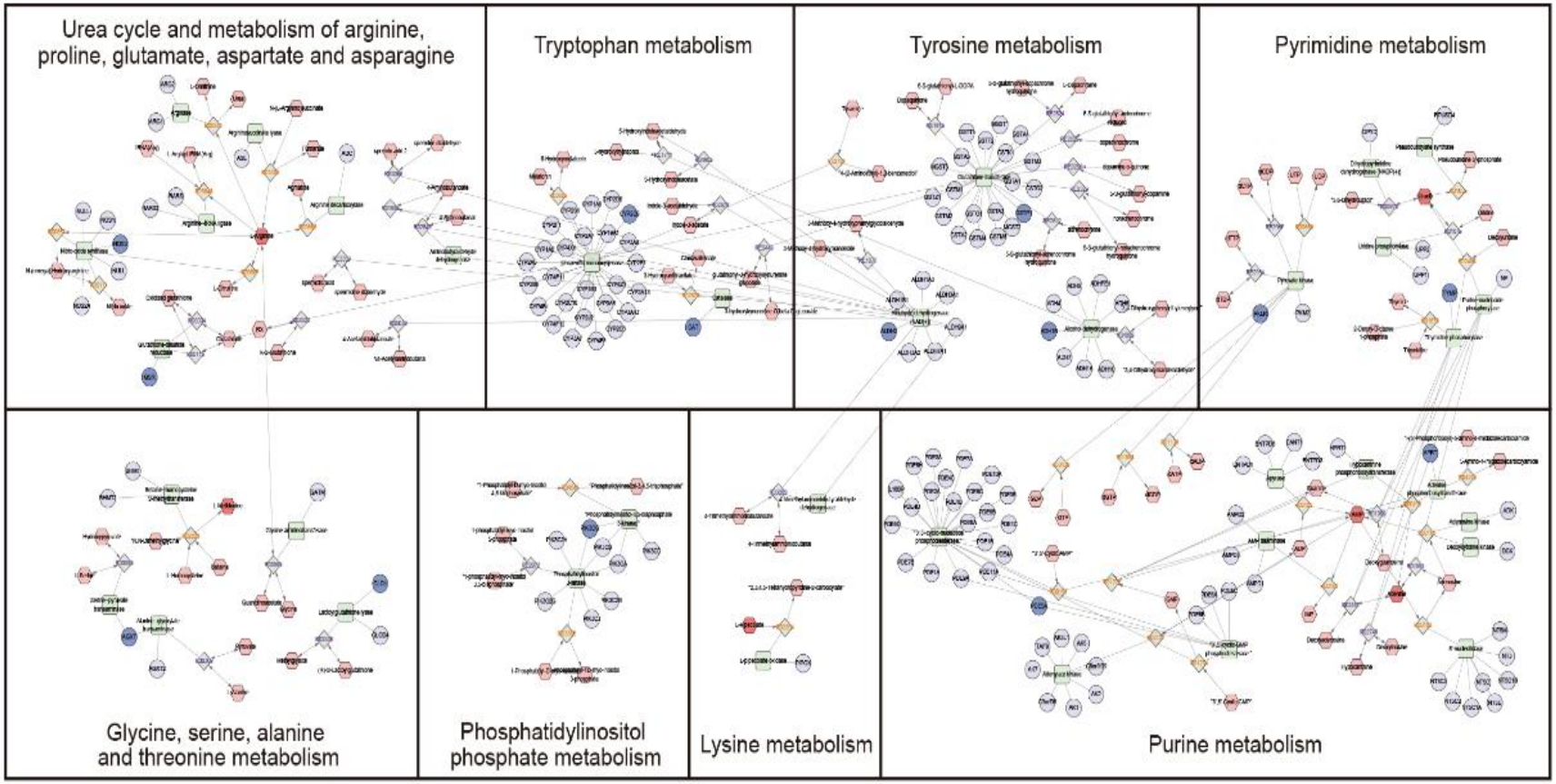

Figure 2-8 The compound-reaction-enzyme-gene networks of the key metabolites and targets

The red hexagons, grey diamonds, green round rectangle, and purple circles represent the active compounds, reactions, proteins and genes, respectively. The key metabolites, proteins and genes were magnified. The pathways with a blue background are significantly regulated in the cortex. The pathways with a red background are significantly regulated in both the cortex and hippocampus. (For interpretation of the references to color in this figure legend, the reader is referred to the web version of this article.)

2.3.7 The result of targeted metabolomics analysis

For the pathways enriched by untargeted metabolomics, targeted metabolomics by UHPLC-QQQ-MS/MS was performed in kidney samples for validation. Tissue samples offer advantages in determining organ-specific metabolic fingerprints compared to biological fluids that represent the average metabolic state of the whole organism. As shown in **Figure 2-9**, ACT significantly call backed the kidney levels of metabolites such as threonine, proline, phenylalanine, histidine, serine, arginine, asparagine, urea, kynurenic acid, tryptophan, glutamine, cysteine, leucine, AMP, and NAD^+. In addition, ACT was found to significantly reduce the levels of uridine, 5-hydroxyindole-3-acetic acid, methionine, choline, and oxoglutaric acid, while increased the levels of succinic acid and lactic acid. Furthermore, the results of targeted metabolomics in the kidney were consistent with those of serum detection.

To assess the discriminatory efficacy of the metabolite markers, further receiver operating characteristic (ROC) curve analysis was performed in the validation group. **Figure 2-10** showed that 15 metabolite markers including NAD^+, AMP, urea, kynurenic acid, tryptophan, glutamine, cysteine, leucine, threonine, proline, phenylalanine, histidine, serine, arginine, and asparagine exhibited excellent diagnostic abilities with differences between the Con group and the Mod group. In addition, those markers in kidney were found to have a high sensitivity and specificity with the area under the curve (AUC) of 0.711 or larger. Therefore, it was suggested that such markers were suitable for detecting the kidney damage in DN. Specifically, serine and asparagine exhibited the distinguished ability in the kidney. And in our study, the level of tryptophan was increased significantly in kidney samples and ACT could significantly revert the level of tryptophan and thus play a therapeutic role in DN (**Figure2-11**).

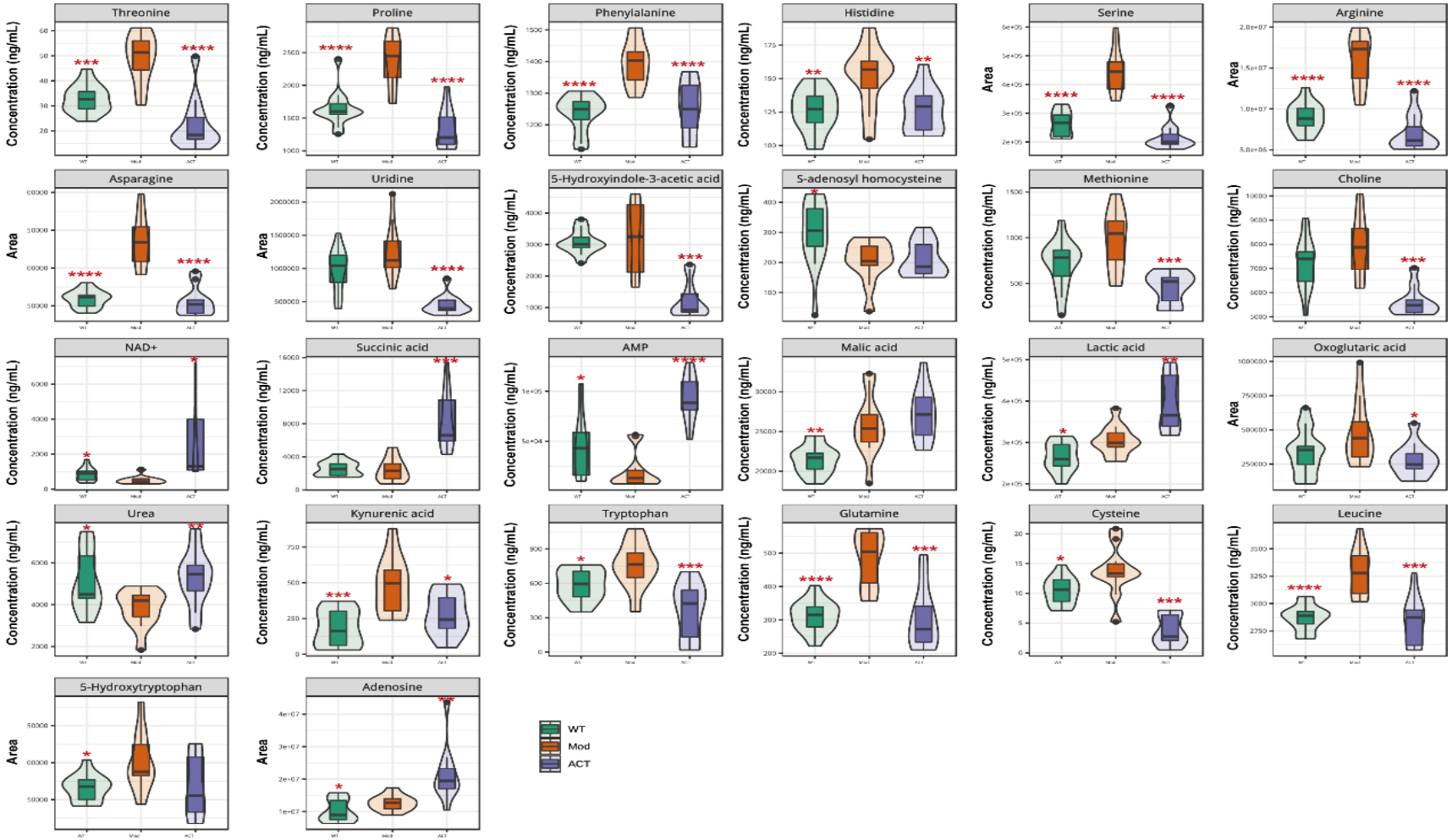

Figure 2-9 Targeted metabolomic analysis in kidney samples

The green represents the WT group, orange represents the MOD group, and purple represents the ACT administration group. **P* < 0.05, ***P* < 0.01, ****P* < 0.001, *****P* < 0.0001 (compared to Mod group).

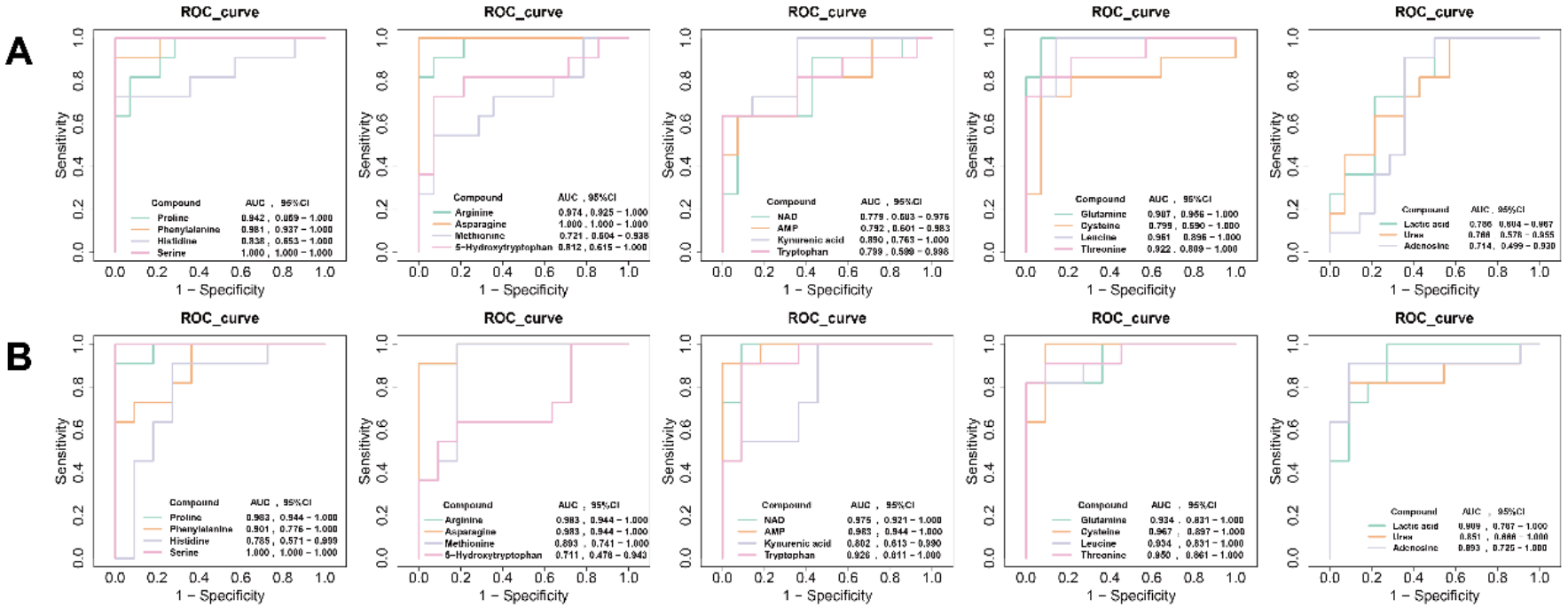

Figure 2-10 Receiver operating characteristic (ROC) curves of metabolites based on targeted metabolomic analysis

This figure demonstrates the ROC curve (Receiver Operating Characteristic Curve) of the model. The ROC curve evaluates the classification performance of the model by depicting the relationship between the True Positive Rate (TPR, also known as sensitivity) and the False Positive Rate (FPR, also known as 1 minus specificity). The horizontal axis (X-axis): False Positive Rate (FPR), representing the proportion of negative samples that are wrongly predicted as positive. The value range is usually from 0 to 1, increasing from left to right. The vertical axis (Y-axis): True Positive Rate (TPR), also known as sensitivity, representing the proportion of positive samples that are correctly predicted as positive. The value range is usually from 0 to 1, increasing from bottom to top. Curve: ROC curve. Ideally, the curve should be close to the top left corner, indicating that the model maintains a low FPR while achieving a high TPR. The diagonal line represents the performance of random guessing. (A) ROC curves of metabolites between Con and Mod groups in kidney samples. (B) ROC curves of metabolites between Mod and ACT group in kidney samples.

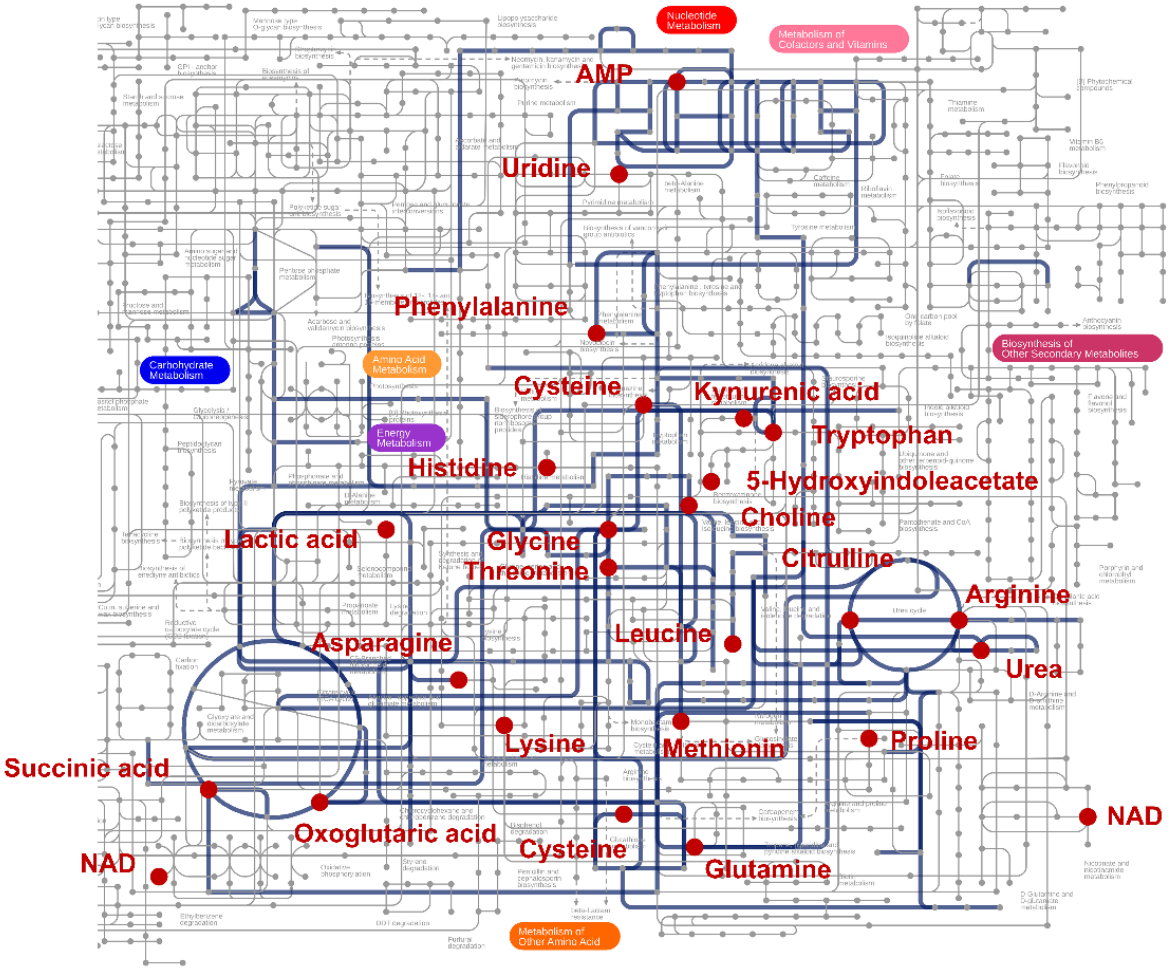

Figure 2-11 Relationship map of differential metabolites

The red dots are metabolites identified from biological samples treated with ACT for DN, which are enriched in the blue metabolic pathway, which mainly involves amino acid metabolism and sugar metabolism.

2.4 Discussion

DN is one of the major complications of DM, which is a major cause of end-stage renal disease[82]. The main cause of DN is a damage to glomerular microvascular structure and function in a chronic high-glucose environment, which is generally considered to be the result of environmental and genetic factors[83]. Metabolic dysregulation has been reported to become an important marker in the pathogenesis[84].

Amino acids are well known to exist in a wide range of organisms and play as active signaling molecules that regulate metabolism such as glycolysis and the tricarboxylic acid cycle, protein synthesis, and the synthesis of nucleic acids and lipids in maintaining homeostasis[85]. Dysregulation of amino acid metabolism is also a pathogenic risk factor for type 2 diabetes (T2D)[86]. Branched-chain amino acids (BCAA) such as valine, leucine and isoleucine are essential amino acids with protein-synthetic properties. Recently, it has been reported that there is a surge in research into the role of BCAA in promoting insulin secretion and predicting DN[87]. In addition, a dietary supplementation of leucine into mice has been reported to reduce insulin resistance, liver steatosis, and early DN development[88]. Furthermore, it has been reported that BCAA responsiveness is elevated in the early stages of type 2 diabetes mellitus (T2DM) to counteract high glucose toxicity, while the progression of DN is further exacerbated by a deficiency of BCAA[89].

On the other hand, it has been reported that levels of BCAA and aromatic amino acids are higher in pre-diabetic and diabetic patients than in normal ones, by a mechanism which circulating amino acids may regulate insulin functions[90-91]. In addition, the plasma levels of aromatic amino acids have been reported to be influenced by renal conditions, because the kidney plays an important role in amino acid synthesis, degradation, conversion, and renal tubular reabsorption[92]. Taken together with that tyrosine and phenylalanine have been shown to play a key role in a predicting risk of future diabetes[92], not only BCAA but also aromatic amino acids seem to become a risk predictor of DM. In this regard, it has been reported that insulin resistance and a T2DM phenotype are induced in mice fed with a diet supplemented with phenylalanine[93]. Thus, these reports strongly support our findings that the level of leucine and phenylalanine are increased in kidney from DN mice treated with ACT. Therefore, the augmentation of BCAA and aromatic amino acids production is likely to contribute to the therapeutic action of ACT in DN.

Ornithine is converted to citrulline, which in turn reacts with aspartic acid to produce

arginine and urea in a urea cycle[94]. It has been reported that plasma citrulline level is associated with DN risk, whereas there is no significant correlation among arginine, ornithine, their ratios and DN risk[95]. However, Abdelsattar *et al*.[96] have shown that the levels of arginine, citrulline, and ornithine in the blood are significantly increased in the early stages of DN, under which the level of arginine is predominant. Similar observations were obtained in this study, and I demonstrated for the first time that ACT significantly reduced the level of arginine in the kidney. Thus, it is suggested that ACT improves the function of urea cycle for its therapeutic effect on DN.

An essential amino acid, tryptophan plays a vital role in human health and disease and is mainly catabolized through a kynurenine pathway to produce kynurenic acid, xanthurenic acid, and quinolinic acid[97]. This metabolic pathway has been reported to be involved in the regulation of immune activation and inflammation linked to obesity and insulin resistance[98]. A case-cohort study has shown that tryptophan levels is initially increase and then deplete as diabetes progresses in severity, suggesting that tryptophan is associated with a higher risk of incident T2D [99]. In this study, the level of tryptophan was increased significantly in kidney samples, and ACT decreased its level. Thus, it is suggested that ACT improves the metabolism of tryptophan in a kynurenine pathway for its therapeutic effect on DN.

The high ratio of asparagine to aspartate has been reported to be associated with an elevated risk of T2D[100]. However, other studies[101] have shown that asparagine is associated with a lower risk of diabetes. In our study, the level of asparagine in *db/db* mice was higher than in normal mice. Taken together with a previous paper that microbial metabolites of imidazole propionate from histidine contribute to the pathogenesis of T2DM[102], ACT is likely to revert the level of histidine in kidney samples. As the relationship between asparagine levels and diabetes is still clinically controversial, further research is needed to address the pattern of changes in asparagine in diabetic patients.

It has been reported that the levels of AMP and GMP are significantly decreased in the extrarenal medulla and increased in the renal cortex, whereas those of ADP and ATP are increased in the renal cortex and outer medulla in the kidneys of high-fat diet-fed and streptozotocin (STZ)-treated DN rats[103]. Therefore, the metabolism of amino acids may play an important role in renal metabolism with not only the basic energy source but also the basal metabolism of the kidney. In our study, the level of AMP in the kidney of the Mod group was significantly reduced, of which condition was improved after the medication, suggesting the

improvement of renal hyperfunction. Thus, these findings allow me to speculate that ACT recovers amino acid metabolism disturbed in DN. Further experiments need to clarify this hypothesis.

2.5 Conclusions

In this Chapter, my findings strongly suggested that ACT delays the progression of DN and improves the degree of histopathological damage to the kidney, which is closely related to the metabolic pathway of amino acid such as tryptophan, glutamine, cysteine, leucine, threonine, proline, phenylalanine, histidine, serine, arginine, and asparagine. Furthermore, the network pharmacology analysis suggests that the actions of ACT are associated with the regulation of signal transduction, the metabolism of carbohydrate, lipid, and amino acid, and mainly the endocrine and immune systems. Thus, this study provides a precious insight and understanding for the clinical treatment of DN with ACT.

CHAPTER 3 Molecular mechanisms of renal protective actions of ACT in rat glomerular cells *in vitro*

3.1 Introduction

In Chapters 1 and 2, I have gradually revealed the therapeutic activity of ACT in the field of nephrosis (CGN-DN) and explored the mechanism of action of ACT *in vivo*. In this Chapter, I examined molecular mechanisms of renal protective actions of ACT in rat glomerular cells *in vitro.*

It has been reported that ACT impedes the proliferation of crescentic cells and the mitigation of crescentic cell adhesion to the glomerular vessel wall and inhibits the necrosis of glomerular fibroblasts[20]. In addition, ACT has been reported to markedly reduces proteinuria and glomerular protein swelling, impedes glomerular cell proliferation, decreases glomerular macrophage permeability, downregulates glomerular cell ICAM-1 expression, and increases the activity of glomerular cell matrix metalloproteinases (MMPs)[104]. MMPs are the pivotal enzymes that degrade various ECM components under physiological and pathological conditions[105]. It has been reported that MMP-2/gelatinase A participates in a variety of renal damage processes such as glomerulosclerosis and interstitial fibrosis. MMP-2 has been reported to promote the transformation of the angiogenic phenotype[106]. Furthermore, MMP-9/gelatinase B has been reported to activate angiogenesis to prerequisite for endothelial cells to form neovascularization[107]. Moreover, both MMP-2 and MMP-9 have been reported to promote neovascularization by acting on other cells or vascular factors.

Mesangial cells, endothelial cells, and podocytes are recognized as structural cells of the glomerulus. Mesangial cells in the glomerulus play an important role in maintaining the integrity of the glomerular capillary bed and the metabolic balance of the mesangial matrix [108-109]. In the pathogenesis of kidney disease, various pathological factors directly affect glomerular mesangial cells, causing hypertrophy and excessive proliferation of glomerular mesangial cells. The abnormal accumulation and deposition of ECM components such as collagen and fibronectin (FN) in the mesangial area constitute an important pathological basis for glomerular fibrosis and sclerosis[110-111]. Connective tissue growth factor (CTGF), which is a very important pro-fibrotic factor, plays an important role in the occurrence and development of kidney disease associated with glomerular fibrosis[112-114]. Transforming growth factor β1

(TGF-β1) is a major renal fibrosis promoting factor that participates in mesangial cells proliferation, the synthesis and deposition of ECM proteins[115], and glomerular sclerosis and interstitial fibrosis of the renal tubules[116].

Glomerular endothelial cells directly contact the blood through the glomerular filtration barrier. In addition, proteinuria is one of the signs of widespread damage to glomerular endothelial cells in kidney disease[117-118]. It has been reported that angiotensin II (Ang II) induces damage and apoptosis of glomerular endothelial cells following to the development of kidney disease[119-121]. In addition, it has been reported that Ang II promotes the production of various cytokines including TGF-β1 to accumulate cell proliferation matrix[122]. Furthermore, the increased activity of Ang II has been reported to augment changes in renal glomerular hemodynamics, glomerular capillary pressure, the excretion of urinary albumin, the infiltration of mononuclear macrophages in the glomerulus, and the synthesis and aggregation of ECM, leading to renal injury[115].

Podocytes, which are attached to the outer side of the glomerular basement membrane (GBM), form a filtration barrier with the glomerular basement membrane and capillary endothelial cells. Thus, changes in podocytes are associated with the occurrence of proteinuria related kidney disease. Furthermore, the changes in the level of nephrin and synaptopodin, which are podocyte injury markers[123], have been reported to objectively explain the morphology and activity of podocytes[124-130].

In this Chapter, to elucidate the molecular mechanisms of the therapeutic actions of ACT for kidney disease, I systematically studied the effects of ACT on the expression of such key molecules in mesangial cells, glomerular endothelial cells, and podocytes under inflammation and high-glucose (HG) damage conditions. Furthermore, based on the results of metabolic analysis in the Chapter 1, the effects of two metabolites of ACT, DOPE and DOPAC, on cell morphology and the expression of nephrin were examined in HG-stimulated glomerular podocytes.

3.2 Materials and Methods

3.2.1 Chemicals and reagents

ACT was isolated from the Dihuangye as Chapter 1. The purity of ACT was over 98%. DTG is from Sichuan Meidakang Company, with an ACT content of approximately 40%. Dimethyl sulfoxide (DMSO) (Cat# D2650) and collagenase IV (Cat# C8160) were purchased

from Sigma (Germany). Fetal bovine serum (FBS) (Cat# 10099-141), trypsin (Cat# 25200-072), DMEM/F12 medium (Cat# C11330500BT), RPMI1640 basal medium (Cat# 11875085) were purchased from Gibco (USA). PVDF membrane (0.45 um) (Cat# IPVH00010) was purchased from Millipore (Germany). Developing liquid (Cat# YA0371), fixative (Cat# YA0381), photographic film (Cat# YA0360) were purchased from Eastman Kodak Company (USA). D-glucose was purchased from Shanghai Sangon Biological Engineering Co., Ltd (Shanghai, China); RIPA buffer (high), Phenylmethanesulfonyl fluoride (PMSF), SDS-PAGE Gel Kit were purchased from Solarbio (Beijing, China); RPMI 1640 Media (Cat# SH30807.01) and low glucose DMEM (Cat# SH30002.01) were purchased from Hyclone (USA). High glucose DMEM (Cat# 12800-058) was purchased from GIBCO (USA).

3.2.2 Antibodies

Vascular endothelial growth factor (VEGF) (Cat# K003244P), transferrin (Cat# T8010), 3-(4,5)-dimethylthiahiazo (-z-y1)-3,5-di-phenytetrazoliumromide (MTT) (Cat# M8180), radio immunoprecipitation assay lysis buffer (RIPA) (Cat# R0020), PMSF (Cat# P0100), acrylamide (30%, 29:1) (Cat# A1010), tris(Hydroxymethyl)aminomethane (Tris) (PH 8.8) (Cat# T1010), BCA protein assay kit (Cat# PC0020), rainbow protein marker (Cat# PR1930), ECL western blotting substrate (Cat# PE0010-A/B), rabbit anti-matrix metalloproteinase-9 (MMP-9) antibody (Cat# bs-4593R), rabbit anti-matrix metalloproteinase-2 (MMP-2) antibody (Cat# bs-4599R), rabbit anti-CTGF antibody (Cat# bs-0743R), rabbit anti-AngII antibody (Cat# bs-0587R), and rabbit anti-TGF-β antibody (Cat# bs-0086R) were purchased from Bioss (USA). Anti-GAPDH antibody (Cat# ab37168) was purchased from Abcam (UK). Anti-rabbit IgG and HRP-linked antibody (Cat# 7074) were purchased from Cell Signaling Technology (USA). β-Actin rabbit monoclonal antibody (mAb) was purchased from Cell Signaling Technology (Beverly, MA, USA). Rabbit polyclonal antibody to nephrin was purchased from Abcam (Cambridge, MA, USA).

3.2.3 Animals

Male Sprague-Dawley (SD) rats were used for the separation of glomerular cells. The rats were purchased from Shanghai JSJ Laboratory Animal Technology Co. Ltd, SCXK (HU) 2018-0004 & SCXK (HU) 2013-0006 (Shanghai, China).

3.2.4 Isolation and culture cells

3.2.4.1 The culture of primary rat kidney cells

Renal lavage *in situ*: SD rats were anesthetized with 8% chloral hydrate injection and positioned supine. The chest and abdomen were sterilized, and the thoracic aorta was dissected, blood was perfused with sterile cold PBS to wash the kidneys, while the renal vein was incised to facilitate fluid outflow. After 1-2 min, the kidneys turned pale. The renal cortex was cut into 1-2 mm^3 pieces after the medulla was removed. The renal cortex was ground and passed through 80, 120, and 200 cell Strainers to collect the glomeruli.

3.2.4.2 Isolation and culture of rat glomerular endothelial cells

The isolated glomeruli were digested using 0.1% type collagenase IV, and the resulting precipitate was collected. Subsequently, 2×10^4 glomeruli were seeded in culture flasks coated with 1% gelatin. A specialized endothelial cell culture medium, comprising DMEM, 20 mmol/L HEPES, 20% FBS, 0.66 U/mL insulin, 20 ng/mL vascular endothelial growth factor, and 100 μg/mL heparin sodium, was added. Following three days of static culture, daily observations were made to confirm glomerular adherence. Once full adherence was achieved, media exchange and purification were routinely performed during the third week[131-132)].

3.2.4.3 Isolation and culture of rat glomerular mesangial cells

The collected glomeruli underwent centrifugation at 3000 r/min for 10 min, discarding the supernatant. Subsequently, 5 mL of 0.5 g/L type collagenase IV was added, and the mixture was transferred to a sterile centrifuge tube. A 37 ℃ water bath was employed for digestion with shaking for 30 min. The digestion process was halted using RPMI-1640 containing 20% FBS at 1500 r/min for 10 min, followed by discarding the supernatant. The cells were resuspended in RPMI-1640 medium with 20% FBS and seeded in T25 flasks. Incubation occurred in a 37 ℃, 5% CO_2 environment for 3-5 days, ensuring no disturbance to the flasks for the initial 3 days. On the 5th day, the first medium change was performed, and subsequent changes occurred every 3 days until the 14th day, when the cells underwent their first digestion[133)].

3.2.4.4 Isolation and culture of rat glomerular podocytes

Glomeruli were obtained through rinsing with DMEM/F12, resulting in the observation of numerous intact Bowman's capsule glomeruli under an inverted microscope. After collection in a centrifuge tube, 0.1% type collagenase IV was added for digestion at 37 ℃ for 10 min, followed by supernatant removal through centrifugation at 800 r/min for 5 min. The glomeruli were then resuspended in complete medium (containing 10% FBS, 100 U/mL penicillin, 100 U/mL streptomycin, 5 μg/mL insulin, 5 μg/mL transferrin, and 5 μg/mL sodium selenite), and seeded in gelatin-coated T25 culture flasks at a density of 15-20 glomeruli per mL. Placed in a 5% CO_2 incubator, by the third day, most glomeruli adhered to the flask wall, with cobblestone-like podocytes emerging from a few. Following a medium exchange, numerous podocytes crawled out from the glomeruli, exhibiting cobblestone-like structures with visible foot processes on the outermost cells. After 10 days of culture, the cells underwent passaging through differential trypsin digestion. The podocytes in the incubator were removed, and after a wash with preheated sterile PBS at 37 ℃, 0.25% trypsin was added to the culture flask for digestion lasting 3-5 min. Under an inverted microscope, podocytes exhibited shrinkage and rounding, with a small portion detaching from the surface. Initial digested cells were discarded, replaced with preheated complete medium, and completely detached using an elbow pipette. After collection, the cells underwent another round of passage through a 200-mesh screen to remove glomeruli. Following collection and screening, centrifugation was performed at 1000 r/min for 5 min before resuspending in complete medium and inoculating into T25 flasks for further incubation. On the second day of passage, the culture medium was changed, while maintaining the aforementioned conditions for one week, with media changes occurring every three days until differentiation, when cells were utilized for corresponding experiments[134-135)].

3.2.5 MTT assay

Three types of renal cells in logarithmic growth phase, displaying robust growth status, were selected. The cell suspension concentration was adjusted, and the aliquot of the suspension (100 μL) was added to each well. The plate was gently shaken to evenly distribute the cells at a density of 8000 cells per well, with sterile PBS used to fill the edge wells. Subsequently, the cells were incubated in a 5% CO_2 atmosphere at 37 ℃ until they formed a monolayer on the bottom surface of a flat-bottomed 96-well plate with 100 μL medium per well and six replicates. Additionally, zero-setting wells (containing complete medium, MTT reagent, and dimethyl

sulfoxide) as well as control wells (containing cells, complete medium, MTT reagent, and DMSO) were prepared. ACT intervention concentrations were prepared at 12.5 μmol/L, 25 μmol/L, 50 μmol/L, and 100 μmol/L. DTG intervention concentrations based on the content of ACT (40%) were set at 19.5 mg/L, 39.1 mg/L, 78.2 mg/L, and 156 mg/L. After 12, 24, 48, or 72 h, the cells were observed under an inverted microscope. After careful flushing 2-3 times with PBS, 10 μL of MTT solution (5 mg/mL, or 0.5% MTT) was added to each well, and the culture was continued for another 4 h. Then, 100 μL of formazan solution was added to each well, mixed appropriately, and the incubation was continued in the cell incubator until the formazan was completely dissolved under the microscope. Absorbance was measured at 570 nm.

3.2.6 Western Blot analysis

According to the MTT test results, the ACT intervention concentration was set at 25 μmol/L (L), 50 μmol/L (M), and 100 μmol/L (H). The intervention concentration of DTG based on the content of ACT (40%) was set at a higher 156 mg/L.

The cell culture medium was aspirated and washed once with serum-free medium. To 1 mL of RAPA, 10 μL PMSF was added to achieve a final PMSF concentration of 1 mM. The lysate was added in a ratio of 150 to 250 μL per well in a 6-well plate based on the cell number. The lysed sample was centrifuged at 10000×g for 5 min, and the supernatant was discarded. Protein content was determined using the BCA kit instructions. RIPA was added to adjust the volume of each sample to 20 μL. Finally, 5 μL (5×) buffer was added for mixing, and the protein was fully denatured by boiling for 10 min. The sample volume of the pre-staining marker was 5 μL each time. SDS-PAGE was conducted, and the concentrated gel portion was subjected to constant pressure electrophoresis at 80 V for about 20 min. The separated gel portion was then subjected to constant pressure electrophoresis at 150 V until the leading edge of bromophenol blue was below the electrode wire. A sandwich structure was used for membrane transfer, employing 200 mA constant current electric transfer for 100 min while maintaining a voltage of 80 V. After membrane transfer, the membrane was removed and rinsed three times with TBST. A blocking solution of 5% skim milk powder was applied at room temperature for 2 h. TBST was used for three additional rinses. According to the primary antibody instructions, the molecular weight band range obtained by Western blot was predicted,

and the membrane was accordingly cut. The primary antibody and GAPDH one were diluted in TBST buffer containing 5% BSA. The cut membranes were incubated in the primary antibody dilution (1:200) and GAPDH (1:4000), respectively, overnight at 4 ℃ on a shaker. TBST was used for three additional rinses. HRP-labeled goat anti-rabbit secondary antibody was diluted to 1:5000 with TBST buffer, and the membrane was placed in the secondary antibody diluent and incubated for 1 h at room temperature. TBST was used for three additional rinses. The ECL luminescent reagent A and reagent B were mixed in equal volume in the dark, and the luminescent solution was evenly applied to the PVDF membrane protein surface in the dark room. After incubating for 3 min, the residual solution was slightly absorbed. The exposure time was adjusted multiple times with different time gradients to achieve the best effect. The film was then scanned or photographed.

3.2.7 Statistical analysis

Statistical analysis of the data was carried out using SPSS (v 25), and the results were presented as mean ± standard error of the mean (SEM). The t-test was employed for datasets with normal distribution and equal variance, while the non-parametric rank sum test was applied for datasets exhibiting abnormal distribution. Significance was attributed to cases where $P < 0.05$, and trends were identified when $P < 0.1$. Graded data were assessed for significant differences using a nonparametric rank sum test. Graphs were generated using GraphPad Prism (v 9.5).

3.3 Results

3.3.1 Effect of ACT and DTG on cell viability in LPS-stimulated mesangial cells

First, MTT assay was performed to evaluate the protective effects of ACT and DTG on cell viability in rat mesangial cells stimulated for 24, 48, and 72 h with LPS. As shown in Figure 3-1, the model group exhibited a decline in cell viability compared to the blank group at the 24 h of LPS stimulation. Different concentrations of ACT showed protective effects on cell viability compared to the model group; significant protective effects were detectable at 50 μmol/L and 100 μmol/L of ACT. The DTG group also demonstrated a significant protective effect on cell viability at 39.1 mg/L, 78.2 mg/L, and 156 mg/L in a dose-dependent manner. After 48 h of LPS stimulation. As shown in **Figure 3-1**, cell viability was decreased in the

model group as compared to the blank group. However, both ACT and DTG were found to dose-dependently increase the cell viability in the model group. Following the 72 h of LPS stimulation, cell viability was reduced in the model group as compared to the blank group. Similarly, both ACT (50 μmol/L) and DTG (78.2 mg/L and 156 mg/L) administration was found to increase cell viability in the model group in a dose-dependent manner.

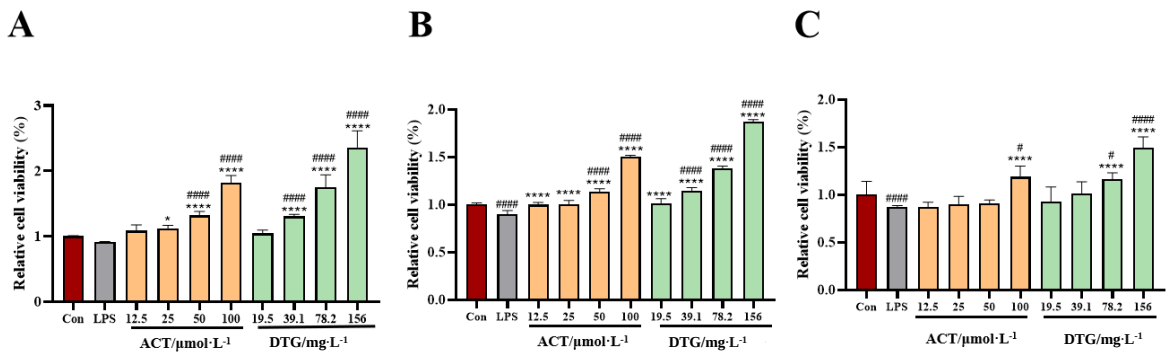

Figure 3-1 Effect of ACT and DTG on cell viability in LPS-stimulated rat mesangial cells

Rat mesangial cells were treated for 24h (A), 48h (B), and 72h (C) with ACT (12.5-100 μmol/L) and DTG (19.5-156 μmol/L) in the presence and absence of LPS (1 μg/mL), and then the cell viability was measured as described in the Materials and Methods. $^{\#}P < 0.05$, $^{\#\#}P < 0.01$, $^{\#\#\#}P < 0.001$, $^{\#\#\#\#}P < 0.0001$ (compared to the Con group); $^{*}P < 0.05$, $^{**}P < 0.01$, $^{***}P < 0.001$, $^{****}P < 0.0001$ (compared to the LPS group).

3.3.2 Effect of ACT and DTG on cell viability in IL-1β-stimulated mesangial cells

Next, MTT assay for evaluating ACT and DTG actions was similarly demonstrated in IL-1β-stimulated rat mesangial cells. As shown in **Figure 3-2**, cell viability was decreased in the model group as compared to the blank group. Both ACT and DTG were found to exhibit protective effect similarly and dose-dependently on cell viability in IL-1β-stimulated rat mesangial cells at individual treatment periods (24-72 h).

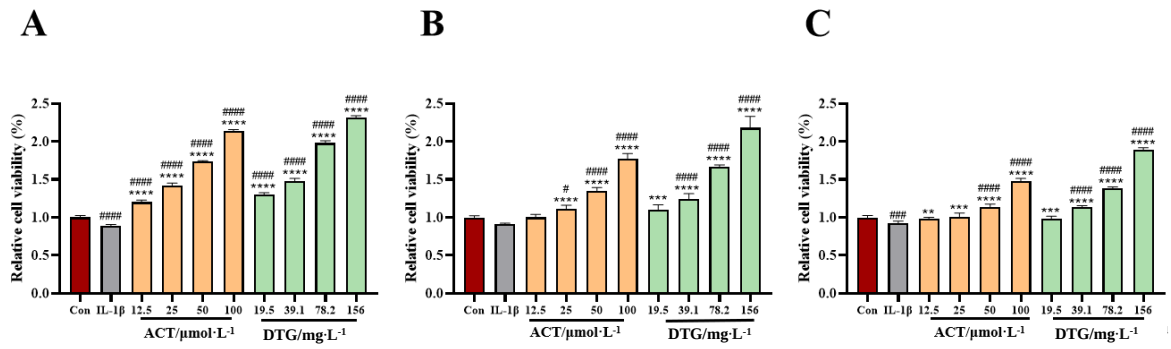

Figure 3-2 Effect of ACT and DTG on cell viability in IL-1β-stimulated rat mesangial cells

Mesangial cells were treated for 24h (A), 48h (B), and 72h (C) with ACT (12.5-100 μmol/L) and DTG (19.5-156 μmol/L) in the presence and absence of IL-1β (10 ng/mL), and then the cell viability was measured as described in the Materials and Methods. $^{\#}P < 0.05$, $^{\#\#}P < 0.01$, $^{\#\#\#}P < 0.001$, $^{\#\#\#\#}P < 0.0001$ (compared to the Con group); $^{*}P < 0.05$, $^{**}P < 0.01$, $^{***}P < 0.001$, $^{****}P < 0.0001$ (compared to the IL-1β group).

3.3.3 Effect of ACT and DTG on cell viability in IL-1β-stimulated glomerular endothelial cells

To clarify whether ACT and DTG exhibit the protective effect on other structural cells of the glomerulus, the similar MTT assay was performed in rat glomerular endothelial cells treated for 12-48 h with IL-1β. As shown in **Figure 3-3**, IL-1β stimulation for up to 48 h was found to decrease the cell viability of endothelial cells. In addition, both ACT (12.5-100 μmol/L) and DTG (19.5-156 mg/L) were found to recover the cell viability of endothelial cells in a dose-dependent manner.

3.3.4 Effect of ACT and DTG on cell viability in HG-stimulated glomerular endothelial cells

Since ACT showed therapeutic efficacy in DN in Chapter 2, the effects of ACT on cell viability was examined in HG-stimulated rat glomerular endothelial cells. As shown in **Figure 3-4**, HG stimulation was found to decrease the cell viability of glomerular endothelial cells in a treatment-time-dependent manner. Both ACT (12.5, 25, 50, and 100 μmol/L) and DTG (19.5, 39.1, 78.2, and 156 mg/L) were found to dose-dependently recovered the cell viability in HG-stimulated glomerular endothelial cells.

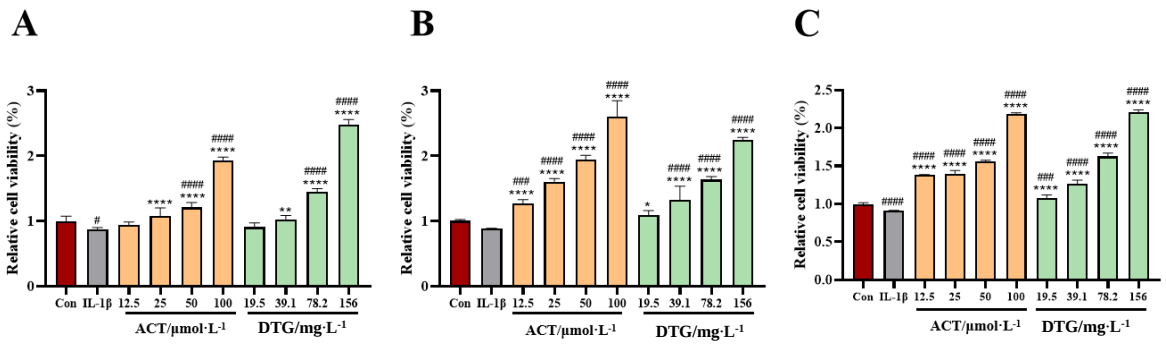

Figure 3-3 Effect of ACT and DTG on cell viability in IL-1β-stimulated rat glomerular endothelial cells

Rat glomerular endothelial cells were treated for 24h (A), 48h (B), and 72h (C) with ACT (12.5-100 μmol/L) and DTG (19.5-156 μmol/L) in the presence and absence of IL-1β (10 ng/mL), and then the cell viability was measured as described in the Materials and Methods. $^{\#}P < 0.05$, $^{\#\#}P < 0.01$, $^{\#\#\#}P < 0.001$, $^{\#\#\#\#}P < 0.0001$ (compared to the Con group); $^{*}P < 0.05$, $^{**}P < 0.01$, $^{***}P < 0.001$, $^{****}P < 0.0001$ (compared to the IL-1β group).

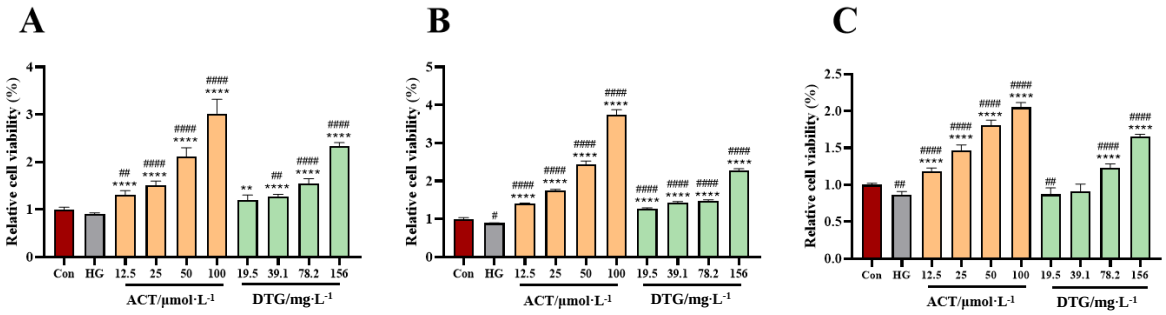

Figure 3-4 Effect of ACT and DTG on cell viability in HG-stimulated rat glomerular endothelial cells

Glomerular endothelial cells were treated for 24h (A), 48h (B), and 72h (C) with ACT (12.5-100 μmol/L) and DTG (19.5-156 μmol/L) in the presence and absence of HG (30 mmol/mL), and then the cell viability was measured as described in the Materials and Methods. $^{\#}P < 0.05$, $^{\#\#}P < 0.01$, $^{\#\#\#}P < 0.001$, $^{\#\#\#\#}P < 0.0001$ (compared to the Con group); $^{*}P < 0.05$, $^{**}P < 0.01$, $^{***}P < 0.001$, $^{****}P < 0.0001$ (compared to the HG group).

3.3.5 Effect of ACT and DTG on cell viability in IL-1β-stimulated glomerular podocytes

To investigate whether ACT and DTG exhibit the protective effect on another structural cells of the glomerulus, the similar MTT assay was performed in rat glomerular podocytes. As shown in **Figure 3-5**, when the cells were stimulated for 12, 24, and 48 h with IL-1β, the cell viability was slightly decreased in a time-dependent manner. In addition, both ACT (12.5, 25, 50, and 100 μmol/L) and DTG (19.5, 39.1, 78.2, and 156 mg/L) were found to dose-dependently augment the cell viability in the IL-1β-stimulated podocytes.

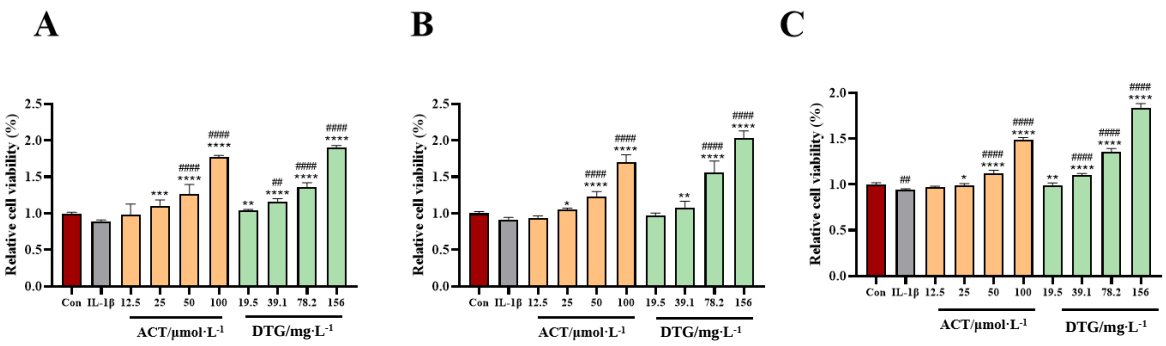

Figure 3-5 Effect of ACT and DTG on cell viability in IL-1β-stimulated rat glomerular podocytes

Rat glomerular podocytes were treated for 24h (A), 48h (B), and 72h (C) with ACT (12.5-100 μmol/L) and DTG (19.5-156 μmol/L) in the presence and absence of IL-1β (10 ng/mL), and then the cell viability was measured as described in the Materials and Methods. $^{\#}P < 0.05$, $^{\#\#}P < 0.01$, $^{\#\#\#}P < 0.001$, $^{\#\#\#\#}P < 0.0001$ (compared to the Con group); $^{*}P < 0.05$, $^{**}P < 0.01$, $^{***}P < 0.001$, $^{****}P < 0.0001$ (compared to the IL-1β group).

3.3.6 Effect of ACT and DTG on the production of MMP-2 and MMP-9 in IL-1β-stimulated rat mesangial cells, glomerular endothelial cells, and glomerular podocytes

Renal fibrosis in renal failure is closely related to abnormal ECM metabolism [115]. As the renal ECM remodeling has been reported to be regulated by MMPs such as MMPs-2 and -9 [105-106], whether the production of MMP-2 and MMP-9 was controlled by ACT in rat mesangial cells, glomerular endothelial cells, and glomerular podocytes. When the mesangial cells were treated with IL-1β (described as Mod), the production of MMP-2 and MMP-9 was augmented **(Figure 3-6A)**. The increase production of MMP-2 and MMP-9 was suppressed by ACT in a dose-dependent manner. In addition, DTG was found to decrease the production of MMPs-2

and -9 in rat mesangial cells. Furthermore, the similar suppressive action of ACT and DTG was detectable in the IL-1β-stimulated glomerular endothelial cells **(Figure 3-6B)** and glomerular podocytes **(Figure 3-6C)**.

3.3.7 Effect of ACT and DTG on the production of CTGF and TGF-β in LPS-stimulated rat mesangial cells

Since CTGF and TGF-β1 have been reported to plays an important role in the occurrence and development of kidney disease as pro-fibrotic factors, I examined whether ACT and DTG regulated the production of CTGF and TGF-β1 in rat mesangial cells. As shown in **Figure 3-7**, LPS augmented the production of CTGF and TGF-β and the increased protein level of both factors was decreased by ACT in a dose-dependent manner. In addition, the similar reduction of CTGF and TGF-β production was detectable in DTG treatment.

3.3.8 Effect of ACT and DTG on the production of AngII in HG-stimulated rat glomerular endothelial cells

Since AngII has been reported to participate in the occurrence and development of kidney disease by affecting vascular functions [119-121], I examined whether ACT and DTG influenced the production of AngII in HG-stimulated rat glomerular endothelial cells. As shown in **Figure 3-8**, when endothelial cells were cultured under HG condition, the production of AngII was increased. The augmented level of AngII was decreased by ACT and DTG, and ACT in a dose-dependent manner.

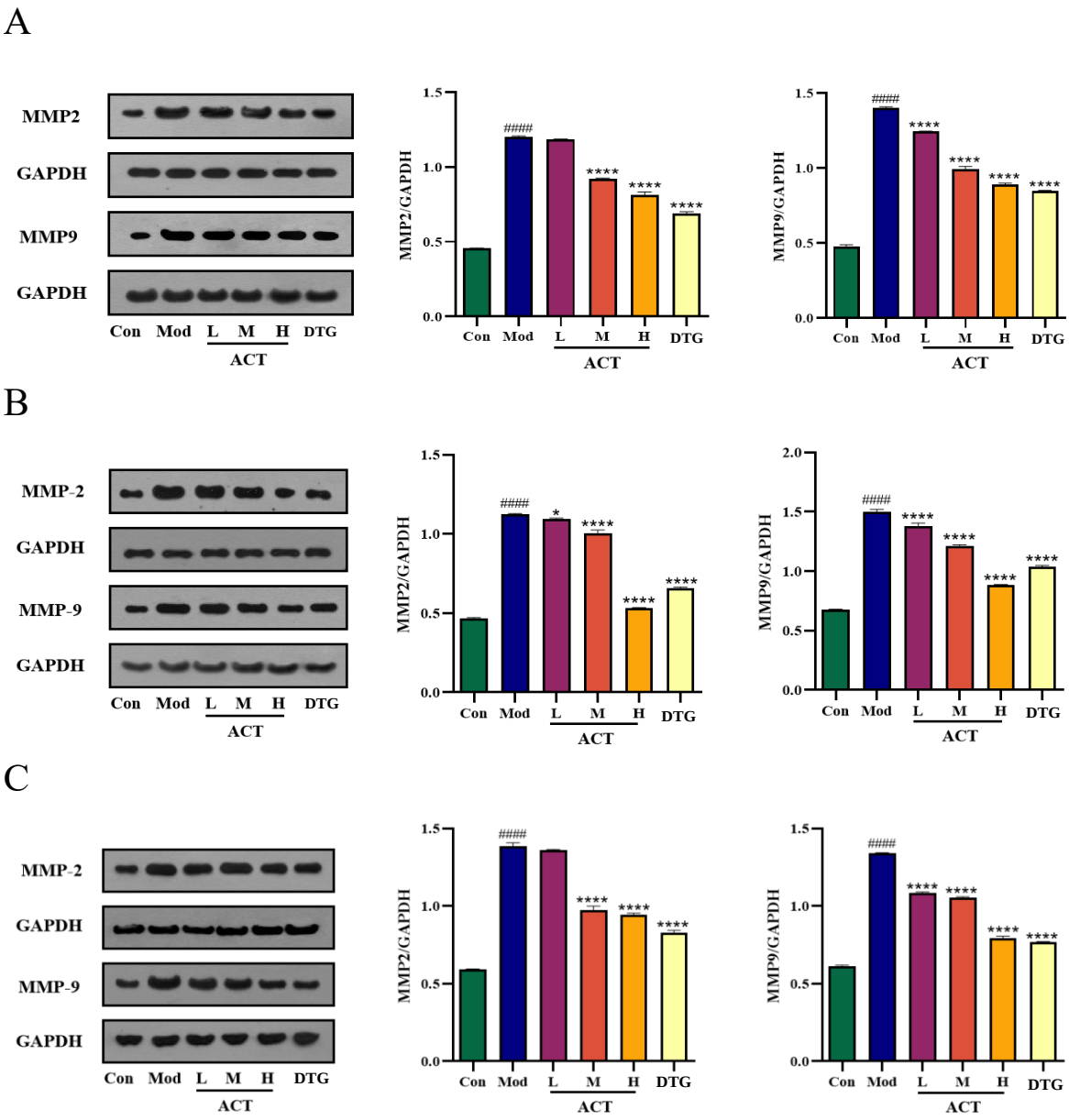

Figure 3-6 Effect of ACT and DTG on MMP-2 and MMP-9 protein expression in IL-1β-stimulated rat mesangial cells, glomerular endothelial cells, and glomerular podocytes

Rat mesangial cells (A), glomerular endothelial cells (B), and glomerular podocytes (C) were treated for 24 h with ACT (25, 50, and 100 μmol/L indicating L, M, and H, respectively) and DTG (156 mg/L), and then Western blot analysis was performed as described in the Materials and Methods. The detected MMP-2 and MMP-9 protein were corrected for that of GAPDH (left panels in A-C), and then the relative amounts of MMP-2 (middle panels in A-C) and MMP9 (light panels in A-C), respectively, were shown as mean ± SD. $^{\#}P < 0.05$, $^{\#\#}P < 0.01$, $^{\#\#\#}P < 0.001$, $^{\#\#\#\#}P < 0.0001$ (compared to the Con group); $^{*}P < 0.05$, $^{**}P < 0.01$, $^{***}P < 0.001$, $^{****}P < 0.0001$ (compared to the Mod group).

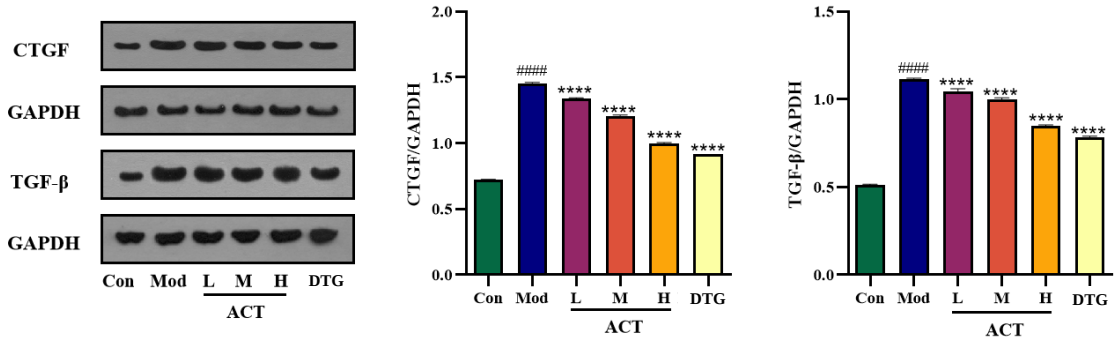

Figure 3-7 Effect of ACT and DTG on the production of CTGF and TGF-β in LPS-stimulated rat mesangial cells

Mesangial cells were treated for 24 h with ACT (25, 50, and 100 μmol/L indicating L, M, and H, respectively) and DTG (156mg/L), and then Western blot analysis was performed as described in Figure 3-6. The detected CTGF and TGF-β protein were corrected for that of GAPDH (left panel), and then the relative amounts of CTGF (middle panel) and TGF-β (light panel) were shown as mean ±SD. $^{\#}P < 0.05$, $^{\#\#}P < 0.01$, $^{\#\#\#}P < 0.001$, $^{\#\#\#\#}P < 0.0001$ (compared to the Con group); $^{*}P < 0.05$, $^{**}P < 0.01$, $^{***}P < 0.001$, $^{****}P < 0.0001$ (compared to the Mod group).

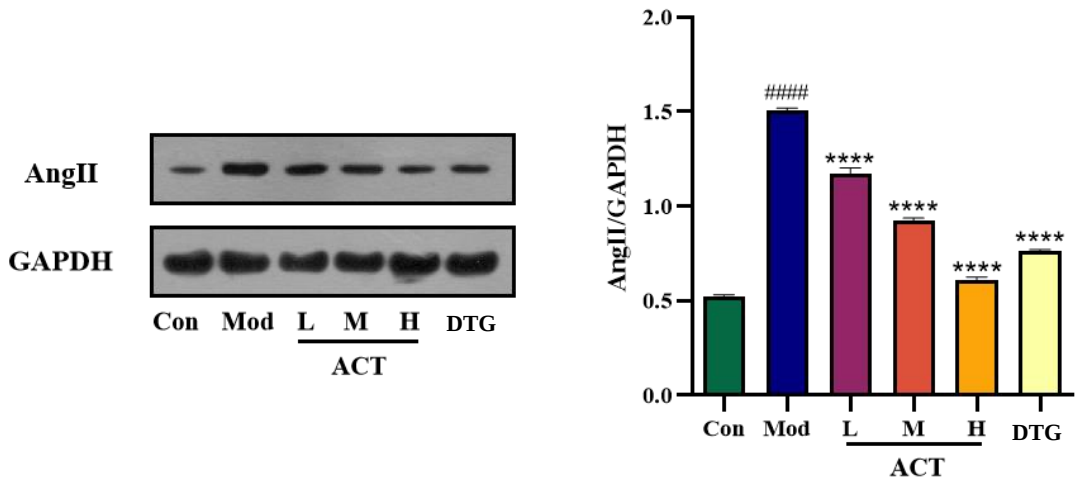

Figure 3-8 Effect of ACT and DTG on the production of AngII in HG-stimulated rat glomerular endothelial cells

Rat glomerular endothelial cells under HG conditions were treated for 24 h with ACT (25, 50, and 100 μmol/L indicating L, M, and H, respectively) and DTG (156mg/L), and then Western blot analysis was performed as described in Figure 3-6. The detected AngII protein was corrected for that of GAPDH (left panel), and then the relative amounts of AngII (light panel) were shown as mean ± SD. $^{\#}P < 0.05$, $^{\#\#}P < 0.01$, $^{\#\#\#}P < 0.001$, $^{\#\#\#\#}P < 0.0001$ (compared to the Con group); $^{*}P < 0.05$, $^{**}P < 0.01$, $^{***}P < 0.001$, $^{****}P < 0.0001$ (compared to the Mod group).

3.3.9 Effect of ACT and its metabolites on podocytic functions and the production of nephrin in HG-stimulated rat glomerular podocytes

Functional changes in podocytes have been reported to be associated with the occurrence of proteinuria related kidney disease. In addition, the changes in the level of nephrin have been reported to be associated with the morphology and activity of podocytes[70-76]. Therefore, metabolites of ACT *in vivo* were analyzed in the CGN model rats in Chapter 1, and the presence of DOPE and DOPAC as metabolites was confirmed. Based on this result, whether ACT, DOPE, and DOPAC influenced the podocyte functions was examined under HG conditions *in vitro*. When podocytes were cultured under HG conditions, a significant retraction of the podocytic process, and a decrease in the number of podocytes, the cell body area, and the expression of nephrin were observed **(Figure 3-9 A)**. When the cells were treated with ACT, the production of nephrin was augmented by ACT at 50 and 100 μmol/L ($P < 0.05$), but not 200 μmol/L. Furthermore, there was no change in the level of nephrin in DOPE (50, 100, and 200 μmol/L)-treated podocytes. However, DOPAC at 100 μmol/L was found to increase the production of nephrin in HG-stimulated podocytes ($P < 0.05$), while there was no alteration in DOPAC at 50 and 200 μmol/L **(Figure 3-9 B and C)**.

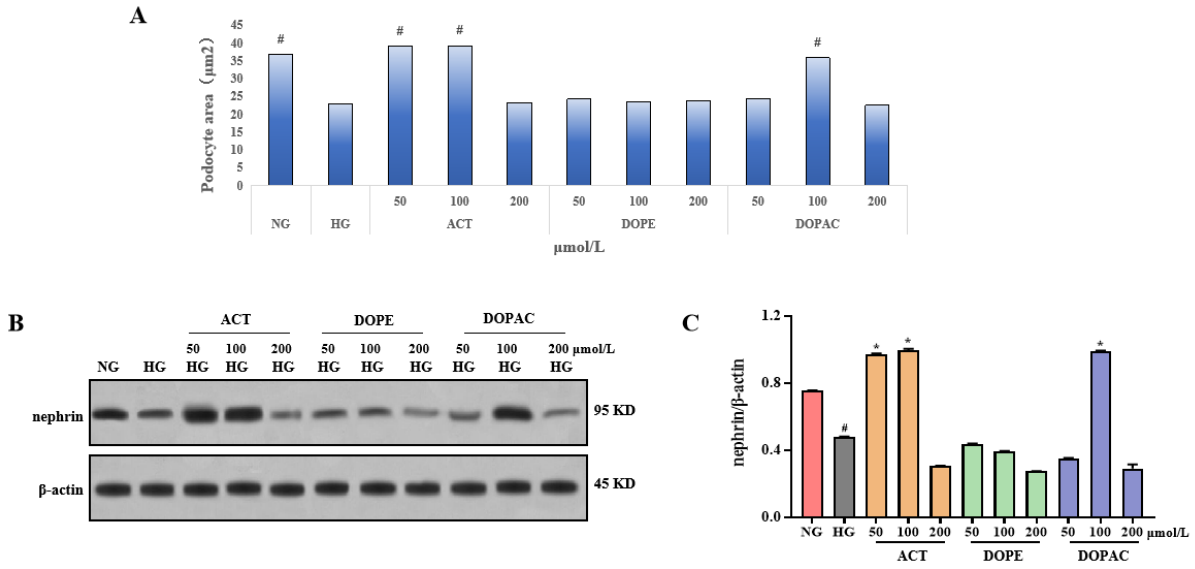

Figure 3-9 The alteration of cell morphology and regulation of nephrin expression by ACT, DOPE, and DOPAC in HG-stimulated glomerular podocytes

Glomerular podocytes were treated for 24 h with ACT (50, 100, and 200 μmol/L), DOPE (50, 100, and 200 μmol/L), and DOPAC (50, 100, and 200 μmol/L) in the presence or absence of HG (30 mmol/mL). The significant retraction of the podocytic process was shown in panel A. Western blot analysis was performed to measure the protein level of nephrin and β-actin (panel B) as described in Figure 3-6, and then the relative amounts of nephrin against β-actin were shown as mean ± SEM (panel C). $^{\#}P < 0.05$, $^{\#\#}P < 0.01$, $^{\#\#\#}P < 0.001$ (compared to NG group); $^{*}P < 0.05$, $^{**}P < 0.01$, $^{***}P < 0.001$ (compared to HG group).

3.4 Discussion

The glomerulus, a capillary ball within the renal corpuscle, is a critical component responsible for blood filtration. The glomerulus with branches of the renal artery purifies blood through a filtration membrane created by the capillary wall, which functions as a primary blood filter [136]. Inflammatory damage to the glomerulus impairs kidney function, leading to various manifestations such as edema, hypertension, hematuria, proteinuria, and the accumulation of toxins in the body, profoundly impacting human health[137]. In this Chapter, I demonstrated that ACT as well as DTG improved cell viability of rat mesangial cells and glomerular endothelial cells and podocytes under inflammatory and HG-exposed conditions. Taken tother with *in-vivo* findings in Chapters 1 and 2, ACT is likely to exhibit the prevention and curing action for renal impairment in CGN and DN.

It has been reported that renal tubulointerstitial fibrosis stands out as a crucial indicator for measuring the chronic progression of kidney disease. TGF-β1 has been identified as a key fibrogenic factor, capable of inducing the formation and development of renal interstitial fibrosis through various pathways. In addition, CTGF has been reported to play a positive role in tissue fibrosis processes[138-140]. As TGF-β is involved in humoral immunity, fibroblast-derived CTGF induces the production of TGF-β1, which plays a crucial role in promoting cell proliferation and the synthesis of ECM components. Furthermore, multiple stimuli have been reported to facilitate the excessive secretion of CTGF in renal cells, which in turn promotes cell proliferation and ECM deposition following to the occurrence and development of renal fibrosis.

MMP is a family of zinc- and calcium-dependent proteinase secreted as a zymogen [141-143]. MMP-2 and MMP-9 are particularly well-studied members of the MMP family in kidney diseases. It has been reported that MMP-2 plays a crucial role in various renal damage processes including glomerulosclerosis and interstitial fibrosis[143-145], and that MMP-2 facilitates the transformation of the angiogenic phenotype, while MMP-9 activates angiogenesis for endothelial cell neovascularization[146]. In addition, both MMP-2 and MMP-9 have been shown to promote neovascularization by influencing other cells or vascular factors[147-151]. On the other hand, renal fibrosis is caused by the accumulation of interstitial collagen (types I, II, and III), glycoproteins (fibronectin and laminin), and proteoglycans[145]. In addition, MMP-2 and MMP-9 have been reported to alleviate renal fibrosis by specifically degrading type-IV collagen, a major component of the basement membrane, thereby disrupting the tissue barrier[152]. Furthermore, MMP-2 has been reported to proteolytically activating TGF-β, which promotes

epithelial-mesenchymal transition[153]. Moreover, MMP-9 has been reported to be involved in the release of vascular endothelial growth factor (VEGF), which may contribute to renal physiology and pathology.

McMillan *et al.*[154] have reported a significant increase in the gene expression and production of MMP-9 in glomerular visceral epithelial cells of rats with passive Heymann nephritis. As the augmentation of MMP-9 expression seems to be associated with the development of proteinuria, it is suggested that the heightened expression of MMP-9 provides a crucial role in the degradation of collagen in the glomerular capillary basement membrane, resulting in increased permeability and the production of proteinuria in membranous nephropathy. Therefore, the overexpression of MMP-2 and MMP-9 may lead to excessive degradation of collagen in the glomerular basement membrane, which might be a possible pathogenesis for membranous nephropathy. In this Chapter, both ACT and DTG reduced the IL-1β augmented production of MMP-2 and MMP-9 in rat glomerular mesangial cells, endothelial cells, and podocytes. Thus, these results suggest that ACT and DTG exhibit therapeutic actions to kidney disease by improving the MMP2/9-mediated excessive degradation of type-IV collagen in glomerular basement membrane.

The local activation of Renin-Angiotensin System (RAS) is a major characteristic in the occurrence and development of various chronic kidney diseases. Angiotensin II (Ang II) plays a dominant role in regulating blood volume, hemodynamics, and homeostasis of the internal environment in the body[155]. Previous studies have shown that the locally elevated Ang II level in the kidney is closely related to the occurrence and development of renal diseases in hypertension and diabetes[156-157]. Thus, local elevation of Ang II in the kidney may cause not only intraglomerular hypertension but also the growth factor and/or cytokine-associated glomerular sclerosis. In this Chapter, my findings indicated that ACT and DTG decreased the HG-augmented production of Ang II in glomerular endothelial cells. Therefore, it is strongly suggested that ACT has the potential to improve intraglomerular hypertension and glomerular sclerosis in kidney disease treatments.

Nephrin is a transmembrane protein in podocytes, of which main role is to maintain the structural and functional integrity of podocytes[158-159]. In this Chapter, I demonstrated for the first time that HG stimulation decreased the production of nephrin in glomerular podocytes. In addition, ACT (50-200 μmol/L) reversed the level of nephrin in the HG-stimulated podocytes. Furthermore, there was no alteration of nephrin production in DOPE (50-200 μmol/L) and

DOPAC (50 and 200 μmol/L))-treated ells. Although the reason why DOPAC at only 100 μmol/L promoted the production of nephrin is unclear at this time, it is possible that not only ACT itself but also its metabolite, DOPAC is the active component in the regulation of nephrin production in HG-damaged podocytes *in vivo*. Further experiments are needed to clarify this hypothesis.

3.5 Conclusion

In this Chapter, as molecular mechanisms for the improvement and protective actions of ACT on renal function in CGN and DN, I demonstrated that ACT promoted cell viability in rat mesangial cells, glomerular endothelial cells, and glomerular podocytes under inflammatory and HG conditions. In addition, I found that ACT suppressed the production of MMPs, CTGF, TGF-β, and AngII, which are closely related to the occurrence of renal dysfunction, in those cells *in vitro*. Furthermore, ACT was found to facilitate the production of nephtrin, which is involved in the regulation of podocyte functions. Therefore, these results suggest that ACT is a potent therapeutic candidate for the treatment of kidney disease with impaired mesangial cells, and glomerular endothelial cells and podocytes.

GENERAL DISCUSSION AND CONCLUSION

Since DTG Capsule have therapeutically shown the improvement and protective activity with high safety for kidney functions by reducing urinary protein[160], chronic nephritis[7] and DN[8], the main active ingredient of DTG Capsule is not well understood, which seriously affects the clinical usage and global promotion. It is worth mentioning that ACT is the most abundant component in DTG, containing about 35%, and in DTG capsules about 12%. It has been reported that ACT possesses various pharmacological activities such as kidney protection, anti-oxidation, neuroprotection, liver protection, and anti-tumorigenesis. Dai *et al.*[161] have reported that 27 endogenous metabolites are detected in serum and urine from DTG-treated DN rats, and that DTG influences the production of TGF-β1 in renal tissues and mesangial cells. Similarly, ACT has been reported to exist as metabolites in diabetic renal injury model after DTG administration[10]. In the present study, metabolites of ACT were identified in serum, urine, and feces in CGN rats and DN mice. In addition, the administration of ACT relieved symptoms of both renal insufficiencies. Furthermore, Gan *et al.*[162] found that utilizing human peripheral blood lymphoid Th22 cells revealed that ACT exhibited the inhibition of the cell proliferation and differentiation, antigen presentation, inflammatory factor secretion, and the induction of the differentiation of lymphocytes to Th22 cells in kidneys, suggesting that ACT participates in the control of immune system. Therefore, ACT is likely to be the main active ingredient of DTG to elicit therapeutically the multiple actions for kidney disease such as CGN and DN.

Diabetes mellitus (DM) is a chronic disease characterized by hyperglycemia and abnormal metabolism of not only carbohydrates but also lipids and amino acids[64]. The most common complication of DM is DN, which is the final stage of the disease state characterized by histological and functional destruction of the glomerulus[65-66]. In the present metabonomic study using DN mice, ACT showed a significant alleviation of disease progression and an improvement in renal pathological tissue damages. Noteworthy, ACT significantly improved the levels of citrulline and tryptophan, which are the landmark amino acids in the early stage of DN. In addition, the metabolism of serine and asparagine was related to restore the renal functions in DN treated with ACT. Furthermore, ACT displayed a clear protective effect on glomerular podocytes damaged by high glucose. Thus, these results suggested that ACT is therapeutically applicable for the early stage of DN due to not only the improvement of

abnormal amino acid metabolism but also the protection of glomerular podocytes.

Computer biology methods such as network pharmacology and molecular docking are useful in predicting drug targets and mechanisms of actions[80]. This study using a network pharmacology analysis indicated that a total of 293 targets for ACT and 1748 targets for DN were extracted, with 122 targets overlapping between them, and in the network pharmacology research of ACT on CGN, there also a total of 293 targets for ACT were extracted and 975 targets for CGN were obtained, there were 84 targets of intersection. In addition, the "component-target-pathway" network revealed that targets in signaling transduction pathways such as AKT2, AKT1, MAPK1, HRAS, MAPK10, EGFR, MAPK8, MAPK14, IGF1R, and SRC were associated with the pharmacological actions of ACT in DN and CGN. Although the causes and symptoms are not necessarily identical in CGN and DN[163-165], the inflammatory response is seemed to be common in both diseases[166]. Such predicted signaling factors have been reported to be involved in various inflammatory responses to dysregulation of renal integrity and be therapeutic targets for drugs[43,167]. Taken together with my preliminary experiment of molecular docking that ACT interacted with MAPK1, HRAS, AKT1, and EGFR **(Schema 1)**, it is suggested that ACT exerts the improvement and protective effects on renal dysfunction through binding to predicted-candidate-signaling molecules in DN and CGN.

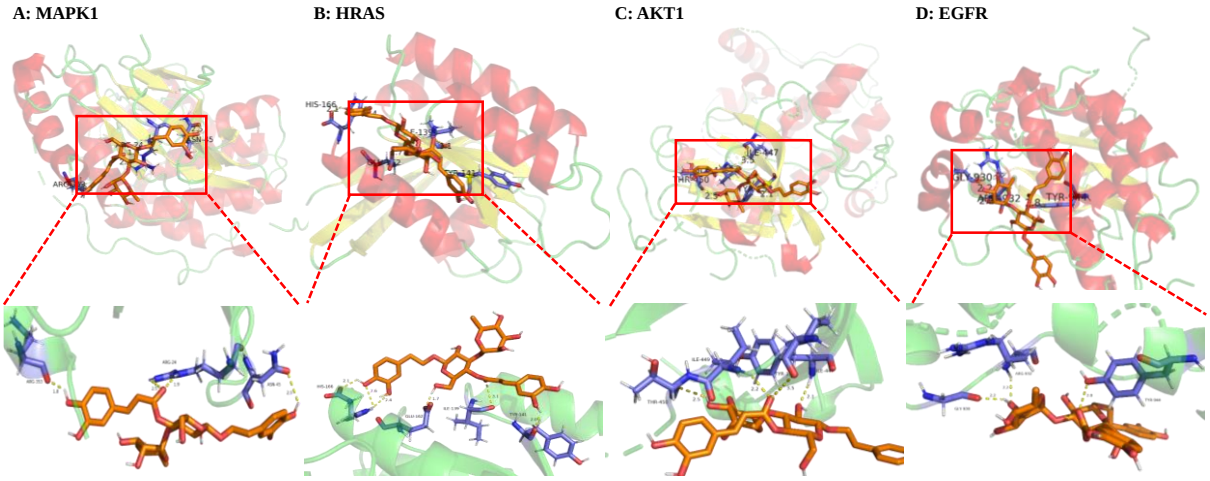

Schema 1 Screening of ACT-GN targets by molecular docking

Molecular docking studies of ACT with MAPK1 (F), HRAS (G), AKT1 (H), and EGFR (I) proteins. Molecules were depicted by a stick model, the hydrogen bonds were depicted by a dotted line, and the distance was shown in angstroms.

The glomerulus is a critical component responsible for blood filtration. The glomeruli formed by the branches of the renal arteries purify the blood through a filtration membrane created by the capillary walls, and then serve as the primary blood filte[168-169]. Inflammatory damage to the glomerulus impairs kidney function, leading to various manifestations such as edema, hypertension, hematuria, and proteinuria, under which toxins are accumulated in the body to profoundly influence human health[170]. In this study, ACT had a significant protective effect on rat mesangial cells, glomerular endothelial cells, and podocytes under inflammation and HG damage conditions *in vitro*. In addition, such actions of ACT on those glomerular cells were more effective than that of DTG. A previous study by Ding *et al*. [28] has shown that ACT effectively reduces proteinuria and the expression of podocyte injury markers such as nephrin and synaptopodin, leading to the alleviation of podocyte injury in puromycin rat nephropathy model. In addition, Ding *et al*.[28] have reported that ACT restores podocyte viability, reduces abnormal migration ability, protects podocyte cytoskeleton, and reinstates the expression of nephrin protein in puromycin-induced podocyte injury models *in vitro*. My experiments used a HG induced rat primary podocyte injury model to explore the role and mechanism of ACT, which was consistent with the results by Ding *et al*.[28]. The therapeutic and protective effects of ACT were validated through different podocyte injury models. Therefore, the restoration of function of impaired podocytes by ACT may be a useful pharmacological effect in the treatment of renal failure. Taken together with the fact that similar actions were detectable in mesangial cells and glomerular endothelial cells, it is suggested that ACT is a more effective glomerular function-improving agent than DTG in the treatment of renal failure.

Patients with renal dysfunction including hemodialysis are well known to be itching due to dry skin, under which scratching behavior is repeated, resulting in poor skin regeneration (wound healing) [171]. Skin itching is one of the common clinical complications in maintenance hemodialysis (MHD) patients with an incidence rate of approximately 60 to 90%[172]. Currently, the pathogenesis of skin itching in MHD patients is not well understood, peripheral neuropathy, the cutaneous accumulation of uremic toxins, and secondary hyperparathyroidism are considered as candidate pathogenicity factors[173]. A previous study by Pessemier B.D. *et al*.[174] have shown that IL-33 released by damaged skin epithelial cells activates the expression of ST2 in skin dendritic cells. In addition, the activated dendritic cells migrate to intestinal lymph nodes,

where CD^{+4} T cells differentiate into CD^{+4} Th2 cells to produce an immune response[175], suggesting the interaction between the skin and intestine through the "gut skin axis". Furthermore, it has been reported that tryptophan produced by gut microbiota is involved in skin itching, while lactic acid bacteria and bifidobacteria produce γ-aminobutyric acid, which in turn suppresses skin itching[176]. In this study, ACT improved immune response and amino acid metabolism in CGN and DN *in vivo* and *in vitro*. In addition, ACT suppressed the production of MMPs, which participate in the degradation of renal ECM in kidney diseases[105-106], in three glomerular derived cells. Given that ECM remodeling is requisite for wound healing[177], it is presumed that ACT and its metabolites, which are systemically present in CGN and DN, exert their effects on the dysregulation of wound healing due to skin dryness. In this regard, my previous report has shown that ACT and its derivatives, CA and DOPE, promote the production of MMP-2 and MMP-9, whereas MOPE and HVA do not affect both production [178]. Although it needs to study whether ACT and its derivatives, as well as DTG, might be transferred to skin tissues needs to be investigated, they have potential as a novel useful topical agent for improving wound healing.

In conclusion, the present study demonstrated that ACT improved the symptoms of nephritis by the inhibition of inflammatory responses, the regulation of immune function, and the improvement of tissue hemodynamics and hemorheology in CGN rats. In addition, ACT exhibited similar protective activities due to the reduction of not only histopathological but also functional damage to the kidney in DN. Furthermore, the network pharmacology analysis suggests that the actions of ACT are associated with the regulation of signal transduction, the metabolism of carbohydrate, lipid, and amino acid, and mainly the endocrine and immune systems. Moreover, as molecular mechanisms for the improvement and protective actions of ACT to renal functions in CGN and DN, ACT is likely to re-activate the viability of glomerular component cells and suppress the expression of nephritis-inducing factors related closely to the occurrence of renal dysfunction **(Schema 2)**. Thus, these results strongly suggest that ACT is a crucial active component in DTG for the treatment of kidney disease. Given that ATC metabolites existed in the blood and kidneys, ACT is likely to not only improve systemically

metabolic regulation, but also restore glomerular component cell functions in renal failure patients. Thus, this study is believed to contribute to the development of new therapeutic and preventive agents for kidney disease.

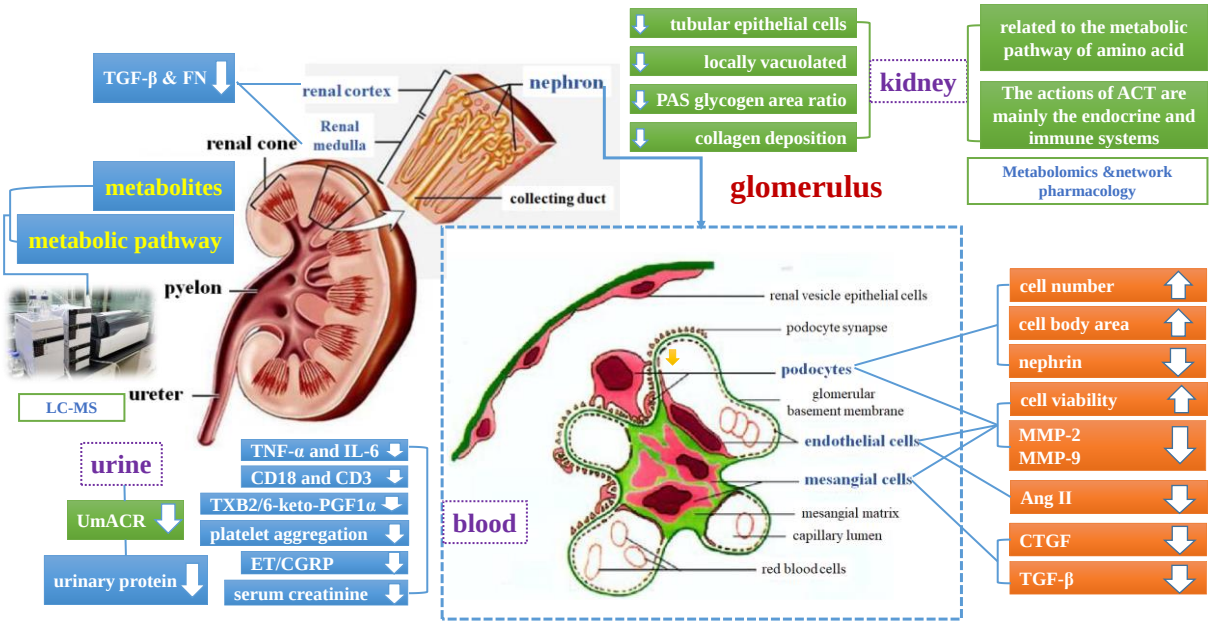

Schema 2 Mechanisms of the therapeutic actions of ACT against nephropathy

ACKNOWLEDGMENTS

First of all, I would like to express my gratitude to my supervisor, Professor Takashi Sato, for his patient guidance and energetically support in the process of doctoral dissertation preparation. And when I was in the laboratory, Tokyo University of Pharmacy and Life Sciences for engage in advanced studies gave me great assistance too.

Most importantly, I would like to express my special gratitude to Professor Akira Ito and Professor Baolin Bian for their great help and opportunities in academic research.

Meanwhile, I wholeheartedly thank Dr. Keisuke Imada for numerous help when I was in Japan. And I thank Sihua Yang and all of the students who were in the laboratory at the same time in Japan. As well as the teachers and classmates of our Chinese team.

I sincerely appreciate to Dr. Bo Yuan for his great and nice assistance.

Finally, I would like to acknowledge my sincere thanks to my family who give me great encouragement and support. I love you all.

REFERENCE

1. Chinese Pharmacopoeia Commission, *Ch.p*, 2020, Part one .
2. Beijing Municipal Health Bureau*, Beijing Standard of Chinese Herbal Medicines,* 1998, PP. 111-12.
3. Li S.Z., *Compendium of Materia Medica* (Jinling edition), ed. By Wang Q.G., Chinc Press of Trasitional Chinese Medicine, 2020, PP. 561-65.
4. Xiao P., *New Chinese Medicine Records*, Chemical Industry Press, PP. 390-95 (2002).
5. Ji X.Q., Sun P., Qi J.J., Lian D.Q., Li X.E., Study on distribution and dynamic accumulation of catalpol andtotal iridoid in fresh *Rehmannia glutinosa, Chin. J. Chin Mater.Med.*, **39,** 466-70 (2014).
6. Chong W.X., Observation on the therapeutic effect of Dihuang Ye Total Glycoside Capsules in the treatment of stage 1 and 2 proteinuria in chronic kidney disease, *Heilongjiang. J. TCM.*, **1**, 64-65 (2017).
7. Gao C.S., Tian J., Total glucosides of yellow leaves in adjuvant treatment of idiopathic membranous nephropathy in phase II efficacy, *Clin. J. Med. Officer*, **45**, 914-917 (2017).
8. Liu G.H., Xue F.P., Zhang W., Zhang N., Observation on the therapeutic effect of rehmannia glutinosa leaf total glycosides capsule on diabetes nephropathy, *Chin. J. Integr. Tradit. Western Nephrol.,* **19**, 990-992 (2018).
9. Bian B.L., Wang H.J., Yang J., Comparison of the Content of Glycosides in Five Different Medicinal Materials, *Chin. J. Chin Mater. Med.*, **35**, 739-740 (2010).
10. Li J.H., Li J., Wang J.Y., Cui Y., Research progress on chemical components and pharmacological effects of the leaves of Rehmannia glutinosa, *Chin. J. Gerontology*., **36**, 4926-4927 (2016).
11. Chen C.H., Song T.Y., Liang Y.C., Hu M.L., Acteoside and 6-*O*-acetylacteoside downregulate cell adhesion molecules induced by IL-1b through inhibition of ERK and JNK in human vascular endothelial cells. *J. Agric. Food Chem.,* **57**, 8852-8859 (2009).
12. Speranza L., Franceschelli S., Pesce M., Reale M., Menghini L., Vinciguerra I., De Lutiis M.A., Felaco M., Grilli A., Antiinflammatory effects in THP-1 cells treated with verbascoside, *Phytother. Res,* **24**, 1398-1404 (2010).

13. Song H.S., Sim S.S., Acteoside inhibits alpha-MSH-induced melanin production in B16 melanoma cells by inactivation of adenyl cyclase, *J. Pharm. Pharmacol.,* **61**, 1347-1351 (2009) .
14. Cui Q., Pan Y., Zhang W., Zhang Y., Ren S., Wang D., Wang Z., Liu X., Xiao W., Metabolites of dietary acteoside: profiles, isolation, identification, and hepatoprotective capacities, *J. Agric. Food Chem.*, **66**, 2660-2668 (2018).
15. Gong W., Zhang N., Cheng G., Zhang Q., He Y., Shen Y., Zhang Q., Zhu B., Zhang Q., Qin L., Rehmannia glutinosa libosch extracts prevent bone loss and architectural deterioration and enhance osteoblastic bone formation by regulating the IGF-1/PI3K/mTOR pathway in streptozotocin-induced diabetic rats, *Int. J. Mol. Sci.*, **20,** 3964 (2019).
16. Ran Z., Ju B., Cao L., Hou Q., Wen L., Geng R., Liao Y., Hu J., Yang J., Microbiome-metabolomics analysis reveals the potential effect of verbascoside in W. Gao *et al.* alleviating cognitive impairment in *db/db* mice, *Food Funct.*,**14**, 3488–3508 (2023).
17. Wang H., Xu Y., Yan J., Zhao X., Sun X., Zhang Y., Guo J., Zhu C., Acteoside protects human neuroblastoma sh-sy5y cells against beta-amyloid-induced cell injury, *Brain. Res.*, **1283**, 139–147 (2009).
18. Etemad L., Zafari R., Moallem S.A., Vahdati-Mashhadian N., Skouei S.Z., Hosseinzadeh H., Teratogenic effect of verbascoside, main constituent of lippia citriodora leaves, in mice, *Iran. J. Pharm. Res.,* **15**, 521-525 (2016).
19. Dai X.X., Su S.L., Cai H.D., Wei D.D., Zheng T.Y., Zhu Z.H., Yan H., Shang E.X., Guo S., Qian D.W., Duan J.A., Comparative pharmacokinetics of acteoside from total glycoside extracted from leaves of rehmannia and dihuangye total glycoside capsule in normal and diabetic nephropathy rats, *Biomed. Chromatogr.,* **31,** 28543613 (2017).
20. Hayashi K., Nagamatsu T., Ito M., Hattori T., Suzuki Y., Acetoside, a component of stachys sieboldii miq, may be a promising antinephritic agent: effect of acteoside on crescentic-type anti-gbm nephritis in rats, *Jpn. J. Pharmacol.*, **65**, 143-151 (1994).
21. Wu Y.T., Lin L.C., Tsai T.H., Measurement of free hydroxytyrosol in microdialysates from blood and brain of anesthetized rats by liquid chromatography with fluorescence detection, *J. Chromatogr. A.*, **1216**, 3501-3507 (2009).
22. Koo K.A., Kim S.H., Oh T.H., Kim Y.C., Acteoside and its aglycones protect primary

culures of rat cortical cells from glutamate-induced excitotoxicity, *Life Sci.*, **79**, 709-716 (2006).

23. Peipei W., Shixia H., Li G., Jianmei L., Lin J., Liangmo C., Ming Y., Yi H., Kaisaier A., Pharmacokinetic study on acteoside in rats, *Chin. J. Chin. Mater. Med.,* **21**, 3312-3315 (2012).
24. Su D., Li W., Xu Q., Liu Y., Song Y., Feng Y., New metabolites of acteoside identified by ultra-performance liquid chromatography/quadrupole-time-of-flight MS(E) in rat plasma, urine, and feces, *Fitoterapia.*, **112**, 45-55 (2016).
25. Wang Y., Feng R., He C., Su H., Ma H., Wan J.B., An integrated strategy to improve data acquisition and metabolite identification by time-staggered ion lists in UHPLC/Q-TOF MS-based metabolomics, *J. Pharm. Biomed.Ana*l., **157**, 171-179 (2018).
26. Wang Z., Ma B., Ma C., Zheng C., Zhou B., Guo G., Xia T., Region identification of Xinyang Maojian tea using UHPLC-Q-TOF/MS-based metabolomics coupled with multivariate statistical analyses, *J. Food Sci.*, **86**, 1681-1691 (2021).
27. Miyase T., Koizumi A., Ueno A., Noro T., Kuroyanagi M., Fukushima S., Akiyama Y., Takemoto T., Studies on the Acyl Glycosides from Leucoseptrum japonicum (MIQ.) Kitamuraet Murata, *Chem. Pharm. Bull*, **30**, 2732 (1982).
28. Ding F.R., Si N., Bian B.L., Ding J., The effect of acteoside on puromycin nephropathy and podocyte injury model, *Chin. J. Nephrol.*, **34**, 30-35 (2018).
29. Wen Y., Huo S., Zhang W., Xing H., Qi L., Zhao D., Li N., Xu J., Yan M., Chen X., Pharmacokinetics, Biodistribution, Excretion and Plasma Protein Binding Studies of Acteoside in Rats, *Drug. Res. (Stuttg),* **66**, 148-153 (2016).
30. Amaro D., Carreño E., Steeples L.R., Oliveira-Ramos F., Marques-Neves C., Leal I., Tubulointerstitial nephritis and uveitis (TINU) syndrome: a review, *Br. J. Ophthalmol.*, **104** ,742-747 (2020).
31. Harikrishnan R., Devi G., Van D.H., Balamurugan P., Arockiaraj J., Balasundaram C., Hepatic antioxidant activity, immunomodulation, and pro-anti-inflammatory cytokines manipulation of κ-carrageenan (κ-CGN) in cobia, Rachycentron canadum against Lactococcus garvieae, *Fish Shellfish Immunol.*, **119**, 128-144 (2021).
32. Gahmberg C.G., Leukocyte adhesion: CD11/CD18 integrins and intercellular adhesion molecules, *Curr. Opin. Cell. Biol*, **9**, 643-650 (1997).

33. Zhang X., Zhao C.L., He L., A study on the β2 adhesion molecule in tegrins and L-selectins in patients with proliferative glom erulonephritis, *J. Chin. Physician.*, **18**, 52-54 (2006).
34. Segerer S., Nelson P.J., Chemokines, chemokine receptors, and renal disease from basic science to pathophysiologic and therapeutic studies, *J. Am. Soc. Nephrol.*, **11**, 152-176 (2000).
35. Thati M., Bryce A.K., Berend I., The emerging role of coagulation proteases in kidney disease, *Nat. Rev. Nephrol.*, **12**, 94–109 (2016).
36. Zhang X., Zhao C.L., Zhang W.H., He L., Yin Y.M., The expressinon of β2 adhesion molecule integrins and L-selectins in proliferative Glomerulonephritis patients, *Chin. J Prac. Med.*, **2**, 966-968 (2003).
37. Tshilela K.A., Ikeuchi H., Matsumoto T., Kuroiwa T., Sakurai N., Sakairi T., Kaneko Y., Maeshima A., Hiromura K., Nojima Y., Glomerular cytokine expression in murine lupus nephritis, *Clin. Exp. Nephrol.,* **20**, 23-29 (2016).
38. Zhong X., Li X., Liu F., Tan H., Shang D., Omentin inhibits TNF-α-induced expression of adhesion molecules in endothelial cells via ERK/NF-κB pathway, *Biochem. Biophys. Res. Commun.*, **425**, 401-406 (2012).
39. Choi H.J., Kim N.E., Kim B.M., Seo M., Heo J.H., TNF-α-Induced YAP/TAZ Activity Mediates leukocyte-endothelial adhesion by regulating VCAM1 expression in endothelial cells, *Int. J. Mol. Sci.*, **19**, 3428 (2018).
40. Page M.J., Bester J., Pretorius E., The inflammatory effects of TNF-α and complement component 3 on coagulation, *Sci. Rep.*, **8**, 1812 (2018).
41. Shobeiri P., Seyedmirzaei H., Karimi N., Rashidi F., Teixeira A.L., Brand S., Sadeghi-B.D., Rezaei N., IL-6 and TNF-α responses to acute and regular exercise in adult individuals with multiple sclerosis (MS): a systematic review and meta-analysis, *Eur. J. Med. Res.*, **27**, 185 (2022).
42. Zhang J., Mi Y., Zhou R., Liu Z., Huang B., Guo R., Wang P., Lu Y., Zhou Y., Quan S., The TLR4-MyD88-NF-κB pathway is involved in sIgA-mediated IgA nephropathy, *J. Nephrol.*, **33**, 1251-1261 (2020).
43. Su H., Lei C.T., Zhang C., Interleukin-6 signaling pathway and its role in kidney disease: An update, *Front. Immunol.*, **8**, 405 (2017).
44. Eitner F., Westerhuis R., Burg M., Weinhold B., Gröne H.J., Ostendorf T., Rüther

U., Koch K.M., Rees A.J., Floege J., Role of interleukin-6 in mediating mesangial cell proliferation and matrix production in vivo Ostendorf, Ulrich Rüther, Karl-Martin Koch, Andrew J. Rees, Jürgen Floege, *Kidney Int.*, **51**, 69-78 (1997).

45. Abbott F., Ryan J.J., Ceska M., Matsushima K., Sarraf C.E., Rees A.J., Interleukin-1β stimulates human mesangial cells to synthesize and release interleukins-6 and -8, *Kidney Int.*, **40**, 597-605 (1991).
46. Magno A.L., Herat L.Y., Carnagarin R., Schlaich M.P., Matthews V.B., Current knowledge of IL-6 cytokine family members in acute and chronic kidney disease, *Biomed.*, **7**, 19 (2019).
47. Ruef C., Budde K., Lacy J., Northemann W., Baumann M., Sterzel R.B., Coleman D.L., Interleukin 6 is an autocrine growth factor for mesangial cells, *Kidney Int.*, **38**, 249-257 (1990).
48. Tesar V., Masek Z., Rychlík I., Merta M., Bartůnková J., Stejskalová A., Zabka J., Janatková I., Fuciková T., Dostál C., Becvár R., Cytokines and adhesion molecules in renal vasculitis and lupus nephritis, *Nephrol. Dial. Transplant.*, **13**, 1662-1667 (1998).
49. Knight K.R., Collopy P.A., Martin T.J., O'Brien B.M, Regulation of microvascular prostacyclin and thromboxane with inhibitors of arachidonic acid metabolism, *Prostaglandins*, **33**, 445-457 (1987).
50. Brunkwall J.S., Stanley J.C., Jackson T., Andersson D., Bergqvist D., Papaverine effects on PGI2 and TXA2 release from the canine vascular wall, *PGs. Leukot Essent Fatty Acids.*, **46**, 175-182 (1992).
51. Ho-Tin-Noé B., Boulaftali Y., Camerer E., Platelets and vascular integrity: how platelets prevent bleeding in inflammation, *Blood*, **131**, 277-288 (2018).
52. Mackie I., Cooper P., Lawrie A., Kitchen S., Gray E., Laffan M., Guidelines on the laboratory aspects of assays used in haemostasis and thrombosis, *Int. J. Lab. Hematol.*, **35**, 1-13 (2013).
53. Wang Z., Wang C., Zhang W., Wang L., Lei T., Changes of TXA2 and PGI_2 during postoperative hypertensive crisis in patients with hypertensive intracerebral hemorrhage, *J. Huazhong. Univ. Sci. Technolog. Med. Sci.*, **28**, 87-89 (2008).
54. Zhang Z.F., Zhao Y.T., Shi X.Y., The changes in serum TXB_2 and 6-keto-$PGF_{1\alpha}$ in 62 cases with renal disease, *Chin. J. Int. Med.*, **28**, 25-27 (1989).
55. Zdrojewski Z., Lizakowski S., Raszeja-Specht A., Skibowska A., Rutkowski B.,

Influence of spontaneous platelet aggregation on progression of glomerular disease, *Nephron.*, **92**, 36-42 (2002).

56. Ferroni P., Basili S., Davi G., Platelet Activation, Inflammatory Mediators and Hypercholesterolemia, *Curr. Vasc. Pharmacol.*, **1**, 157-169 (2003).
57. Finsterbusch M., Norman M.U., Hall P., Kitching A.R., Hickey M.J., Platelet retention in inflamed glomeruli occurs via selective prolongation of interactions with immune cells, *Kidney Int*., **95**, 363-374 (2019).
58. Guan Z., VanBeusecum J.P., Inscho E.W, Endothelin and the renal microcirculation, *Semin. Nephrol.,* **35**, 145-155 (2015).
59. Liu Z., Zhang M., Huo Q., Zhu T., Changes in ET-1, Plasma Neuropeptide Y, and CGRP in Child Patients With Congenital Heart Disease Complicated With Pulmonary Hypertension Before and After Operation, *Clin. Pediatr. (Phila).*, **60**, 56-63 (2021).
60. Ginsberg P., Panzer U., Asada N., Tissue-resident memory T cells in renal autoimmune diseases, *Front. Immunol.*, **14**, 1111521 (2023).
61. Eddy A.A., Molecular basis of renal fibrosis, *Pediatr. Nephrol.*, **15**, 290-301 (2000).
62. Bai Y., Wang W., Yin P., Gao J., Na L., Sun Y., Wang Z., Zhang Z., Zhao C., Ruxolitinib alleviates renal interstitial fibrosis in UUO mice, *Int. J. Biol. Sci.*, **16**, 194-203 (2020).
63. Gharaee-Kermani M., Wiggins R., Wolber F., Goyal M., Phan S.H., Fibronectin is the major fibroblast chemoattractant in rabbit anti-glomerular basement membrane disease, *Am. J. Pathol.*, **148**, 961-967 (1996).
64. ElSayed N.A., Aleppo G., Aroda V.R., Bannuru R.R., Brown F.M., Bruemmer D., Collins B.S., Hilliard M.E., Isaacs D., Johnson E.L., Kahan S., Khunti K., Leon J., Lyons S.K., Perry M.L., Prahalad P., Pratley R.E., Seley J.J., Stanton R.C., Gabbay R.A., on behalf of the American Diabetes Association, Classification and Diagnosis of Diabetes: Standards of Care in Diabetes-2023, *Diabetes Care.*, **46** , S19-S40 (2023).
65. Magliano D.J., Boyko E.J., IDF DIABETES ATLAS [Internet], IDF Diabetes Atlas 10th edition scientific committee 10th edition. Brussels: International Diabetes Federation, PMID: 35914061 (2021).
66. Mauer S.M., Steffes M.W., Goetz F.C., Sutherland D.E., Brown D.M., Diabetic nephropathy. A perspective, *Diabetes*, **2**, 52-55 (1983).
67. Samsu N., Diabetic Nephropathy: Challenges in Pathogenesis, Diagnosis, and

Treatment, *Biomed. Res. Int.*, 1497449 (2021).

68. Sharma K., Mccue P., Dunn S.R., Diabetic kidney disease in the db/db mouse, *Am. J. Physiol.-Renal Physiol.*, **284**, 12736165 (2003).

69. Tesch G.H., Lim A.K., Recent insights into diabetic renal injury from the db/db mouse model of type 2 diabetic nephropathy, *Am. J. Physiol.-Renal Physiol.,* **300**, F301-F310 (2011).

70. Azushima K., Gurley S.B., Coffman T.M., Modelling diabetic nephropathy in mice, *Nat. Rev. Nephrol.*, **14**, 48-56 (2018).

71. Chen M.L., Wen J., Xie L.S., Fan J.M., Efficacy of total glycosides from Rehmannia glutinosa Libosch leaf extract for diabetic nephropathy: a meta-analysis, *JEBM*, **11**, 1293-1298 (2021).

72. Parving H.H., Lehnert H., Bröchner-Mortensen J., Gomis R., Andersen S., Arner P., The effect of irbesartan on the development of diabetic nephropathy in patients with type 2 diabetes, *N Engl J Med*., **345,** 870-8(2001).

73. Palmer A.J., Tucker D.M., Valentine W.J., Roze S., Gabriel S., Cordonnier D.J., Cost-effectiveness of irbesartan in diabetic nephropathy: a systematic review of published studies, *Nephrol Dial Transplant*., **20**, 1103-9(2005).

74. Wang X., Shen Y., Wang S., Li S., Zhang W., Liu X., Lai L., Pei J., Li H., PharmMapper 2017 update: a web server for potential drug target identification with a comprehensive target pharmacophore database. *Nucleic. Acids Res.,* **45**, W356-W360 (2017).

75. Daina A., Michielin O., Zoete V., Swisstargetprediction: updated data and new features for efficient prediction of protein targets of small molecules, *Nucleic. Acids Res.*, **47**, 357-364 (2019).

76. Gfeller D., Michielin O., Zoete V., Shaping the interaction landscape of bioactive molecules, *Bioinformatics*, **29**, 3073-3079 (2013).

77. Stelzer G., Rosen N., Plaschkes I., Zimmerman S., Twik M., Fishilevich S., Stein T.I., Nudel R., Lieder I., Mazor Y., Kaplan S., Dahary D., Warshawsky D., Guan-Golan Y., Kohn A., Rappaport N., Safran M., Lancet D., The genecards suite: from gene data mining to disease genome sequence analyses, *Curr. Protoc. Bioinformatics.*, **54**, 1-30 (2016).

78. Zhou Y., Zhang Y., Lian X., Li F., Wang C., Zhu F., Qiu Y., Chen Y., Therapeutic target database update 2022: facilitating drug discovery with enriched comparative data of

targeted agents, *Nucleic. Acids. Res.*, **50**, D1398-D1407 (2022).

79. Wishart D.S., Feunang Y.D., Guo A.C., Lo E.J., Marcu A., Grant J.R., Sajed T., Johnson D., Li C., Sayeeda Z., Assempour N., Iynkkaran I., Liu Y., Maciejewski A., Gale N., Wilson A., Chin L., Cummings R., Le D., Pon A., Knox C., Wilson M., DrugBank 5.0: a major update to the DrugBank database for 2018, *Nucleic. Acids Res.*, **46**, D1074-D1082 (2018).
80. Szklarczyk D., Gable A.L., Lyon D., Junge A., Wyder S., Huerta-Cepas J., Simonovic M., Doncheva N.T., Morris J.H., Bork P., Jensen L.J., Mering C.V., STRING v11: protein-protein association networks with increased coverage, supporting functional discovery in genome-wide experimental datasets, *Nucleic. Acids Res.*, **47**, D607-D613 (2019).
81. Zhou Y., Zhou B., Pache L., Chang M., Khodabakhshi A.H., Tanaseichuk O., Benner C., Chanda S.K., Metascape provides a biologist-oriented resource for the analysis of systems-level datasets, *Nat. Commun.*, **10**, 1523 (2019).
82. Zhang L., Wang Z., Zhang X., Zhao L., Chu J., Li H., Sun W., Yang C., Wang H., Dai W., Yan S., Chen X., Xu D., Alterations of the Gut Microbiota in Patients with Diabetic Nephropathy, *Microbiol. Spectr.*, **10**, e0032422 (2022).
83. Gong W., Chen C., Xiong F., Yang Z., Wang Y., Huang J., Liu P., Huang H., CKIP-1 ameliorates high glucose-induced expression of fibronectin and intercellular cell adhesion molecule-1 by activating the Nrf2/ARE pathway in glomerular mesangial cells, *Biochem. Pharmacol.*, **116**, 140-152 (2016).
84. Lyu C., Sun Y., Immunometabolism in the pathogenesis of vitiligo, *Front. Immunol.*, **13**, 1055958 (2022).
85. Liu L., Xu J., Zhang Z., Ren D., Wu Y., Wang D., Zhang Y., Zhao S., Chen Q., Wang T., Metabolic Homeostasis of Amino Acids and Diabetic Kidney Disease, *Nutrients*, **15**, 184 (2022).
86. Arneth B., Arneth R., Shams M., Metabolomics of Type 1 and Type 2 Diabetes, *Int. J. Mol. Sci.*, **20**, 2467 (2019).
87. Holecek M., Branched-chain amino acids in health and disease: metabolism, alterations in blood plasma, and as supplements, *Nutr*. Metab., **15**, 33 (2018).
88. Chen K.H., Chen Y.L., Tang H.Y., Hung C.C., Yen T.H., Cheng M.L., Shiao M.S., Chen J.K., Dietary leucine supplement ameliorates hepatic steatosis and diabetic nephropathy

in db/db mice, *Int. J. Mol. Sci*, **19**, 1921 (2018).

89. Saleem T., Dahpy M., Ezzat G., Abdelrahman G., Abdel-Aziz E., Farghaly R., The profile of plasma free amino acids in type 2 diabetes mellitus with insulin resistance: association with microalbuminuria and macroalbuminuria, *Appl. Biochem. Biotechnol.*, **188**, 854-867 (2019).
90. Sun Y., Gao H.Y., Fan Z.Y., He Y., Yan Y.X., Metabolomics signatures in type 2 diabetes: a systematic review and integrative analysis, *J. Clin. Endocrinol. Metab.,* **105**, dgz240. (2020).
91. Wang T.J., Larson M.G., Vasan R.S., Cheng S., Rhee E.P., Mccabe E., Lewis G.D., Fox C.S., Jacques P.F., Fernandez C., O'Donnell C.J., Carr S.A., Mootha V.K., Florez J.C., Souza A., Melander O., Clish C.B., Gerszten R.E., Metabolite profiles and the risk of developing diabetes, *Nat. Med.*, **17**, 448-453 (2011).
92. Zhang S., Li X., Luo H., Fang Z.Z., Ai H., Role of aromatic amino acids in pathogeneses of diabetic nephropathy in chinese patients with type 2 diabetes, *J. Diabetes Complications*, **34**, 107667 (2020).
93. Zhou Q., Sun W., Chen J., Zhang H., Liu J., Lin Y., Lin P., Wu B., An Y., Huang L., Sun W., Zhou X., Li Y., Yuan Y., Zhao J., Xu W., Zhao S., Phenylalanine impairs insulin signaling and inhibits glucose uptake through modification of irβ, *Nat. Commun.,* **13**, 4291 (2022).
94. Clark T.C., Tinsley J., Sigholt T., Macqueen D.J., Martin S.A.M., Arginine, ornithine and citrulline supplementation in rainbow trout: Free amino acid dynamics and gene expression responses to bacterial infection, *Fish Shellfish Immunol.*, **98**, 374-390 (2020).
95. Cao P., Huang B., Hong M., Jiang Y., Cao R., Chi C., Cao Y., Li S., Association of amino acids related to urea cycle with risk of diabetic nephropathy in two independent cross-sectional studies of chinese adults, *Front. Endocrinol.*, **13**, 983747 (2022).
96. Abdelsattar S., Kasemy Z.A., Elsayed M., Elrahem T.A., Zewain S.K., Targeted metabolomics as a tool for the diagnosis of kidney disease in type ii diabetes mellitus, *Br. J. Biomed. Sci.*, **78**, 184-190 (2021).
97. Song P., Ramprasath T., Wang H., Zou M.H., Abnormal kynurenine pathway of tryptophan catabolism in cardiovascular diseases, *Cell. Mol. Life Sci.*, **74**, 2899-2916 (2017).
98. Qi Q., Li J., Yu B., Moon J.Y., Chai J.C., Merino J., Hu J., Ruiz-Canela M., Rebholz C.,

Wang Z., Usyk M., Chen G.C., Porneala B.C., Wang W., Nguyen N.Q., Feofanova E.V., Grove M.L., Wang T.J., Gerszten R.E., Dupuis J., Salas-Salvado J., Bao W., Perkins D.L., Daviglus M.L., Thyagarajan B., Cai J., Wang T., Manson J.E., Martinez-Gonzalez M.A., Selvin E., Rexrode K.M., Clish C.B., Hu F.B., Meigs J.B., Knight R., Burk R.D., Boerwinkle E., Kaplan R.C., Host and gut microbial tryptophan metabolism and type 2 diabetes: an integrative analysis of host genetics, diet, gut microbiome and circulating metabolites in cohort studies, *Gut*, **71**, 1095-1105 (2022).

99. Yu E., Papandreou C., Ruiz-Canela M., Guasch-Ferre M., Clish C.B., Dennis C., Liang L., Corella D., Fito M., Razquin C., Lapetra J., Estruch R., Ros E., Cofan M., Aros F., Toledo E., Serra-Majem L., Sorli J.V., Hu F.B., Martinez-Gonzalez M.A., Salas-Salvado J., Association of tryptophan metabolites with incident type 2 diabetes in the predimed trial: a case-cohort study, *Clin. Chem.*, **64**, 1211-1220 (2018).

100. Luo H.H., Feng X.F., Yang X.L., Hou R.Q., Fang Z.Z., Interactive effects of asparagine and aspartate homeostasis with sex and age for the risk of type 2 diabetes risk, *Biol. Sex Differ.*, **11**, 58 (2020).

101. Rebholz C.M., Yu B., Zheng Z., Chang P., Tin A., Kottgen A., Wagenknecht L.E., Coresh J., Boerwinkle E., Selvin E., Serum metabolomic profile of incident diabetes, *Diabetologia*, **61**, 1046-1054 (2018).

102. Koh A., Molinaro A., Stahlman M., Khan M.T., Schmid C., Manneras-Holm L., Wu H., Carreras A., Jeong H., Olofsson L.E., Bergh P.O., Gerdes V., Hartstra A., Brauw M., Perkins R., Nieuwdorp M., Bergstrom G., Backhed F., Microbially produced imidazole propionate impairs insulin signaling through mtorc1, *Cell*, **175**, 947-961 (2018).

103. Wang Z., Fu W., Huo M., He B., Liu Y., Tian L., Li W., Zhou Z., Wang B., Xia J., Chen Y., Wei J., Abliz Z., Spatial-resolved metabolomics reveals tissue-specific metabolic reprogramming in diabetic nephropathy by using mass spectrometry imaging, *Acta Pharm. Sin.,* **B 11**, 3665-3677 (2021).

104. Watanabe N., Shikata K., Shikata Y., Sarai K., Omori K., Kodera R., Sato C., Wada J., Makino H., Involvement of MAPKs in ICAM-1 Expression in Glomerular Endothelial Cells in Diabetic Nephropathy, *Acta. Medica. Okayama*, **65**, 247-257 (2011).

105. Xu L., Zhao B.L., Tang T.P., Ren X.Z., Chinese herbs for benefiting qi and resolving stasis delay the progression of fibrosis in mesangial proliferative glomerulonephritis by regulating activity of NF-κB to restrain the expression of MMP-2 and MMP-9. *CJTCMP*,

34, 3001-3005 (2019).

106. Hu Y.J., Ren X.Z., The research progress of relationship between mesangial proliferative glomerulonephritis and MMP-2, TIMP-2 in traditional Chinese medicine. *J. Zhejiang Univ. Med. Sci.*, **38**, 1342-1345 (2014).
107. Aresu L., Benali S., Garbisa S., Gallo E., Castagnaro M., Matrix metalloproteinases and their role in the renal epithelial mesenchymal transition, *Histol. Histopathol,* **26**, 307-313 (2011).
108. Miner J.H., The glomerular basement membrane, *Exp. Cell Res.*, **318**, 973-978 (2012).
109. Fogo A.B., Kon V., The glomerulus – a view from the inside – the endothelial cell, *Int. J. Biochem. Cell Biol.*, **42**, 1388-1397 (2010).
110. Imig J.D., Zhao X.Y., Elmarakby A.A., Pavlov T., Editorial: Interactions between podocytes, mesangial cells, and glomerular endothelial cells in glomerular diseases, *Front. Physiol.*, **13**, 849693 (2022).
111. Hu C., Sun L., Xiao L., Han Y., Fu X., Xiong X., Xu X., Liu Y., Yang S., Liu F., Kanwar Y.S., Insights into the mechanisms involved in the expression and regulation of extracellular matrix proteins in diabetic nephropathy, *Curr. Med. Chem.*, **22**, 2858-2870 (2015).
112. Du Y.G., Zhang K.N., Jiang X.E., Chai K.F., Protective effects and mechanisms of panax nologinoside on rat mesangial cells induced by high glucose, *J. Zhejiang Chin. Med. Univ.*, **39**, 647-653 (2015).
113. Luo D., Wang Y., Ding X., Hu Y., Effect of nobiletin on LPS-induced inflammatory injury of mesangium cells by regulating AMPK /NLRP3 signaling pathway, *Trad. Chin. Drug Res. & Clin. Pharma.*, **35**, 224-229 (2024).
114. Li X.G., Liu H.Y., Liu G., Sun Y., Li J., Guan G.J., Effects of high glucose on expressions of connective tissue growth factor and its receptor in cultured human mesangial cells, *J. Shandong Univ. Health. Sci.*, **49**, 99-102 (2011).
115. Yu H., Advances in the pathogenesis of IgA nephropathy, *J. Inner. Mongolia Med. Univ.*, **36**, 90-94 (2017).
116. Kalliakmani P., Nakopoulou L., Tsakas S., Gerolymos M., Papasotiriou M., Goumenos D.S., Urinary interleukin-6 (IL-6) and transforming growth factor (TGF-β) levels in corticosteroid treated patients with IgA nephropathy. *Clin. Nephrol.*, **76**, 144-

150 (2011).

117. Zhao L., Zhao J., Wang X.L., Chen Z.X., Peng K.X., Lu X.H., Meng L.H., Liu G., Guan G.G., Wang F., Serum response factor induces endothelial-mesenchymal transition in glomerular endothelial cells to aggravate proteinuria in diabetic nephropathy, *Physiol. Genomics.*, **48**, 711-718 (2016).
118. Satchell S.C., Braet F., Glomerular endothelial cell fenestrations: an integral component of the glomerular filtration barrier, *Amer. J. Phys.*, **296**, F947-F956 (2009).
119. Xing Y.F., Peng H., Li C.M., Ye Z.C., Li M., Lou T.Q., Effect of high glucose on renin-angiotensin system in rat glomerular endothelial cells and its associated mechanism. *Chin. J. Neph.*, **11**, 831-837 (2011).
120. Luo J.H., Chen X.M., Research progress on the role and regulatory mechanism of renal tubular epithelial cell transdifferentiation in the process of renal interstitial fibrosis, *Urol. Nephro. FMS.*, **25**, 829-831 (2005).
121. Meng H., Zhou X.P., X.J., Luo H.M., Yuan H.L., Xiong L.Y., Changes in levels of CyPA and AngII in peripheral blood of patients with acute kidney injury and influence of hemodialysis on them, *Shandong Med. J.*, **55**, 10-12 (2015).
122. Abduweli A., Research progress of drugs related to diabetes nephropathy. *Chin. Pract. Med.*, **6**, 255-256 (2011).
123. Kravets I., Mallipattu S.K., The role of podocytes and podocyte-associated biomarkers in diagnosis and treatment of diabetic kidney disease, *J. Endocr. Soc.*, **4**, 35-44 (2020).
124. Jia M., Zhang Y.M., Xu A.P., Lv J., Lai D.Y., Influence of fenofibrate on Nephrin in primary cultured rat podocytes under high glucose, *Chin. J. Diabetes*, **21**, 935-938 (2013).
125. Yang L.Y., Lin X., Lan M.L., Progress in the application of podocyte protein markers in primary podocyte disease, *Chin. Modern Doctor*., **61**, 116-119 (2023).
126. Wang Z., Sun W.S., Wu X.L., Li R.P., Progress on the effects of traditional Chinese medicine on the cytoskeleton and pore membrane related proteins of renal podocytes. *Shaanxi J. Trad. Chin. Med.*, **10**, 1437-1438 (2013).
127. Audzeyenka I., Bierżyńska A., Lay A.C., Podocyte bioenergetics in the development of diabetic nephropathy: The role of mitochondria, *Endocrinology*, **163**, bqab234 (2022).
128. Guo L.Q., Chen X.W., Liu H.F., Podocyte marker proteins and podocyte diseases, *Chin. J. Integr. Tradit. Western Nephrol.*, **2**, 173-176 (2008).

129. Chen Y., Podocyte injury and diabetes nephropathy, *Chin. J. Pract. Inter. Med.,* **27**, 1876-1879 (2007).
130. Gao Y., Yang L., Wang J.R., Yang W.X., Zang L.P., Mesangial podocyte axis in renal tubulointerstitial lesions of IgA nephropathy, *J. Clin. Exp. Pathol.*, **34**, 73-76 (2018).
131. Ma H.G., Liu H.Q., Liu Z.D., Tang Y.Y., Primary culture and identification of rat glomerular microvascular endothelial cells, *J. physiol.*, **7**, 926-930 (2021).
132. Mei F., Zhang D.D., Ma J.L., Sun X., Zhang Z.Q., Wang Y., Effects of hypoxia on the expression of transforming growth factor-β1 and transdifferentiation related proteins in rat glomerular endothelial cells. *Qinghai Sci. Tech.*, **27**, 23-26 (2020).
133. Chen C., Hu D.J., Zhang S., Dong P., Xu Y., Liu N.L., Effects of carnosic acid on high glucose-induced rat mesangial cells by regulating PINK1/Parkin signaling pathway. *Chin. J. Gero.*, **23**, 5830-5834 (2023).
134. Gu J., Zhang C.J., Jia L., Yang X.P., Primary culture of rat podocytes and its specific expression of Nephrin, *Guangdong Med.*, **38**, 825-829 (2017).
135. Tao Y.H., Wang Y.M., Peng W.Z., Primary culture and identification of rat glomerular podocytes, *J. Sichuan. Univ. Med. Sci.*, **44**, 987-990 (2013).
136. Ma L.L., Ni H.L., Zou X.R., Yuan Y.Y., Luo C., Liu B.Y., Wang F.Y., Xi Y., Chu Y.D., Xu P.G., Qiu X.H., Li S., Bu S.Z ,. Mori cortex prevents kidney damage through inhibiting expression of inflammatory factors in the glomerulus in streptozocin-induced diabetic rats, *Iran. J. Basic. Med. Sci.*, **20**, 715-721 (2017).
137. Caulfield J.P., Farquhar M.G., The permeability of glomerular capillaries to graded dextrans: Identification of the basement membrane as the primary filtration barrier, *J. Cell Biol.*, **63**, 78-83 (1974).
138. Ramazani Y., Knops N., Elmonem M.A., Nguyen T.Q., Arcolino F.O., Heuvel L., Levtchenko E., Kuypers D., Goldschmeding R., Connective tissue growth factor (CTGF) from basics to clinics, *Matrix Biol.*, **68-69**, 44-66 (2018).
139. Wahab N., Cox D., Witherden A., Mason R.M., Connective tissue growth factor (CTGF) promotes activated mesangial cell survival via up-regulation of mitogen-activated protein kinase phosphatase-1 (MKP-1). *Biochem. J.*, **406**, 131-138 (2007).
140. Lipson K.E., Wong C., Teng Y., Spong S., CTGF is a central mediator of tissue remodeling and fibrosis and its inhibition can reverse the process of fibrosis, *Fibrogenesis & Tissue Repair*, **5**, S24 (2012).

141. Narula S., Tandon C., Tandon S., Role of matrix metalloproteinases in degenerative kidney disorders, *Curr. Med. Chem.*, **25** ,1805-1816 (2018).

142. Lenz O., Elliot S.J., Stetler-Stevenson W.G., Matrix metalloproteinases in renal development and disease, *J. Am. Soc. Nephrol.*, **11**, 574-581 (2000).

143. Cheng Z.Y., Liu L., Wang Z., Cai Y.Y., Xu Q., Chen P.S., Hypoxia activates Src and promotes endocytosis which decreases MMP-2 activity and aggravates renal interstitial fibrosis, *Int. J. Mol. Sci.*, **19**, 581 (2018).

144. Cavdar Z., Ozbal S., Celik A., Ergur B.U., Gunel I.E., Ural C., Camsari T., Guner G.A., The effects of alpha-lipoic acid on MMP-2 and MMP-9 activities in a rat renal ischemia and re-perfusion model, *Biotech. Histochem.*, **89**, 304-314 (2014).

145. Cheng Z.Y, Limbu M.H, Wang Z, Liu J, Liu L, Zhang X.Y, Chen P.S, Liu B.C, MMP-2 and 9 in chronic kidney disease, *Inter. J. Mol. Sci.*, **18**, 63-70 (2017).

146. Zhang J.H., Wang S.R., He Y.X., Yao B.Y., Zhang Y., Regulation of matrix metalloproteinases 2 and 9 in corneal neovascularization, *Chem. Biol. Drug Des.*, **95**, 485-492 (2020).

147. Lelongt B., Legallicier B., Piedagnel R., Ronco P.M., Do matrix metalloproteinases MMP-2 and MMP-9 (gelatinases) play a role in renal development, physiology and glomerular diseases?, *Curr. Opin. Nephrol. Hypertens.*, **10**, 7-12 (2001).

148. Cavdar Z., Ural C., Celik A., Arslan S., Terzioglu G., Ozbal S., Yildiz S., Ergur U.B., Guneli E., Camsari T., Akdogan G., Protective effects of taurine against renal ischemia/reperfusion injury in rats by inhibition of gelatinases, MMP-2 and MMP-9, and p38 mitogen-activated protein kinase signaling, *Biotech. Histochem.*, **92**, 524-535 (2017).

149. Hood J.D., Cheresh D.A., Role of integrins in cell migration and invasion. *Nat. Rev. Cancer*, **2**, 91-100 (2002).

150. Zakiyanov O., Kalousová M., Zima T., Tesař V., Matrix metalloproteinases in renal diseases: A critical appraisal, *Kidney Blood Press. Res.*, **44**, 298-330 (2019).

151. Hicklin D.J., Ellis L.M., Role of the vascular endothelial growth factor pathway in tumor growth and angiogenesis, *J. Clin. Oncol.*, **23**, 1011-1027 (2005).

152. Mathalone N., Marmor S., Rahat M.A., Lahat N., Oron Y., Geyer O., MMP expression in leaking filtering blebs and tears after glaucoma filtering surgery, *Graefes. Arch. Clin. Exp. Ophthalmol*, **249**, 1047-1055 (2011).

153. Tang G.Y., Li S., Zhang C., Chen H.Y., Wang N., Feng Y.B., Clinical efficacies, underlying mechanisms and molecular targets of Chinese medicines for diabetic nephropathy treatment and management, *Acta. Pharm. Sin. B.*, **11**, 2749-2767 (2021).
154. McMillan J.I., Riordan J.W., Couser W.G., Pollock A.S., Lovett D.H., Characterization of a glomerular epithelial cell metalloproteinase as matrix metalloproteinase-9 with enhanced expression in a model of membranous nephropathy, *J. Clin. Inv.*, **97**, 1094-1101 (1996).
155. Liu N., Chen Z.L., Clinical effect of Haikun Shenxi Capsule combined with angiotensin converting enzyme inhibitor in the treatment of chronic glomerulonephritis, *Clin. Res.*, **30**, 104-108 (2022).
156. Rüster C., Wolf G., Angiotensin II as a morphogenic cytokine stimulating renal fibrogenesis, *J. Am. Soc. Nephrol.*, **22**, 1189-1199 (2011).
157. Singh R., Singh A.K., Leehey D.J., A novel mechanism for angiotensin II formation in streptozotocin-diabetic rat glomeruli, *Am. J. Physiol. Renal Physiol.*, **288**, F1183-F1190 (2005).
158. Putaala H., Soininen R., Kilpeläinen P., Wartiovaara J., Tryggvason K., The murine nephrin gene is specifically expressed in kidney, brain and pancreas: inactivation of the gene leads to massive proteinuria and neonatal death, *Hum. Mol. Genet.*, **10**, 1-8 (2001).
159. Li X.Z, Chuang P.Y., Agati V.D.D., Dai Y., Yacoub R., Fu J., Xu J., Taku O., Premsrirut P.K., Holzman L.B., He J.C., Nephrin preserves podocyte viability and glomerular structure and function in adult kidneys, *J. American Society Nephrol.*, **26**, 2361-2377 (2015).
160. Zhong W.X., Observation on the therapeutic effect of Dihuang Ye Total Glycoside Capsules in the treatment of stage 1 and 2 proteinuria in chronic kidney disease. *Heilongjiang J. Trad. Chin. Med.*, **1**, 64-65 (2017).
161. Dai X.X., Su S.L., Cai H.D., Wei D.D., Yan H., Zheng T.Y., Zhu Z.H., Shang E.X., Guo S., Qian D.W., Duan J.A., Protective effects of total glycoside from Rehmannia glutinosa leaves on diabetic nephropathy rats via regulating the metabolic profiling and modulating the TGF-β1 and Wnt/β-catenin signaling pathway, *Front. Pharmacol.,* **9**, 1012 (2018).
162. Gan L., Li X.Z., Zhu M.Y., Chen C., Luo H.M., Zhou Q.L., Acteoside relieves mesangial cell injury by regulating Th22 cell chemotaxis and proliferation in IgA nephropathy,

Renal Failure, **40**, 364-370 (2018).

163. Ammirati A.L., Chronic kidney disease, *Rev. Assoc. Med. Bras (1992).*, **66**, s03-s09 (2020).
164. Liu C.L., Yang M.Q., Tang Z.S., Liu Y.R., Song Z.X., Zhang X., Yang X.J., Zhao Y.T., Research on the improvement effect of Saposhnikovia divaricate (Trucz.) Schischk on rheumatoid arthritis based on the "component-target-pathway" association, *Anal. Biochem.*, **674**, 55-60 (2023).
165. Zhang X.Y., Wang S., Shu L.X., Zhao S., Yan X.X., Jia. G.X, Zhang Y., Zhang W.Q., Qian W.X., Yang B., Li Y.B., Rapid screening of hepatotoxic components in Uncariae Ramulus Cum Uncis based on "component-target-pathway" network, *J. Pharm. Biomed. Anal.*, **219**, 36-38 (2022).
166. Teratani G., Awano S., Soh I., Yoshida A., Kinoshita N., Hamasaki T., Takata Y., Sonoki K., Nakamura H., Ansai T., Oral health in patients on haemodialysis for diabetic nephropathy and chronic glomerulonephritis, *Clin. Oral. Investig.*, **17**, 483–489 (2013).
167. Yu W.N., Lei Q.Y., Yang L., Qin G.H., Liu S.S., Wang D, Ping Y., Zhang Y., Contradictory roles of lipid metabolism in immune response within the tumor microenvironment, *J. Hematol. Oncol.*, **14** ,187 (2021).
168. Pollak M.R., Quaggin S.E., Hoenich N.A., Danen E.H., The glomerulus: the sphere of influence, *Clin. J. Am. Soc. Nephrol.,* **9**, 1461- 1469 (2014).
169. Caulfield J.P., Farquhar M.G., The permeability of glomerular capillaries to graded dextrans : Identification of the basement membrane as the primary filtration barrier, *J. Cell Biol.*, **63**, 102-110 (1974).
170. Panzer U., Huber T.B., Immune-mediated glomerular diseases: new basic concepts and clinical implications, *Cell Tissue Res.*, **385**, 277-279 (2021).
171. Shemin D., Bostom A.G., Laliberty P., Dworkin L.D., Residual renal function and mortality risk in hemodialysis patients, *Am. J. Kidney Dis.*, **38**, 85-90 (2001).
172. Narita I., Alchi B., Omori K., Sato F., Ajiro J., Saga D., Kondo D., Skatsume M., Maruyama S., Kazama J.J., Akazawa K., Gejyo F., Etiology and prognostic significance of severe uremic pruritus in chronic hemodialysis patients, *Kidney Int.*, **69**, 1626-1632 (2006).
173. Trachtenberg A.J., Collister D., Rigatto C., Recent advances in the treatment of uremic pruritus, *Curr. Opin. Nephrol. Hypertens.*, **29**, 465-470 (2020).

174. Pessemier B.D., Grine L., Debaere M., Maes A., Paetzold B., Callewaert C., Gu-Skin axis: current knowledge of the interrelationship between microbial dysbiosis and skin conditions, *Microorganisms*, **9**, 353 (2021).

175. Ziegler S.F., Artis D., Sensing the outside world: TSLP regulates barrier immunity, *Nat. Immunol.*, **11**, 289-293 (2010).

176. Fang Z.F., Li L.Z., Zhang H., Zhao J.X., Lu W.W., Chen W., Gut microbiota, probiotics, and their interactions in prevention and treatment of atopic dermatitis: A review, *Front. Immunol.*, **12**, 720393 (2021).

177. Tracy L.E., Minasian R.A., Caterson E.J., Extracellular matrix and dermal fibroblast function in the healing wound, *Adv. Wound Care (New Rochelle)*, **5**, 119–136 (2016).

178. Si N., Kanazawa H., Okuyama K., Imada K., Wang H.J., Yang J., Zhao H.Y., Bian B.L., Ito A., Sato T., Involvement of catechols in acteoside in the activation of promatrix metalloproteinase-2 and membrane type-1-matrix metalloproteinase expression via a phosphatidylinositol-3-kinase pathway in human dermal fibroblasts, *Biol. Pharm. Bull.*, **41**, 1-8 (2018).